MASTER THESIS

Regional climate regulation by different land cover types: comparing homogeneous and heterogeneous structures in agricultural landscapes

LEILA SCHUH

Global Change Ecology (M.Sc.)

University of Bayreuth, Germany

✉ leilaschuh@yahoo.com

30 August 2017

Supervision by

DR. WOLFGANG BABEL

Department of Micrometeorology

University of Bayreuth

PROF. DR. THOMAS KOELLNER

Professorship of Ecological Services

University of Bayreuth

Elite Network of Bavaria

UNIVERSITÄT BAYREUTH

Content

List of Figures

List of Tables

Abbreviations

DLM	Digital landscape model
GIS	Geographical Information System
IPCC	Intergovernmental Panel on Climate Change
LAI	Leaf Area Index
LC	Land cover
LH	Latent heat
LST	Land surface temperature
LWD	Long wave down- welling radiation
MODIS	Moderate-resolution imaging spectroradiometer
NA	No data available (missing values)
NSE	Nash Sutcliffe Efficiency
SEWAB model	Soil energy water atmosphere balance model
SH	Sensible heat
SVAT model	Soil vegetation atmosphere transfer model
SWD	Short wave down-welling radiation
RMSE	Root mean squared error
r	Pearson correlation coefficient
R^2	Coefficient of determination

Acknowledgements

I would like to thank my supervisors, Dr. Wolfgang Babel and Prof. Dr. Thomas Koellner, for the opportunity to write this thesis and for their support during the process of doing so. Heartfelt thanks to Dr. Wolfgang Babel for his exceptional mentoring and encouragement. I would like to thank my technical adviser, Dr. Martin Wegmann, for his generous assistance. Furthermore, I thank Prof. Dr. Christoph Thomas for inviting me into his research group, for his expertise and for his support when I broke my arm. Special thanks go to Dr. Wolfgang Babel, Prof. Dr. Christoph Thomas and Prof. Dr. Thomas Koellner for allowing me to explore my fields of interest and offering this exciting topic, and to the whole Micrometeorology group for their team spirit and welcoming mentality.

I would not have been able to get this far without the help of my family and friends. Heartfelt thanks go to Asja Bernd, Hannah Hepp, Gabriel Brownell, Tejas Bhagwat, Regina Pöhlmann, Joe Premier, Benjamin Leutner, Craig Walton, Detchema Limbrock, Ilse Schuh, Julian Schuh, Gert Haumberger, Ursula Schmeikal and Bernd Schmeikal. Thank you for your input, encouragement, patience, food deliveries, and support when the goal seemed unreachable. Any remaining mistakes are solely my own.

Furthermore, I thank Dr. Heinz-Theo Mengelkamp and Dr. Wolfgang Babel for providing the Soil Energy Water Balance (SEWAB) model utilized in this study, and the Bayerische Vermessungsverwaltung for providing land cover data. Spatial data on land surface temperature and topography was provided by NASA.

Declaration of Originality

I hereby certify that I am the sole author of this thesis and that no part of this thesis has been published or submitted for publication or with the aim of obtaining an academic title elsewhere.

I certify that, to the best of my knowledge, my thesis does not infringe upon anyone's copyright nor violate any proprietary rights and that any ideas, techniques, quotations, or any other material from the work of other people included in my thesis, published or otherwise, are fully acknowledged in accordance with the standard referencing practices.

_____ _____

Location and Date Leila Schuh

Abstract

The agricultural sector is under pressure to produce more food for a growing world population. At the same time, the world's leading scientists warn of rising temperatures and increasing frequency and intensity of extreme events. Modern agricultural production involves large areas of continuous crop fields. Such homogenous landscapes are prone to be strongly affected by, and contribute to summer droughts and heat waves. During such extreme events, regional climate regulation is important for the specific area, but also influences the global climate. Through interaction with the atmosphere, the land surface influences important climatic variables, such as the sensible heat flux, the latent heat flux, the ratio of the turbulent fluxes (Bowen ratio) and the land surface temperature. However, different vegetation types provide the ecosystem service of regional climate regulation to different extents. This study aims to answer the question, whether we can increase the resilience of agricultural areas to summer droughts and heat waves by landscape structuring. The influence of forest patches in crop growing areas, on the turbulent fluxes and on land surface temperature, is investigated. Methodologically, a micrometeorological model is utilized in conjunction with remote sensing data. The research site is located in Bavaria, where rising temperatures and increasing summer extremes are projected. Confirming the effect of forest islands, average and maximum land surface temperatures are lower over heterogeneous than over homogenous agricultural landscapes. Furthermore, the partitioning of energy is found to be balanced by forest patches in the year 2003, when a strong heat wave struck Europe. Accordingly, heterogeneous agricultural landscapes provide the means to increase regional climate regulating ecosystem services.

1. Introduction

In the 21st century the world population faces multiple challenges, characterized by interdependencies and global extent. Climate change and environmental degradation have become a serious concern to societal development. Environmental degradation includes, amongst other threats, resource depletion, biodiversity loss, pest infestations, shortage of arable lands, soil deterioration and soil loss. (Pielke et al., 2013; Pielke & Niyogi, 2013) The IPCC leaves no doubt that climate change is as much real as it is threatening (IPCC, 2013). Rising temperatures, irregularities in rainfall patterns and higher frequencies of extreme events are expected to cause water shortages, and excess water in other places. Some of the most concerning climate change projections in Western Europe are increasing summer droughts and summer heat waves (Meehl & Tebaldi, 2004; Miralles, 2012).

Our economies are based to a great deal on natural resources. However traditionally, we do not account for the goods and services we receive free of charge from nature (MA, 2005; Grunewald et al., 2015). Such externalities may be the input of water or clean air into economic production, or the environment functioning as a sink for our by-products. In the last decades, accounting for ecosystem goods and services has become increasingly important and is expected to contribute to a better representation of services provided by nature in the economic system, and to make the conservation of ecosystems feasible (MA, 2005; Grunewald, et al., 2015; Koellner, 2012).

Food provisioning is one of the most important services at the base of human life on earth, which is affected by environmental and societal challenges. It is also a sphere, where the distinction between ecosystem services and input by humans is difficult. In the last decades, global food production has stagnated and decreased in many places (Pielke & Niyogi, 2013). At the same time, the agricultural sector is under pressure to feed a growing world population. Changing environmental conditions diminish the chances to achieve global food security. Scientific-based, practical solutions to increase the resilience and adaptive capacity of agricultural landscapes to climate change are on request (Pielke et al., 2013; Pielke & Niyogi, 2013).

Agricultural landscapes play a contradicting role regarding ecosystem services. On the one hand they can be considered a main source of food provisioning services. On the other hand, especially intensive agriculture has been found to diminish other ecosystem

services, such as climate and water regulation. The transformation of small-scale, subsistence farming to large, homogenous crop growing areas is largely responsible for adverse environmental effects of the food sector (Power, 2010; Kovacs-Hostyanszki et al., 2017; Grunewald et al., 2015).

The question arises, whether we can influence the agricultural sector's capacity to provide ecosystem services through the way we structure the landscape. The study at hand analyses homogenous versus heterogeneous agricultural landscapes. Homogenous structures are defined as areas of merely crop fields next to each other. Heterogeneity is provided by forest patches mixed in among food growing areas. The ecosystem service under investigation is regional climate regulation.

Regulating ecosystem services have received considerable attention by the scientific community and so has the ecosystem type forest, while agricultural lands have been studied less intensively (Vihervaara et al., 2010; Viglizzo et al., 2016; McDonough et al., 2017). In order to understand and quantify local and regional climate regulation by ecosystems, a better understanding of the mechanisms driving such services is necessary (Viglizzo et al., 2016).

The role of forests to regulate global climate has been studied extensively (Vihervaara et al., 2010). However, regional climate regulation may have been overlooked in our attempts to diminish and adapt to climate change. Coarse climate models may have been missing an essential part in their computations, namely land surface atmosphere interactions. The land surface interacts with the atmosphere on the local and regional scale, the effect of which can aggregate and ultimately influence the climate worldwide (Pitman, 2003).

The type of vegetation plays an important role in the interaction of land surface and atmosphere. Trees have deep roots to retrieve water, they have a higher capacity to regulate their stomata and a lower albedo, compared to agricultural crops. Furthermore, permanent vegetation cover is essential in the regulation of the regional climate. Especially when crop fields are harvested during hot and dry summer months, high levels of evaporation lead to water depletion in the ground. As a result, energy from the sun translates largely into the sensible heat flux. Consequently, hot and dry conditions are perpetuated (Teuling et al., 2010).

Land surface temperature and the turbulent energy fluxes give insight into the regional climate. The sensible heat flux (SH) and the latent heat flux (LH), as well as their ratio (Bowen ratio), are relevant climatic variables, because they contain information about the division of radiant energy and water. Land surface temperature (LST) is a common climatic measure, which can be retrieved from satellite imagery. In the study at hand, these are the climate variables under investigation (Gerber & Decker, 1960; Arya, 1988; Foken, 2010; Seneviratne et al., 2010).

This study aims to answer the question, whether heterogeneous agricultural landscapes provide regional climate regulating ecosystem services, in comparison to homogeneous crop fields.

Methodologically, a micrometeorological model is utilized, in conjunction with satellite remote sensing data. The soil vegetation atmosphere transfer (SVAT) Model provides simulations of sensible and latent heat flux and of land surface temperature with high temporal, but no horizontal spatial resolution. The land surface temperature product retrieved from satellite, comes at a spatial resolution of approximately 1 km^2 and as eight-day aggregations. An approach based on the analyses of individual pixel was followed in the spatial analysis, similar to Alavipanah et al. (2015). The data from both sources is compared and investigated for distinctions between homogenous and heterogeneous agricultural landscape structures.

2. Theoretical Background

2.1 Problems of Modern Agriculture

The agricultural sector is of great importance to human well-being now and in the future. According to the Food and Agriculture Organisation (FAO) "[a]griculture in the 21st century faces multiple challenges; it has to produce: more food and fiber to feed a growing population with a smaller rural labor force, more feedstocks for a potentially huge bioenergy market, contribute to overall development in the many agriculture-dependent developing countries, adopt more efficient and sustainable production methods and adapt to climate change." (FAO, 2005)

An increase in global demand for food is expected to continue in the 21st century. Some studies suggest that wheat production will have to more than double by the mid-century (Pielke & Niyogi, 2013). However, in the last decades, agricultural production has declined worldwide. Agriculture as a sector is characterized by its dependence on nature. Climate is one of the main limiting factors to production. Since the Neolithic revolution about 12,000 years ago, agricultural produce and methods were adapted to local and regional climatic conditions. Nature's ability to provide the necessary ecosystem services has declined and scientists warn that climate change may impose further threats to agricultural production (Pielke et al., 2013; Pielke & Niyogi, 2013; IPCC, 2013; Bahrenberg et al., 1999)

In the second half of the 20th century, the agricultural sector has undergone massive restructuring. As part of the green revolution, the "modern", technology intensive type of agriculture was exported from the industrialized nations to less "developed" countries. Humans transformed agricultural landscapes from biodiversity rich, not very productive lands to lucrative, biodiversity poor plant communities. Small-scale, subsistence farming was removed to make way for large, homogenous fields that are worked by heavy machinery and the use of herbicides and pesticides has increased rapidly since then (Bahrenberg et al., 1999).

In western Europe, rural restructuring (German: *Flurbereinigung*) was a planned operation. This heavy state intervention fostered the development of "large-scale capitalist farms", involving fields of greater size being worked and managed by less people (Renes, 2009). Renes points out that the 15 member states that were part of the European Union in the year 2000, together employed less than a third of their labor force of 1950, and managed half the number of farms (Renes, 2009). In the process of merging arable lands, natural vegetation was removed. This included the slashing of hedgerows, bushes and trees along waterways and roads, and the removal of forest islands between crop fields. Corridors of natural vegetation used to connect agricultural landscapes, and even reach into villages in Germany, before the restructuring of agricultural landscapes started to destroy these biotopes (Bahrenberg et al., 1999).

The conversion of traditional, extensive production to intensive farming led to a steep increase in crop yield. However, a plateau was reached and in most places harvest declined. This unexpected development has led agronomists to formulate the hypothesis of decreasing yield. The hypothesis states that the difference between input and output

declines, until a point after which yield decreases, even with additional input of capital and labor (Pielke & Niyogi, 2013). Crop damage through the extensive use of fertilizers is a visible example (Bahrenberg et al., 1999; Hutson & Roberts, 1990). Despite ongoing innovations, it is worth recognizing that "unfortunately, a limit to yield may exist" (Pielke & Niyogi, 2013).

Not only was modern agriculture unable to keep its promises to infinitely increase yields, it also created a whole new range of problems. Agriculture contributes to the deterioration of the ecosphere's mass balance through its production methods. Organic and inorganic contaminants are placed in the soil and can infiltrate into the groundwater. Nitrogen is a major component of fertilizers and transforms easily into nitrate, which is mobile in soils. The uptake of nitrate by plants occurs only in shallow soil layers, and with excess water, nitrate is easily washed out. The use of fertilizers heavily contributes to the accumulation of substances such as nitrogen and phosphorus in terrestrial and aquatic ecosystems (Jury et al., 1991; Bahrenberg et al., 1999).

Extensive use of pesticides and lack of habitat have led to a decline in insect biodiversity in industrial croplands. While some fauna harms crops, other insects, such as spiders and ground beetles, control pests (Bahrenberg et al., 1999). Furthermore, some insects act as pollinators and are therefore essential for the functioning of the terrestrial ecosystems. Allocating the ecosystem services pollination and pest control spatially, patches of natural vegetation are essential because they provide habitat and retreat for insects, and thus indirectly influence the provision of agricultural services positively (Grunewald & Bastian, 2015).

Erosion is another threat to the productivity of arable lands increased by the intensification of farming. It depends on external factors such as precipitation, wind, temperature, landscape structure and vegetation; and on soil internal factors including soil type and structure, rooting depth and soil chemistry. Particularly wide, open fields are prone to wind, but also water erosion. After the harvest, the soil lays bare, without protection from vegetation, leaving crop fields especially prone to erosion (Bahrenberg et al., 1999). Wind increases evaporation from the bare soil and also increases transpiration by plants, because the surrounding air is continuously moved away. To prevent soil loss and limit evaporation, fields have been traditionally protected by wind breaks, such as hedgerows. Crop production is impacted by the state of erosion regulating ecosystem services.

Despite technical progress agriculture continues to depend on the ecosystem services provided by nature. The sector is threatened by the deterioration of such services, and moreover, climate change is expected to adversely impact agriculture. While farming techniques have greatly expanded the possibilities and crop breeding was able to increase heat and drought resistance of plants, climatic changes continue to pose limits to agricultural potential. Changes in mean temperature, shifts of precipitation patterns and new developments in magnitude and frequency of extreme events threaten the chance for a food secure world (Pielke et al., 2013).

2.2 Climate Change and Agriculture

"Climate change caused by human activities is having a massive impact on the Earth's ecosystem, influencing both physical and social activities. The negative environmental associated impacts are compromising the sustainable development of humans and therefore of human society. Climate change has been defined as the alteration of the state of the climate where changes in the mean and the variation of its properties can be easily identified." (Aleixandre-Benavent, 2017).

Temperature and precipitation are projected to be the most influential variables for crop production under changing climatic conditions on a global scale (Aleixandre-Benavent, 2017). Climate experts agree that climate change will come with rising average temperatures worldwide (IPCC, 2013). Global and regional land surface temperatures rose in the last century, with the latest decades displaying the most warming (Pielke et al., 2013; Aleixandre-Benavent, 2017). Furthermore, the IPCC projects a change in precipitation patterns, leading to water scarcity in some places and waterlogging in others (IPCC, 2013). An increase in hydrological extremes can already be observed (Pielke et al., 2013). Particularly when preceded by drought, extreme rain events increase the risk of water erosion. On the other hand, a lack of precipitation can have dramatic consequences: "Drought is the primary climate change threat to crops" (Pielke et al., 2013). Rain fed agriculture is particularly dependent on precipitation. However, if overall water availability decreases in an area, irrigation may not be an option either. Dry conditions and high temperatures often occur at the same time, increasing their destructive potential to agricultural production (Pielke et al., 2013).

Experts agree that climate change will come with rising average temperatures worldwide (IPCC, 2013). Global and regional land surface temperatures rose in the last century, with the latest decades displaying most warming (IPCC, 2013; Pielke et al., 2013). There is no doubt that this will have implications on agriculture particularly because temperature and precipitation are the main determinants of water availability. While different plants need different climatic conditions, the overall effect will likely be a decrease of agricultural productivity (Pielke et al., 2013). Some crop models foresee a reduction in grain yield of 2.5 – 16% for every increase of 1°C in the subtropics and tropics. Studies have also indicated a non-linear relationship between temperature and crop yields, pointing towards a threshold somewhere above 30°C in the United States (Pielke et al., 2013). Wheat as a highly temperature sensitive crop, has already suffered from climate change in Southern and Central Europe. Throughout Europe, generally warmer and drier conditions will likely pose a threat to agricultural production (IPCC, 2013). The extent of projected climate change and resulting crop failure varies between 10% and 50% for Europe according to the IPCC (2013).

Europe has experienced higher mean temperatures since the 1950s. There is high agreement among climate models for all emission scenarios that even if average global temperature increase was limited to 2°C compared to preindustrial times, European climate would change significantly from what we are used to today (IPCC, 2013). While projected precipitation changes vary spatially and seasonally, precipitation is projected to decrease during summer, reaching as far northwards as Sweden. In the second half of the 20th century, extremely hot temperature events have increased and low temperature extremes have decreased throughout Europe. An increase in extreme events, especially heavy precipitation events, droughts and heat waves are expected by climate experts. More numerous heat waves between May and September are projected with high confidence. Especially the combination of heatwaves and droughts poses a threat for Europe under climate change (Meehl & Tebaldi, 2004; Miralles, 2012; IPCC, 2013).

The climate report for Bavaria projects the area to be noticeably affected by climate change, in the next decades and beyond (LFU, 2012). While overall precipitation projections are not straightforward, model results for the hydrological summer period show a clear trend. Projections for rain reduction of up to -10% by the midcentury are evaluated as robust. The frequency of dry periods lasting more than seven days can threaten crop production, particularly during hot summer months (LFU, 2012).

Bavaria is one of the regions in Europe that have to expect significant warming. Ten climate projections for the timeframe 2021 to 2050 were evaluated for the climate report. The results showed a minimum warming of +0.8°C and maximum of +1.9°C. Half of the projections saw a rise of +1.2°C, compared to the timeframe 1971–2000. The rise in mean annual temperature was significant for all projections. This trend is expected to continue throughout the second half of the 21st century. Furthermore, extremely hot days with temperatures above 25°C to 30°C are projected to become more frequent throughout the whole of Bavaria (LFU, 2012).

However, "[c]limate effects are not new, neither is the farmer's ability to adapt" (Pielke et al., 2013). Throughout the world, scientists and practitioners are trying to find new ways of growing crops in a changing environment. More research is necessary to broaden our understanding of the interplay between climate and agriculture (Pielke et al., 2013.). Not only is agriculture affected by climatic conditions, but also the climate is influenced by the planet's surface. There is great effort within the scientific community to expand the knowledge base of the interactions between the land surface and the atmosphere.

Given the environmental challenges we will be facing, the aim of this study is to investigate, whether we can structure agricultural landscapes in a way that influences local and regional climate and makes the landscape more suitable for agricultural production in the face of climate change.

2.3 Land Surface Atmosphere Interactions

An essential contribution to regional climate is made by the interaction between the land surface and the atmosphere. The surface of the earth reacts to atmospheric alterations, and vice versa. Correspondingly, the boundary layer is directly influenced by properties of the ground. The two spheres are connected through the land energy balance, the land water balance and the carbon cycle. In the context of this study, the land surface is defined as the earth's surface, including soil, vegetation, human infrastructure, snow and other topographic features (Pitman, 2003).

The land energy balance gives information about the radiation and the energy budget of a region. The radiation budget comprises of the down-welling shortwave (solar) radiation (SWD), the reflected (upwelling) shortwave radiation, the down-welling

longwave radiation (LWD) (emitted by clouds and aerosols) and the upwelling longwave radiation, emitted by the land surface. The energy fluxes include the latent heat flux, the sensible heat flux and the ground heat flux, which leads to a change in the energy storage term of the surface layer. The ground surface plays a major role in the way the available energy is partitioned into the turbulent fluxes. In the land water balance, precipitation is divided into infiltration, causing a change in water content of the soil, evapotranspiration, surface run-off and subsurface run-off (Fig.1) (Arya, 1988; Pitman, 2003; Foken, 2008).

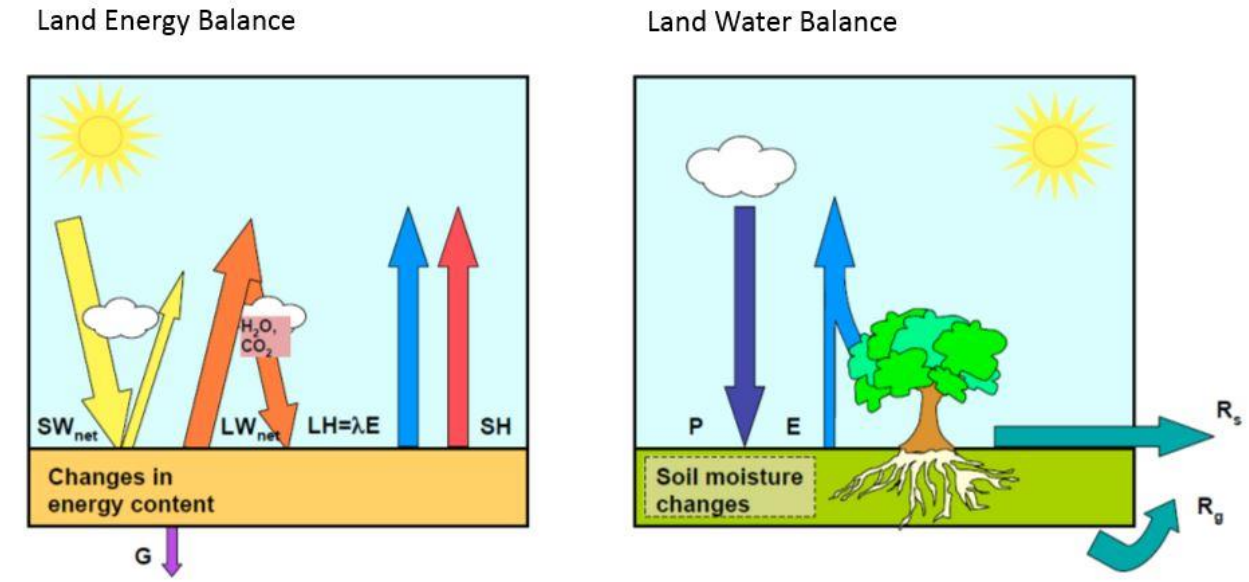

Figure 1: The land energy balance and the land water balance, modified from Seneviratne et al. (2010). SW_{net} refers to net short wave radiation, LW_{net} to net long wave radiation, LH/λE refers to the latent heat flux, SH to the sensible heat flux and G to the ground heat flux. In the water balance, P stands for precipitation, E for evapotranspiration (latent heat flux), R_S for surface runoff and R_g for subsurface runoff.

The sensible heat flux can be interpreted as the transport of warm air through dry air parcels. The latent heat flux connects the land energy balance and the land water balance. It refers to the molecular phase change of liquid water molecules to water vapor. Evapotranspiration comprises of evaporation from the ground and evapotranspiration from vegetated areas. The ratio between sensible heat flux and latent heat flux is called Bowen ratio (Equation 1). This is an important source of information on the division of energy. A high Bowen ratio refers to a high sensible heat flux in comparison to latent heat (Gerber & Decker, 1960; Arya, 1988; Foken, 2010; Seneviratne et al., 2010).

$$\text{Bowen Ratio} = SH / LH \quad (1)$$

The interaction of the components of the land energy and the land water balance plays a major role for droughts and heat waves. Positive feedback loops are responsible that heat waves are more likely to occur during droughts (Miralles et al., 2012). Droughts and heat waves in central Europe are largely driven by two components. Anticyclonic atmospheric circulation patterns lead to cloudless skies and excess radiation arriving at the Earth's surface, which results in the advection of warm air and high land surface temperatures. As a result, soil moisture levels drop below average, leading to a positive feedback on the regional climate system (Meehl & Tebaldi, 2004; Fischer & Serevinate, 2007; Miralles et al., 2012).

Sea surface temperatures affect precipitation patterns, and it is known that El Nino events create hotspots for resulting precipitation anomalies. However, the land surface also affects precipitation, through the amount of what vapor in the air, which is correlated to the amount of soil moisture (Koster et al., 2004). Research on the role of soil moisture and its feedbacks with the atmosphere has increased in the last decades. Not only is the latent heat flux affected by precipitation, rainfall and temperature themselves react to the availability of evapotranspiration. If hot and dry conditions prevail, the ground dries out, increasing the likeliness of prolonged droughts and heat waves (Koster et al., 2004; Miralles et al., 2012).

Teuling et al. (2010) identify a typical non-linear relationship between soil moisture and evapotranspiration. The authors point out that both variables go through three distinct stages during the process of surface drying. During stage (1) the latent heat flux is sustained independently of soil moisture levels, which are still high enough to allow for evapotranspiration. As the ground becomes drier, during stage (2) evapotranspiration is increasingly limited by the availability of soil moisture. Finally, in stage (3) the latent heat drops close to 0, as the ground has dried out and no more water is available in the ground. If hot and dry conditions prevail, the available energy is divided into excessive sensible heat flux and ground heat flux. The latter is very small compared to latent and sensible heat. However, surface temperatures rise as a result of a higher ground heat flux (Teuling et al., 2010; Arya, 1988).

This leads to anomalies in land surface temperature. Furthermore, it perpetuates dry and hot conditions in the boundary layer. Resulting high pressure decreases the likeliness of cloud formation, and therefore of precipitation. This positive feedback loop creates the risk that the severity of droughts and heat waves further increases. On the other hand, if

the latent heat flux is sustained, higher water content has a cooling effect on the lower atmosphere. Colder and moister conditions create low pressure, which increases the likeliness of cloud formation and thus, of precipitation. This would ultimately bring back water into the regional climate system (Fischer et al., 2007; Pitman, 2003).

According to Fisher et al. (2007), soil moisture temperature coupling is of greater importance than the effect of land surface on precipitation. However, both effects are found in the same regions, which are mainly transition zones between wet and dry climate regimes (Koster et al., 2004; Miralles, 2012). In the early 21st century, the Mediterranean region is where the coupling of land surface and atmosphere plays the greatest role for regional climate in Europe. Yet, a trend of increasing land surface temperatures has been observed throughout Europe (Fischer et al., 2007).

As a result of climate change, climatic regimes within Europe are expected to shift northwards. This means that central and eastern Europe will become new zones of transition between dry and wet climates. As a consequence, the coupling of the land surface and the atmosphere will become of increasing importance in countries like Germany. Several climate simulations come to the conclusion that increasing variability in summer temperatures in central Europe will largely be driven by land surface processes (Koster et al., 2004; Fischer et al., 2007; Miralles, 2012).

Agricultural landscapes are at risk of being negatively influenced by these climatic regime shifts. Droughts and heat waves, such as the European extreme event in 2003, can damage and destroy the harvest of a whole year. However, agricultural areas themselves can contribute in the perpetuation, if not creation, of extremely dry and hot summer periods, particularly when harvest occurs during hot and dry summer months. As the soil lays bare without protection from vegetation after the harvest, evaporation levels peak and diminish, leading to excessive sensible heat and increasing land surface temperatures (stage 2 and 3 according to Teuling et al., 2010).

While the effect of soil moisture on summer droughts and heat waves is comparatively well understood, the role of vegetation is less clear. One way the ground surface influences the land energy balance, is by its albedo. Dark surfaces, such as forests, have a low albedo compared to bare soil, agricultural lands or snow. A high albedo means that a larger fraction of the global radiation is reflected back into the sky. Therefore, less

radiation penetrates the ground, which means that the turbulent fluxes receive a smaller fraction of the overall energy budget (Pitman, 2003).

Furthermore, vegetation influences the division of energy and water by its capacity to uptake water by the roots and regulate the release of water molecules through stomata. Teuling et al (2010) found that there is a clear difference between European forest and grassland, in the way they respond under hot and dry conditions. At the beginning of such extreme events, forest displays higher levels of sensible heat flux than grassland. However, the above explained stage (2) and (3) in the process of surface drying are more severe in grasslands than in forest. Due to shallow roots and nearly no capacity to regulate stomata, grasslands have very little means to hold moisture in the ground. Therefore, they dry out quickly and as stage (3) is reached, the sensible heat flux above grasslands exceeds that over forest. Trees, with their deep root system and highly developed stomatal regulation, are able to sustain a latent heat flux and therefore also a stable Bowen ratio (Teuling et al., 2010).

In this study, homogenous and heterogeneous agricultural landscapes are distinguished by the presence of forest patches. Trees are expected to influence the interaction between the land surface and the atmosphere due to vegetation characteristics (see above). Furthermore, forest islands represent permanent vegetation, whereas crop fields repetitively pass through the cycle of sowing, growing and harvesting.

Based on the processes outlined above, the hypotheses of the study at hand are as follows:

1. A peak in sensible heat flux and surface temperature and a minimum in latent heat flux are delayed and diminished over heterogeneous agricultural landscapes during hot summer months.
2. The Bowen ratio remains more stable over heterogeneous agricultural landscapes.
3. The average land surface temperature is lower over heterogeneous than over homogeneous agricultural landscapes.
4. Heterogeneous agricultural landscapes are more resilient to heat waves.

3. Micrometeorological Modelling

3.1 Soil Vegetation Atmosphere Transfer (SVAT) Models

The Earth's surface has been altered by human intervention throughout human history, with a trend of growing intensity that is likely to continue or even increase. The resulting modifications of land surface atmosphere interactions play a crucial role in the process of climate change. Thus, the representation of the land surface is an integral ingredient in climate modelling today. Land surface models have been developed as early as the 1960s, and have considerably advanced in the last decades (Pitman, 2003; Sato et al., 2015).

Soil vegetation atmosphere transfer models are process based, bottom-up models, which simulate components of the land energy and water balance individually and combine the results (Babel, 2017). SVAT models can be part of climate models or hydrological models, however, the temporal and spatial operating scales usually differ substantially. Climate models deal with annual time steps as a minimum, usually considering decades to centuries. The relevant processes between the land surface and the atmosphere must be simulated on much smaller temporal scales of usually less than an hour (Pitman, 2003, Petropoulos et al., 2009). Spatially, climate models often generalize over hundreds of square kilometers, whereas most SVAT models are vertical representations of land atmosphere interactions (Petropoulos et al., 2009). Therefore, land surface models must carefully be nested into coarser models if both are to be combined.

Pitman (2003) defines three generations of land surface models, starting in the 1960s with the use of a simple energy balance equation (Manabe, 1969), ignoring the ground heat flux and without representation of diurnal and seasonal cycles. Based on Sellers et al. (1997), Pitman defines first generation models mainly by the level of sophistication in the simulation of evapotranspiration (Pitman, 2003). Evaporation was often limited by the soil water content below a certain threshold. Soil moisture availability was generally determined by a parameter ranging from zero (dry) to 1 (saturated). While such simplified equations may deliver acceptable results when temporally aggregated, the number of soil layers (usually one or two) was not able to represent the distribution of soil temperature and moisture over annual or multiannual timescales. Vegetation was treated implicitly and remained constant over time, with no separate vegetation layer in the model set up (Pitman, 2003).

A major advancement of what Pitman (2003) defines as second generation models, was the inclusion of a separate vegetation layer. While the range of second generation models is large, a common characteristic is that they consider soil and vegetation as separate actors in the energy and water balance. The representation of evapotranspiration advanced considerably, based largely on insights from Monteith and Szeicz (Monteith & Szeicz, 1962; Pitman, 2003). Further improvement comes from the inclusion of stomata response to photosynthetically active radiation, humidity and temperature, drawing from scientific developments of Jarvis, among others (Jarvis 1976). Other vegetation characteristics, such as surface roughness and Leaf Area Index (LAI) also increased model sophistication. Aerodynamic resistance and canopy resistance are both included in second generation models. Water distribution is handled in a more complex way, largely governed by the Richard's equation (Richards, 1931; Pitman, 2003). The improved simulation of evapotranspiration is of great importance, considering that globally, transpiration is responsible for the largest part of the evapotranspiration process. Furthermore, the latent heat flux plays a major role in the partitioning, and consumes a great fraction of solar energy (Sato et al., 2015; Petropoulos et al., 2009).

Further development of land surface models was achieved by the inclusion of the carbon cycle, involving a greater level of expertise from biology and biochemistry. The coupling of transpiration and photosynthesis allows for the simulation of carbon assimilation and net primary productivity (third-generation models according to Pitman, 2003). Another area of development within the land surface modelling community was to develop spatially explicit models. This involves cooperation of scientists from different disciplines, including climatologists, micrometeorologists, ecologists, soil scientists, hydrologists and the remote sensing community (Pitman, 2003; Petropoulos et al., 2009).

3.2 Soil Energy Water Atmosphere Balance (SEWAB) Model

3.2.1 General Model Structure

In the following section, the one-dimensional Soil Energy and Water Balance (SEWAB) Model, utilized in the study at hand, will be explained. The model was developed to be incorporated into climatic circulation models, representing the land surface (Mengelkamp et al., 1997). The SVAT model has been applied to a range of ecosystems, including the Tibetan Plateau (Babel et al., 2014; Biermann et al., 2014; Biermann, 2014),

and has been found to model turbulent fluxes well in a model evaluation initiative by the World Climate Research Program, namely the Project for the Inter-Comparison of Land-Surface Parameterization Schemes (PILPS) (Henderson-Sellers et al., 1996; Mengelkamp et al., 1997).

SEWAB comprises of one vegetation layer and seven soil layers, representing the one-layer concept for vegetation (Mengelkamp et al., 1997). Even though the model has no horizontal resolution, the vegetation fraction can be determined, allowing for distinction between vegetated areas and bare soil at the earth's surface. The vegetation fraction can be set to change dynamically, based on assigned monthly values. However, only one vegetation type can be determined per model run. An extension for modelling snow can be activated, which will determine the occurrence of snow based on precipitation and air temperature (Mengelkamp et al., 1997; Mengelkamp et al., 1999; Mengelkamp et al., 2001).

Input variables include general information, such as location and elevation of the study site. Soil type and vegetation type have to be chosen from a range of available options. Based on this decision, vegetation and soil parameters are determined and can be modified if necessary (Table 3, 4 and 5). Another input requirement is standard meteorological forcing data (Table 2). SEWAB computes on 10-minute time steps, input data can be supplied at coarser temporal resolution. The time-steps of the output data can be determined. Model output includes the surface fluxes, air, surface and soil temperatures and water distribution, including soil moisture and run-off (Mengelkamp et al., 1997; Mengelkamp et al., 1999; Mengelkamp et al., 2001). Figure 2 provides a schematic overview of the model structure.

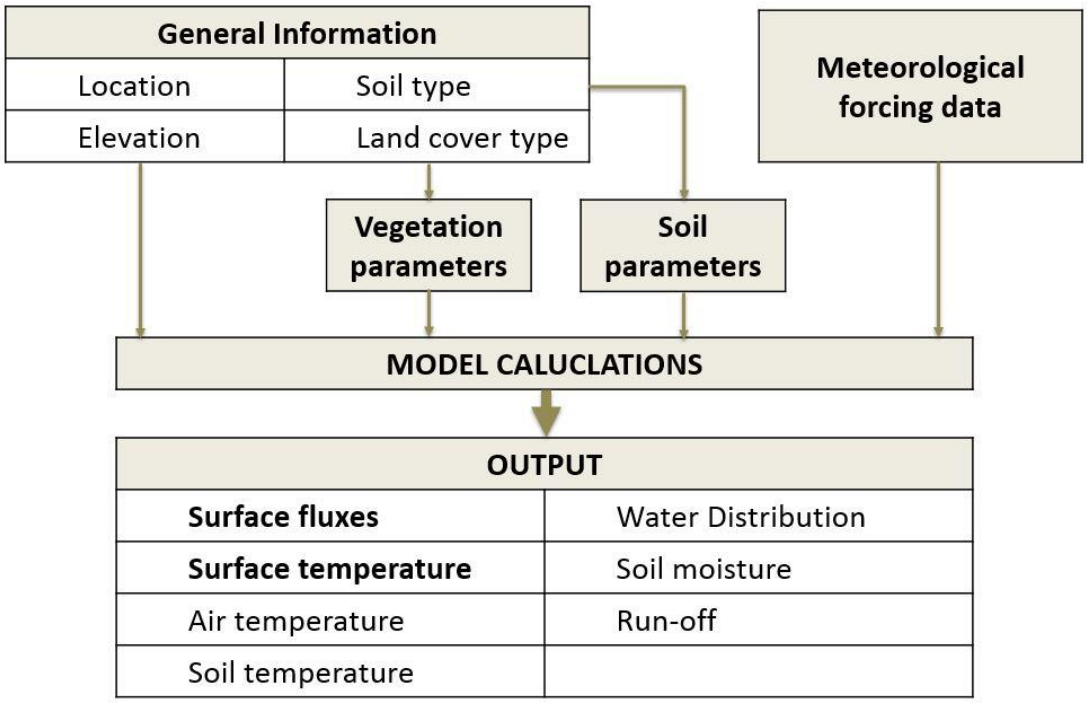

Figure 2: General model structure of SEWAB

3.2.2 Governing Equations

Like all SVAT models, SEWAB is governed by the coupled land energy and land water balance (Mengelkamp et al., 1997; Mengelkamp et al., 2001). No ponding is assumed; therefore, in this model excess water beyond soil saturation becomes runoff (Mengelkamp et al., 1997). The dispersion of temperature through the soil column is calculated with the diffusion equation; the migration of water through unsaturated soil is governed by the Richards equation (Babel et al., 2014; Richards, 1931)

The radiation flux density is calculated from down-welling shortwave and down-welling longwave radiation, under consideration of surface reflectance and emissivity (Table 1). SWD and LWD must either be given in the forcing data, or alternatively they can be parameterised from cloud cover. Albedo and surface emissivity are provided as part of the vegetation and soil parameters and can be adjusted (Mengelkamp et al., 1997; Mengelkamp et al., 1999; Mengelkamp et al., 2001). All components of the energy balance are modelled separately, the land surface temperature is iterated until energy balance is achieved (Mengelkamp et al., 1997; Babel, 2017). Surface temperature is a driving variable for the calculation of sensible and latent heat fluxes, which is done using bulk approaches (Mengelkamp et al., 2001; Babel et al., 2014).

The equation for the ground heat flux is shown in Table 1. It involves the thermal conductivity λ, the temperature of the first soil layer T_1, the surface temperature T_{surf} and the thickness of the first soil layer Δz_1, which is set to 4 cm in the study at hand (Mengelkamp et al., 1997; Mengelkamp et al., 1999; Biermann et al., 2014).

The sensible heat flux is calculated with a bulk-aerodynamic formula (Table 1). The equation involves the air density ρ, the specific heat of air c_p, the C_H Stanton number, the wind speed u_a, the air potential temperature θ_a and the surface potential temperature θ_{surf}. Air density is calculated from the specific gas constant of dry air (287.05 J/kgK) and from air pressure and air temperature, which are both provided in the forcing data. The Stanton number is calculated after Louis (1979) and corresponds to the drag coefficient in the context of momentum. Wind speed is supplied in the standard meteorological data. The consideration of air potential and surface potential temperature accounts for possible temperature gradients between the measurement height and the surface (Louis, 1979; Mengelkamp et al., 1997; Mengelkamp et al., 1999; Mengelkamp et al., 2001). This is particularly important if the canopy is comparatively high, for instance if the vegetation type is forest.

The latent heat flux is comprised of evaporation from the bare soil E_{surf} and evapotranspiration from vegetation E_f (vegetation fraction veg.) The latter is the sum of evaporation from the wet part of the foliage E_r and transpiration from the dry part of vegetation E_{tr} (Table 1) (Mengelkamp et al., 1997; Mengelkamp et al., 2001).

Evaporation from bare soil is calculated from the Schmidt number C_Q, the density of moist air, wind speed, relative humidity at the ground surface α_f, saturation specific humidity at surface temperature $q_s(T_{surf})$, and air specific humidity q_a. The Schmidt number is calculated after Louis 1979, equal to C_H. Relative humidity at the ground surface is calculated after Noilhan and Planton (1989). Specific humidity calculation demands information on air temperature and atmospheric pressure, which are both provided in the forcing data (Louis, 1979; Noilhan & Planton, 1989; Mengelkamp et al., 1997; Mengelkamp et al., 2001).

Evaporation from the wet foliage is calculated with the same equation as evaporation from bare soil, with the exception that relative humidity at the ground surface is not considered (Table 1).

For the calculation of evapotranspiration from the dry part of the foliage, aerodynamic resistance and stomata resistance are considered. Stomata resistance is calculated after Noilhan and Planton (1989).

Table 1: Governing equations for SEWAB (Mengelkamp et al., 1997; Mengelkamp et al., 1999; Mengelkamp et al., 2001; Biermann et al., 2014; Babel et al., 2014)

Variable/component	Equation
Net Radiation	$R_{net} = -R_{swd}(1-a) - R_{lwd} + \varepsilon\sigma T_{surf}^4$
Ground heat flux	$GH = -\lambda \frac{T_{surf} - T_1}{\Delta z_1}$
Sensible heat flux	$SH = -\rho c_p C_H u_a(\theta_a - \theta_{surf})$
Latent heat flux	$E = (1-veg) * E_{surf} + veg * E_f$
Evaporation from bare soil	$E_{surf} = C_Q \rho_w u_a [\alpha_f q_s(T_{surf}) - q_a]$
Evaporation from wet foliage	$E_r = C_Q \rho_w u_a [q_s(T_{surf}) - q_a]$
Transpiration from dry part of vegetation	$E_{tr} = \frac{1}{R_a + R_S} \rho_w [q_s(T_{surf}) - q_a]$

Symbols

a	albedo (–)
C_H	Stanton number (–) (calculated after Louis, 1979)
C_Q	Schmidt number (–) ($C_Q = C_H$) (calculated after Louis, 1997)
c_p	specific heat of air [J kg^{-1}K^{-1}]
q_a	air specific humidity (–)
$q_s(T_{surf})$	saturation specific humidity at surface temperature T_{surf} (–)
R_a	aerodynamic resistance [s m^{-1}]
R_{net}	radiation flux density [W m^{-2}]
R_{lwd}	down-welling longwave radiation [W m^{-2}]

R_S	stomata resistance [s m^{-1}] (after Noilhan & Planton, 1989)
R_{swd}	down-welling shortwave radiation [W m^{-2}]
T_{surf}	surface temperature [K]
u_a	wind speed [m s^{-1}]
Δz_1	thickness of first soil layer [m]
α_f	relative humidity at the ground (–) (after Noilhan & Planton 1989)
ε	emissivity (–)
θ_a	air potential temperature [K]
θ_{surf}	surface potential temperature [K]
λ	soil thermal conductivity [W $m^{-1}K^{-1}$]
ρ	air density [kg m^{-3}]
ρ_w	density of moist air [kg m^{-3}]
σ	Stefan Bolzmann constant (5.67×10^{-8} W m^{-2} K^{-2})

3.2.3 Input Variables and Model Parameters

Meteorological Forcing Data

Standard meteorological data, necessary to operate the SVAT model, includes down-welling shortwave and longwave radiation. If these variables are not available, cloud cover has to be supplied instead, as fractional data (deciles of the visible sky). Further forcing variables are: precipitation, relative humidity, air temperature, wind velocity and air pressure (Mengelkamp et al., 1999). It is noteworthy that SEWAB cannot deal with missing values (NAs) in the forcing data, all data gaps have to be filled. Consistent time steps are a prerequisite for the meteorological data to be accepted by SEWAB. The forcing data has to be delivered together with information about time and date. A detailed list of relevant forcing data is given in Table 2.

Table 2: Forcing data for SEWAB

Cloud cover fraction (range 0–1)	Relative humidity [%]
(Liquid) precipitation [mm]	Down-welling shortwave radiation [W m^{-2}]
Air temperature [°C]	Down-welling longwave radiation [W m^{-2}]
Wind speed [m s^{-1}]	Solid precipitation (optional)
Air pressure [hPa]	

General Input Variables

The mean temperature for the total time period the model is applied to, has to be calculated from the forcing data and included in the section for basic model settings. Further information that has to be inserted into this file includes the measurement heights for air pressure, air temperature and wind speed, as well as latitude, longitude and elevation of the research site (Table 3). Some parameters related to the soil column have to be set: the initial groundwater level, the delay for the penetration of temperature into deeper soil layers and the magnitude of temperature difference between soil layers. The number of soil layers and the depth per soil layer can be adjusted.

Vegetation class and soil class have to be chosen from the available options. This will call on the specified vegetation and soil parameters for the determined class. Vegetation fraction has to be set. It is possible to activate dynamic monthly vegetation fraction. It is further possible to include a dynamically changing Leaf Area Index, which is otherwise provided as a vegetation parameter. A detailed list of general input variables is provided in Table 3. Please note that Table 3 also contains information on modifications for model parameterization and application.

Soil Parameters

The following attributes are specified depending on the chosen soil type: volumetric water content at the point of soil saturation, the moisture potential at saturation, the

saturated hydraulic conductivity, the water content at the wilting point, and the field capacity (Table 4).

Vegetation Parameters

Based on the vegetation type, the following parameters are assigned and can be changed individually if necessary: emissivity, albedo, leaf area index, canopy height, root depth, the roughness length of momentum, the minimum stomata resistance, the influence of photosynthetically active radiation on stomata resistance (RGL), the water storage per leaf area index and the shadow effect for the snow model. Please see Table 5 for a detailed list on vegetation parameters. Table 5 includes information on modifications for model parameterization and application.

4. Study Area and Time

The study area is located between Regensburg and Straubing, two cities in Bavaria. The area has a size of approximately 300 km². One of the main requirements for the area to be suitable was that the average slope remains below 4° to 5°. This is necessary, because the effect of slope and exposure is not included in the code of the SVAT model. Moreover, regional effects due to complex topography cannot be resolved in a 1D model approach.

The study area was requested to show homogenous and heterogeneous agricultural land cover (LC) structure. Additionally, the amount of land cover shared by urban structures and water needs to be kept to a minimum, to avoid distortion of the results of the spatial analysis. Fig.3 shows the location of the study area in Bavaria, as well as the study area and the land cover.

In western Europe, an increase in summer droughts and heat waves is projected (Fischer, 2007). In 2003, one of the worst summer heat waves struck Europe (Miralles, et al. 1012). It caused financial damage throughout the continent, temperature-related deaths and widespread crop failure (Fischer et al., 2007). The heat wave was increased by a pronounced precipitation deficit, starting as early as February and lasting until the end of summer 2003 (Fink 2004). Some authors suggest, that high temperatures early in the year caused vegetation to green sooner than usually, which lead to a soil moisture deficit early in the season. As a result, the latent heat flux was reduced and the sensible heat flux

was increased above normal values, according to Black et al. (2004) and Zaitschik et al. (2006).

To investigate the effect of the summer drought and heat wave 2003 on the turbulent fluxes and land surface temperature, the timeframe between April, until the beginning of November 2003, was investigated. In that timeframe, eight-day aggregations were analyzed, based on the availability of remote sensing data. Only daytime values were considered.

As a reference year, which was not struck by a summer heat wave, the year 2004 was chosen. The climate signal over the snow-free period of the reference year was not extreme and can be considered within a normal range (Wetter online n.d.).

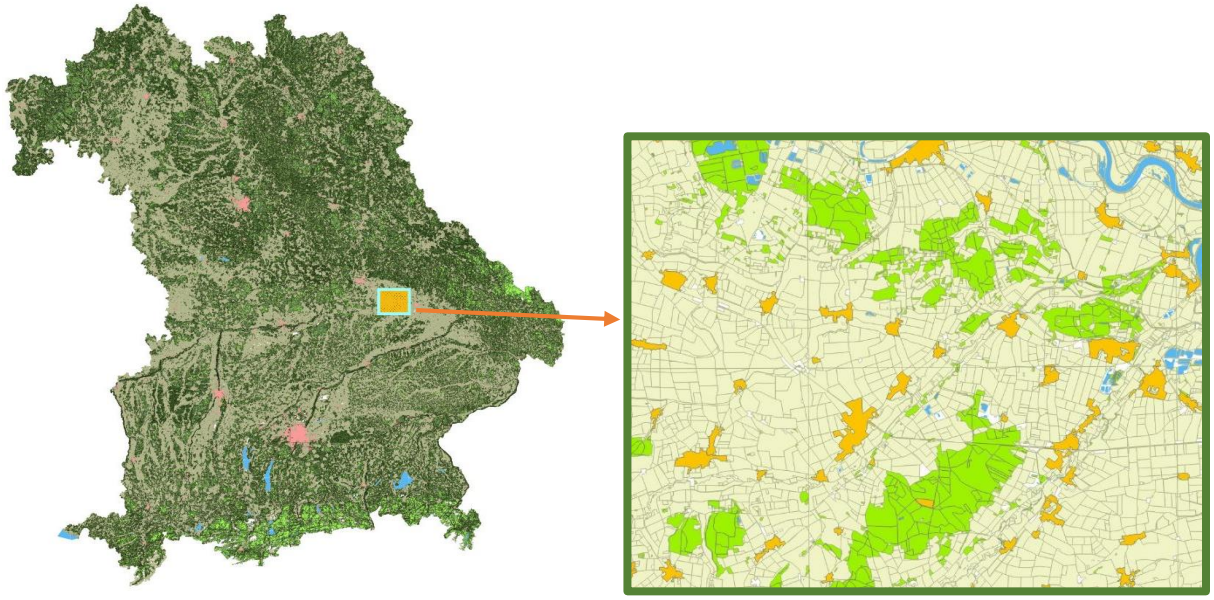

Figure 3: Location of the study area in Bavaria, study area and land cover

5. Methods

5.1 SVAT Model Calibration

SEWAB was calibrated for the land cover types agriculture and forest, at two different research sites, before the model was applied to the actual research area. Model parameterization for land cover type agriculture was undertaken at the research site

Scheyern, and involves settings for winter wheat and for potato/sugar beet. The model was further parameterized for forest at the research site Waldstein. At the research area (see above), SEWAB was applied to agriculture and forest. A detailed list of parameters for model calibration and application is provided in Tables 3–6.

5.1.1 Model Calibration for Land Cover Type: Agriculture

For the calibration of SEWAB to the land cover type agriculture, data was used from a research site called Scheyern, in Bavaria. The estate of the Scheyern Monastery has been a research area for nearly 3 decades. Since 2005, the German Research Foundation for Health and the Environment leases the site and collaborates with the Technical University of Munich and the Helmholtz Centre to conduct sustainability research. The 150 ha large site is one of the best explored agricultural areas, contributing to the development of strategies for environmentally sustainable crop (Helmholtz Zentrum München, 2005). Scheyern is also a Terreno research site and part of the Alpine Observatory of the Helmholtz Institute and the Institute for Technology of Karlsruhe. The site is located about 60 km north of Munich (Helmholtz Gemeinschaft, 2011).

Data from two agricultural fields with different crop rotations was utilized from the site. The fields are located next to each other, with some devices being set up in between them. On the field on the eastern side (in the following referred to as field 17) potato was planted. On field 18 (the field on the western side) winter wheat was grown. Two model runs were conducted, one for land cover type winter wheat and one for potato, the results were combined (see below).

In the process of calibration, meteorological forcing data, site-specific information, and data to evaluate model performance was put to use. All data was made available to the Micrometeorological Department of the University of Bayreuth by the Helmholtz Centre Munich (Helmholtz Zentrum München, 2005).

5.1.1.1 Meteorological Forcing Data

Measurements for the creation of forcing data include values for radiation, precipitation, relative humidity, air temperature, wind velocity and air pressure. However, some measurements did not work or contained errors. A short outline of the measurement

devices is given, as a background for detailed explanation of insufficient data and applied methods to generate missing data.

Short- and longwave radiation fluxes are measured with a CNR1 Net Radiometer, manufactured by Campbell Scientific (Campbell Scientific Inc. 2011). Four devices with 180° viewing angles measure upward and downward welling fluxes. Short wave solar radiation (between 0.3 and 3 micrometers) is measured by two CM3 Pyranometers, capturing down-welling and reflected solar radiation. The far infrared spectrum (5 to 50 micrometers) is measured by two CG3 Pyrgeometers, one facing the sky, the other facing the ground. An integrated heater prevents dew and frost development at the sensor and a PT-100 sensor is installed to measure the temperature of the device itself (Campbell Scientific Inc. 2011).

In the following section, the main data transformation procedures and arising potential error sources are outlined. Variables, which are not mentioned here did not have to be manipulated beyond minor corrections.

Down-welling longwave radiation

The transformation of CG3 measurements to down-welling longwave radiation by the data logger did not work, neither did the Pt-100 measurements. CG3 measurements over both crop fields contain missing values and obvious errors, which were identified by their range. Data for the field, on which winter wheat was grown (field 18) was provided in mV, information on the calibration constant (108.342 Wm^{-2}/mV) was provided by the Helmholtz institute (Helmholtz Zentrum München, 2005). CG3 measurements of both fields were merged, filling gaps in the data of field 18 with data from field 17.

Down-welling longwave radiation was then calculated, utilizing the merged time series of CG3 measurements and air temperature as a replacement for device temperature. The following, adjusted Stefan-Boltzmann equation was applied (Campbell Scientific Inc., 2011; Helmholtz Zentrum München, 2005)**:**

$$E = \frac{V}{C} + 5.67 * 10^{-8} * T^4 \quad (2)$$

Symbols

E Down-welling longwave Radiation

C sensitivity of CG3

V/C CG3 measurements (uncorrected) (difference between LWD and LW emitted by sensor)

T temperature of CG3 measurement device (in Kelvin) (replaced by air temperature)

Stefan Boltzmann Constant 5.67*10-8

Four data gaps remained, one was negligible (2 missing values in February), the second was small in relation to a one-year time series (41 missing values in December). One large data gap of 620 entries occurred in March, another one in August (663 entries). These data gaps were closed using linear interpolation. Therefore, March and August must be inspected with caution during model evaluation.

Relative humidity

Gaps in the data representing relative humidity were closed using linear interpolation. The NA values were spread throughout the year, no large data gaps occurred, which produced a smooth time series subsequent to interpolation.

Air pressure

Air pressure was provided in five-minute steps, which were aggregated to ten-minute steps, creating the mean of two neighboring entries.

5.1.1.2 Model Settings

Geographical Information

General model settings were adjusted to the research site, including latitudinal and longitudinal information and elevation. Scheyern and is located at 44.58695 latitude, 53.73542 longitude and 475.0 m above sea level. A detailed list of model settings is displayed in Table 3.

Measurement Height

Although no information was provided on measurement height, the CNR1 manual states that the device ought to be placed at a minimum height of 1.5 m above the surface "to avoid shading effects of the instruments on the soil and to promote spatial averaging of

the measurement" (Campbell Scientific Inc., 2011). Measurement heights for air pressure, air temperature and wind speed were set to 2 m.

Mean Air Temperature

Mean air temperature for the year 2014 was calculated from the air temperature provided in the forcing data and amounts to 283.25 Kelvin.

Land Cover Class

Vegetation class and relevant parameters were manipulated to improve model performance. Simulations for land cover classes cereal and potato were run individually. However, potato is not an option in the list of vegetation types, therefore sugar beet was chosen as a replacement (see section below for details).

Fractional Vegetation Cover

During an initial model run, the default setting for fractional vegetation cover (0.9) remained unchanged. This was considered a reasonable value, because the timeframe of interest is the main growing season of the crops. In the process of parameterization, monthly values for vegetation fraction were inserted (see below).

Soil class

The dominant soil type at the site is silt loam, with minor parts of Kolluvium and podsol (Helmholtz Zentrum München, 2005; Helmholtz Gemeinschaft, 2011). All Default settings for this soil type were adopted.

Fractional water cover

Since no water is considered in the study at hand, fractional water cover was set to 0.

Initial groundwater level

The default settings for initial groundwater level were incurred, because this setting has proven reasonable when a spin up is run over one year in a study at the Tibetan plateau (Babel, 2014).

Soil specific settings

Furthermore, default settings for the depths of the seven soil layers, the delay and the amplitude of temperature transport through the soil layers were adopted, because these settings have proven reasonable previously (Babel, 2014) (Table 3).

Please see Table 3 for a listing of general model parameter settings for simulations at Scheyern.

5.1.1.3 Model Parameterization

An initial model run was conducted with all default settings for land cover class cereal. This trial run produced strong overestimation of the sensible heat flux in the second half of June and underestimation of the same in the second half of July. Latent heat was underestimated in the second half of June and overestimated in the second half of July. Further model runs were conducted, gradually adding modifications to model settings. The final parameterization settings are presented here.

Consideration of Wind Direction

The measurements, against which the model results are evaluated, were taken by a device installed in between the two agricultural fields. To optimize model results, it was taken into account that either of the two fields influence the device, depending on the wind direction. Accounting for the different crops on field 17 and field 18, the SVAT model was run twice, with adjusted settings simulating winter wheat or potato, respectively. For model evaluation, results from both runs were combined, based on the wind direction.

Land Cover Class

The model contains no specific land cover class for potato, the most similar vegetation types are cereal and sugar beet. Land cover class sugar beet was chosen as a replacement for potato, because canopy height and roughness length in the vegetation settings are closer to potato than to cereal. Further adjustments include the calculation of the albedo for both fields and monthly values for vegetation fraction and leaf area index (see below).

Albedo

The albedo was calculated for field 17 and for field 18. Down-welling shortwave radiation and radiation reflected by the ground surface were measured by the CNR1 device separately for each field. The mean albedo was calculated for the snow free period, because winter is not considered in the study. The calculated average albedo value was implemented as albedo value for both, vegetation and bare soil, since it comprises of both. The calculated mean albedo for field 17 is 0.19, the standard deviation is 0.08. The albedo for field 18 amounts to 0.2 with a standard deviation of 0.09.

Monthly Vegetation Fraction and Leaf Area Index

Continuing over- and underestimation of sensible and latent heat in June and July gave reason to activate the model function allowing to adjust monthly vegetation fraction and Leaf Area Index values. On the field located on the eastern side (field 17), potato was planted on the 22nd of October 2013, and harvested on the 6th of August 2014. On field 18, winter wheat was sowed on April the 17th, 2014 and harvested on the 16th of September the same year.

For the estimation of monthly LAI values, sowing and harvesting dates were taken into consideration. According to Moeller et al. the average LAI for potato ranges between 2.5 and 3 (Moeller et al., 2002). Hermann et.al agree with an average of 2.55, however, within a range of 4.95. Gordon et al. (1997) report similar LAI measurements, with maxima of 3.5. Some studies find higher LAI mean and max values, however, these don't usually apply for rain fed agriculture (Deshi et al., 2015).

Considering wheat, some authors state an average LAI of 2.92, with a range of 6.99 (Hermann et al., 2011). Xiaoyu et al. (2014) conducted a seasonal experiment, measuring an LAI value of 1.63 in the middle of April, an LAI of 3.0 in the middle of May and a decrease to 2.14 at the beginning of June (Xiaoyu et.al., 2014). Based on these findings and in consideration of the plants' growing cycles, monthly LAI and fractional Vegetation settings were installed in the model code. Please see Table 6 for detailed information on monthly values.

*Table 3: SEWAB Input Parameters, including modifications for model parameterization at research sites Scheyern (LC agriculture) and Waldstein (LC forest). Modifications for model application at research area (Straubing) for LC agriculture and LC forest. *Default settings*

Variable/component	**Scheyern**	**Waldstein**	**Straubing Agri.**	**Straubing Forest**
Latitude	44.58695	50.142	48.83	48.83
Longitude	53.74	11.866889	12.56	12.56
Elevation [m above sea level]	475.0	775.0	350.0	350.0
Measurement height for air pressure [m]	2.0	2.0	2.0	2.0
Measurement height for air temperature [m]	2.0	13.0	2.0	2.0
Measurement height for wind speed [m]	2.0	13.0	10.0	10.0
Fractional vegetation cover	monthly	0.9*	monthly	0.9*
Mean air temperature [K]	283.25	280.81	282.03	282.03
Land cover class	Cereal/ sugar beet	Coniferous forest	Sugar beet	Coniferous forest
Soil class	Silt loam	Sandy loam	Silt loam	Silt loam
Soil temperature delay [days]	92.0*	92.0*	92.0*	92.0*
Fractional water cover	0.0*	0.0*	0.0*	0.0*
Initial groundwater level	2.0*	2.0*	2.0*	2.0*
Soil temperature amplitude	8.0*	8.0*	8.0*	8.0*
Number of soil layers	7.0*	7.0*	7.0*	7.0*
Soil layer depths [m]	-0.04 -0.06 -0.2 -0.2 -0.2 -0.3 -1.*			

*Table 4: Soil parameters. *Default settings were used for model calibration in Scheyern (silt loam) and Waldstein (sandy loam), and for model application at Straubing (silt loam).*

Soil parameters	**Sandy Loam (Waldstein)**	**Silt Loam (Scheyern & Straubing)**
Volumetric water content saturation [m^3/m^3]	0.435*	0.485*
Moisture potential at saturation [m]	-0.218*	-0.786 *
Saturated hydraulic conductivity [m/s]	3.41E-005*	7.20E-006*
Wilting point water content [m^3/m^3]	0.114*	0.179*
Field capacity [m^3/m^3]	0.195*	0.255*

*Table 5: Vegetation parameters and modifications for model calibration and application. Calibration for LC type agriculture: cereal and sugar beet in Scheyern. Calibration for LC type forest: coniferous forest in Waldstein. Application at research area: Sugar beet and coniferous forest in Straubing. *Default settings*

Vegetation parameters

	Scheyern cereal	**Scheyern sugar beet**	**Waldstein coniferous forest**	**Straubing sugar beet**	**Straubing coniferous forest**
Emissivity	0.95*	0.96*	0.97*	0.96*	0.97*
Albedo	0.2	0.19	0.07	0.19	0.15*
Leaf Area Index	monthly	monthly	6.0*	monthly	6.0*
Canopy height [m]	1.0*	0.5*	27.0	0.5*	27.0
Root depth	4.0*	4.0*	5.0*	4.0*	5.0*
Roughness length [m]	0.1*	0.03*	2.0*	0.03*	2.0*

Minimum stomata resistance	52.9267*	100*	158.78*	100*	158.78*
RGL for stomata resistance	100*	100*	30.0*	100*	30.0*
Water storage per LAI	0.2*	0.2*	0.2*	0.2*	0.2*
Shadow effect for snow model	0.5*	0.5*	0.95*	0.5*	0.95*

Table 6: Adjusted monthly LAI and fractional vegetation cover values for vegetation type winter wheat and potato at Scheyern.

**sowing or harvest took place in this month and in the year 2013 or 2014 (s.o.)*

Jan	**Feb**	**Mar**	**Apr**	**May**	**Jun**	**Jul**	**Aug**	**Sept**	**Oct**	**Nov**	**Dec**
Winter wheat/ cereal (Field1 8)											
Leaf area index											
0.5	0.5	1.0	2.5	3.0	3.5	3.0	0.9*	0.5	0.5*	0.5	0.5
Fractional vegetation cover											
0.2	0.3	0.5	0.6	0.7	0.8	0.9	0.4*	0.4	0.3*	0.2	0.1
Potato/ sugar beet (Field 17)											
Leaf area index											
0.5	0.5	0.5	0.6*	2.0	3.5	3.0	2.7	0.9*	0.5	0.5	0.5
Fractional vegetation cover											
0.1	0.1	0.2	0.4*	0.5	0.7	0.8	0.9	0.4*	0.3	0.2	0.2

5.1.2 Model Calibration for Land Cover Type: Forest

The SVAT model calibration for the land cover type forest was done with data from the study site Waldstein, which is located in the Lehstenbach catchment area, north of the upper EGER river valley, in the Fichtelgebirge Mountains (Germany, Bavaria) (Serafimovich et al., 2011). The site is one of the main research areas of the Institute of ecology and ecosystems research from the University of Bayreuth (BayCEER) and has been used for intensive ecological and meteorological studies (Matzner 2004; Serafimovich et al 2011). Waldstein-Wiedenbrunnen is also a FLUXNET site (Baldocchi et al. 2001) and has been providing data series on carbon dioxide flux measurements since 1996. At 50° N and 11° E and an elevation of 775 m, the dominant land cover type is deciduous forest, mainly composed of Norway spruce (Picea abies). The canopy height of 27 m remained stable since 2011, according to the micrometeorological department at the University of Bayreuth. Three research sites are located within the Waldstein area: Weidenbrunnen (main tower), Pflanzgarten and Köhlerloh clear cut. The forcing data for SEWAB was taken from the main tower at the Weidenbrunen site and from the Pflanzgarten site, a clear-cut area about 200 m west of Weidenbrunnen and a monitoring site for meteorological parameters since 1994 (Serafimovich et al 2011). Data for the evaluation of model performance was taken from the turbulence tower located at the site.

Data for model calibration at the research site Waldstein was made available by the Micrometeorology Department of the University of Bayreuth.

5.1.2.1 Meteorological Forcing Data

Most meteorological model input data was taken from the Weidenbrunnen site. Where necessary, this data was fused with data from the Pflanzgarten site and with data from the weather station Fichtelberg-Hüttstadl from the German Weather Service (CDC, 2017a).

The variables of interest from The Weidenbrunnen site contain data gaps in the same entry place, which amount to a number of 1,202 NA values per variable at this site. The variables of interest from Pflanzgarten also contain data gaps in the same places as each other, which amount to 140. The gaps in the Weidenbrunnen data and in Pflanzgarten data do not overlap. This allowed for smooth time series being produced for all variables,

except where data gaps had to be closed by linear interpolation. However, no drag on effects are expected to arise from any of the manipulated data gaps.

Precipitation measurements were taken from Pflanzgarten, NAs were filled with data from the German weather service (CDC, 2017a), which are provided as hourly values. These were stretched to 10 minute entries to be usable as SEWAB forcing data.

Measurements for wind velocity were taken from the Weidenbrunnen site. Data gaps were filled with measurements from Pflanzgarten, after linear regression was performed between both data entry series. The model shows an adjusted R-squared value of 0.44. However, only NA values in the data measured at the main tower is replaced by modelled values.

Data gaps in air temperature measurements from the Weidenbrunnen site were filled with data from the Pflanzgarten site, after linear regression was conducted between the two variables. With an R squared value of 0.96, the linear model performs very well.

Relative humidity was measured at the Weidenbrunnen site; gaps were filled with measurements from Pflanzgarten. The linear regression between the two variables performs well with an R squared value of 0.84.

Data gaps in down-welling short wave radiation measured at the main tower were filled with data from Pflanzgarten. Values were modelled with linear regression between the two variables, the intercept was set to 0, to avoid overestimation of night-time values (at night SWD = 0). The R squared value for the model is 0.94.

Down-welling longwave radiation was measured at the main tower. Since no alternative measurements are available from Pflanzgarten, the data gaps were closed by linear interpolation. The location of the two main data gaps was inspected, they are such, that no drag on error is expected. Measurements for air pressure were taken from Pflanzgarten. The 140 data gaps were closed, using linear interpolation.

5.1.2.2 Model Settings

Geographical Information

Geographical information was included in the section for general model settings. Waldstein is located at 50.142 latitude, 11.866889 longitude and at an elevation of 775.0 m

above sea level. Please see Table 3 - 5 for a detailed list of model settings for the research site Waldstein.

Measurement Height

Measurements for air pressure were taken from the Pflanzgarten site. Measurement height for air pressure was set to 2 m, which corresponds to the actual height at the site, not to canopy height at the Weidenbrunnen site. Measurement height for air temperature and wind speed was taken from the Weidenbrunnen site, with a canopy height of 27 m. However, the latter two variables need to be adjusted for high vegetation, because the displacement height does not enter SEWAB model equations. For high vegetation the displacement height reaches up to 3 times the canopy height and influences parameters such as wind speed and friction velocity. SEWAB was designed for low vegetation, such as grassland, where the displacement height is negligible. When SEWAB is run for high vegetation, friction velocity will be underestimated. Therefore, displacement height must be subtracted from canopy height in the model settings. Thus, measurement height for air temperature wind speed are set to 13 m (canopy height – 2/3 *canopy height) (Foken, 2006).

Mean Air Temperature

Mean air temperature for the year 2014 is 280.81 K, as calculated from the forcing data.

Land Cover Class

Coniferous forest was chosen as the dominant land cover class at the site. Most vegetation parameters attached to this land cover class were adopted, including the default setting for LAI of 6.

Fractional Vegetation Cover

The Fractional vegetation cover was set to 0.09 (default value), no monthly vegetation cover was installed. It is presumed that the coniferous forest stand at the Waldstein site has approximately the same vegetation fraction over the whole year.

Soil Class

The dominant soil type at Waldstein is sandy loam according to the German classification system, which developed from weathered granite and gneiss (Serafimovich et al, 2011).

Other settings

In correspondence to model settings for calibration at the research site Scheyern, the default settings for fractional water, initial groundwater level, the depths of the seven soil layers and the delay and amplitude of temperature migration through the soil column, were incurred.

5.1.2.3 Model Parameterization

SEWAB performed considerably well for land cover type forest in the first model run. Only minor modifications were installed into the model settings.

The albedo was calculated with data for down-welling short wave radiation and reflected radiation, the measurements of which were taken at the Weidenbrunnen site. The mean albedo for the snow free period amounts to 0.07, with a standard deviation of 0.008.

The default settings for roughness length is 0.75 m the land cover type coniferous forest and the vegetation parameter section. This value was set to 2m, because canopy height was stable since 2011, when roughness length of 2m was measured by the Micrometeorological Department of the University of Bayreuth.

5.2 Model Application at the Research Area

Subsequent to Model Calibration, SEWAB was applied to the research area. The covered timeframes include the year 2003 as an extremely hot year, and 2004 as a reference year. Data was downloaded, including the year 2002, to allow for a realistic model spin up. Based on the most common crops and tree types in the area, the model was run for land cover type agriculture and forest.

Meteorological forcing data was retrieved from two weather stations represented by the German Weather Service (CDC, 2017a; CDC, 2017b; CDC, 2017c; CDC, 2017d; CDC, 2017e). Most of the necessary input variables were available at the weather station Straubing. Gaps were filled with data from the weather station Regensburg, which is the closest weather station containing the necessary information. The stations are 41 km apart

from each other. No data for longwave, shortwave or net radiation was available from either of the weather stations Straubing, Regensburg, or any other weather station within a range of 80 – 100 kilometers. However, data for cloud cover was available for Straubing and Regensburg. Thus, SEWAB was parameterized with cloud cover information (CDC, 2017e).

The data is provided by the German weather service on their public server. It contains missing values where measurements were of unsuitable quality. The data utilized in the study is provided in hourly time steps. While the model interpolates the data to 10-minute time steps for computation, the output data was delivered as hourly values.

5.2.1 Meteorological Forcing Data

Air temperature and relative humidity

Climate data covering air temperature and relative humidity contained only two missing values per variable, which were closed by linear interpolation.

Precipitation

Precipitation data from Straubing included 181 missing values, with the largest data gap in September 2002. The gaps were closed with precipitation data from the weather station in Regensburg. Precipitation from both weather stations showed similar values over the timeframe under investigation. After the data gaps from Straubing were filled with data from Regensburg, the range of the data remained within the original range of the data from Straubing. Thus, the precipitation time series is considered reasonable. Five NA values remained spread over the whole timeframe, they were closed by linear interpolation.

Wind speed

The data containing information on wind speed contained a total of 23 missing values over the three years, which were spread over the whole time. Linear interpolation was applied to close the data gaps.

Air pressure

The air pressure variable contained 8 missing values over the year 2002, which were filled utilizing linear interpolation.

Cloud cover

Data for cloudiness covers a value range of -1 to 8. However, in the data descriptions a value range of 0 to 8 is explained (CDC, 2017e). According to meteorological convention, this corresponds to the cloud cover fraction of the visible sky, dividing the latter into eight equal squares. Values of -1 were investigated for their time of occurrence, no clear pattern was found. Therefore, values of -1 were set to NA values. Data gaps were then filled with information on cloudiness from the weather station in Regensburg. The remaining data gaps (306 NAs out of 26,304 data entries) were filled with a standard value, which was retrieved from a typical diurnal cycle for cloudiness. A conservative standard value of 4.8 was chosen. The final cloud cover values were normalized to a range of 0 to 1, which is necessary for the variable to be recognized by the SVAT model.

Mean air temperature

The mean air temperature was calculated for the timeframe 2002 to 2004 from the air temperature included in the forcing data. The mean air temperature amounts to 9.03°C/ 282.03 K.

5.2.2 Model settings

The listed model settings at the research area Straubing can be found in Tables 3–5 and in Table 7.

Geographical information

Geographical information of the weather station Straubing was inserted into model settings. The station is located at 12.56 longitude, 48.83 latitude, and at an elevation of 350 m above sea level (CDC, 2017a).

Measurement height

Information on the measurement height of air temperature, air pressure and wind speed was provided by the German weather service. Data on air temperature and air pressure was collected at 2m height, wind speed was measured at 10m height (CDC, 2017b; CDC, 2017c; CDC, 2017d)

Vegetation type

The Thünen Institute provides spatial information on the main crop types in Bavaria for the time steps 1999, 2003, 2007 and 2010 (Thünen Institut, 2014). In the timeframe under investigation, the main crops grown in the research area were winter wheat, potatoes and sugar beet. Of the total agricultural area, between 18% and 42% were dedicated to growing winter wheat, 10% to 33% were covered by potato and on 2% to 22% of croplands, sugar beet was grown.

Two model runs for land cover type agriculture were conducted, one for vegetation type cereal (representing winter wheat), and one for vegetation type sugar beet (representing potato and sugar beet) (Thünen Institut, 2014). The results for both agricultural model runs were compared and put in relation to the results from land cover type forest. As a statistical measure, the root mean squared error was compared. The RMSE, comparing the land surface temperature simulations for winter wheat and sugar beet amounts to 1.03°C. The RMSE for sensible heat flux is 19.61 Wm^{-2}, and for latent heat flux 21 Wm^{-2}. For reference, simulations for forest and potato were compared (RMSE (LST) = 2.11°C, RMSE (SH) = 53.15 Wm^{-2}, RMSE (LH) = 49.55 Wm^{-2}). Simulations for forest and winter wheat were also compared (RMSE (LST) = 1.5°C, RMSE (SH) = 52.74 Wm^{-2}, RMSE (LH) = 45.04 Wm^{-2}). Thus, the difference between winter wheat and potato are smaller than the error between forest and potato and between forest and winter wheat.

On the largest fraction of the study area, either sugar beet or potato was grown (total 12 – 55%) (Thünen Institut, 2014). Thus, sugar beet and potato were the most common crops grown in the study area and period. Based on this information and on the comparison of the model results for winter wheat and for sugar beet, potato/ sugar beet was chosen as the final vegetation type representing the land cover type agriculture.

For the simulation of turbulent fluxes and land surface temperature over forested areas, the vegetation type coniferous forest was chosen. The official land cover data for Bavaria does not distinguish between forest types (Bayerische Vermessungsverwaltung, 2017). Mixed beech forest and deciduous forest, particularly spruce and pine trees, are some of the most common types of forest in Bavaria (Bayerisches Landesamt für Umwelt & Bayerisches Landesamt für Wald und Forstwirtschaft, 2010). According to the Bavarian environment and forestry agencies, beech forest is not found in the Donau region of interest, while coniferous types of trees can be found even in less ideal environments (Bayerisches Landesamt für Umwelt & Bayerisches Landesamt für Wald und Forstwirtschaft 2010). Furthermore, the model was calibrated to coniferous forest and performed well.

Soil type

The research area is located within a region of productive agricultural lands. This is largely owed to fertile soils. The most common soil type is brown soil (BGR n.d.). The most similar soil type available in the model is silt loam.

Vegetation fraction and leaf area index

To simulate land surface temperature and turbulent fluxes over agricultural areas, the settings for monthly vegetation fraction and monthly LAI values are based on the settings for model calibration at Scheyern. The literature based LAI development for winter wheat and potato/sugar beet was adopted (Moeller et al., 2002; Gordon et al., 1997; Hermann et al., 2011; Xiaou et al., 2014). However, harvesting dates were not considered for vegetation fraction or Leaf Area Index values. Thus, smooth changes of monthly vegetation fraction and LAI are implemented into SEWAB. Please see Table 7 for detailed information on vegetation fraction and leaf area index settings for winter wheat and for potato/sugar beet at the research area.

For model application to forested areas, vegetation fraction was set to 0.9. The default value for Leaf Area Index (6.0 for coniferous forest) was adopted (Table 5).

Albedo

Albedo values were adopted from model calibration settings for potato/sugar beet and winter wheat. The albedo for forest was adopted from SEWAB default vegetation parameters for coniferous forest. This decision was made because the calculated albedo for the research site Waldstein is very low (0.07). The SEWAB default albedo for coniferous forest amounts to 0.15 and for deciduous forest to 0.25. Even though coniferous forest was chosen as the type of forest to be implemented, it is not in the interest of the study at hand to increase its dissimilarity to deciduous forest.

Canopy height

Canopy height for wheat and potato/sugar beet was adopted from SEWAB default settings. The default settings for canopy height of coniferous forest is 12 m. However, canopy height at Waldstein is 27 m, and old pine trees can reach heights of up to 36 m, according to the Bavarian agency for forest and forestry (Bayerisches Landesamt für Wald und Fortwirtschaft, n.d.). Thus, canopy height and roughness length were adopted from model calibration settings at Waldstein (canopy height 27 m, roughness length 2 m).

Table 7: Adjusted monthly LAI and fractional vegetation cover values for vegetation type winter wheat and potato/ sugar beet at Straubing. Potato/ sugar beet was chosen as a representative for land cover type agriculture.

Jan	**Feb**	**Mar**	**Apr**	**May**	**Jun**	**Jul**	**Aug**	**Sept**	**Oct**	**Nov**	**Dec**
Winter wheat/ cereal (Field1 8)											
Leaf area index											
0.5	0.5	1.0	2.5	3.0	3.5	3.0	2.0	1.0	0.5	0.5	0.5
Fractional vegetation cover											
0.2	0.3	0.5	0.6	0.7	0.8	0.9	0.7	0.6	0.4	0.2	0.1
Potato/ sugar beet (Field 17)											
Leaf area index											
0.5	0.5	0.5	0.8	2.0	3.5	3.0	2.7	2.0	0.8	0.5	0.5
Fractional vegetation cover											
0.1	0.1	0.2	0.4	0.5	0.7	0.8	0.9	0.7	0.5	0.2	0.2

5.2.3 Simulation of Heterogeneous Landscapes

In order to simulate heterogeneous agricultural landscapes, the simulations for forest and agriculture were combined. The results were added together, assigning a 50% weighing to each land cover type. This proceeding is based on the heterogeneity index created in the spatial analysis (see 5.3). Maximum heterogeneity is presumed to be achieved at a 50% land area share of forest and crop land, respectively. Thus, the simulation of heterogeneous agricultural landscapes can be interpreted as the simulation of maximum heterogeneity in the context of the study at hand.

5.3 Spatial Analysis

A spatial analysis was conducted as part of the study at hand, investigating remotely sensed land surface temperature over homogenous and heterogeneous agricultural landscapes. The data product representing land surface temperature values was generated from the Moderate-resolution imaging spectroradiometer (MODIS) sensor aboard the Aqua platform (MYD2A11) and downloaded from the Earth Explorer website (NASA LPDAAC, 2015). Land cover data was made available by the institution for mapping and geo data survey of Bavaria. The Digital Landscape Model (DLM) is part of the Authoritative Topographic-Cartographic Information System (ATKIS) and represents the official information on land use and land cover in the state of Bavaria (Bayerische Vermessungsverwaltung, 2017).

The DLM was readily available at the University of Bayreuth for the year 2016. It was later retrieved for the year 2003, covering only the study area. However, visual inspection in QGIS revealed only minor differences, which were not actual changes in land cover but in the classification of swampy areas and some urban structures (QGIS Development Team, 2015). The DLM from 2016 contains all urban areas in one vector file, which was considered more appropriate for the study at hand. The two land cover classes, forest and agriculture, we utilized for the analysis of regional climate regulating services provided by forest patches in agricultural areas. Urban areas and water were utilized for visual display.

The MODIS land surface temperature product was acquired from, including April 2003, until early November 2003. The data product consists of as 8-day averages at a spatial resolution of approximately 1 km^2. Daytime averages were analysed in this study. The exact time slots from the 30th of March until the 8th of November can be found in Table 1 in the Appendix.

Most working steps were undertaken in R (R Core Team, 2017), with some steps computed in QGIS (QGIS Development Team, 2015).

Spatial Scale to Define Heterogeneity

To investigate the effect of landscape heterogeneity on land surface temperature, a spatial scale had to be defined, at which to determine the level of heterogeneity. The scale was based on the micrometeorological processes under investigation. Interpreting forests as

flow obstacles, it can be expected that the horizontal influence of forests on air flow over agricultural fields is 20 times the canopy height in upwind direction and 2 times the canopy height in downwind direction (Foken, 2008). With an average canopy height of 20 m - 30 m in the state of Bavaria (Bayerisches Landesamt für Umwelt & Bayerisches Landesamt für Wald und Forstwirtschaft, 2010), the horizontal scale of influence ranges between 400 m and 600 m. The resolution of the utilized remote sensing data is approximately 1 km^2, which is suitable as a spatial extent on which to determine the level of landscape heterogeneity. Thus, the heterogeneity of areas with the extent of the MODIS grid was defined. Investigating land surface temperature over individual pixel has proven feasible before. Alavipanah et al. (2015) show the influence of urban green spaces on surface temperature in Munich. Temperature changes of individual MODIS pixel can be attributed to the underlying land cover type (Alavipanah et al., 2015).

Workflow

The main working stops involved data preparation, including the creation of a suitable extent of the study area. From an exemplary MODIS land surface temperature file with the extent of the study area, a fine raster grid was created. The fine grid was utilized to rasterize the land cover data. The resulting raster file was aggregated back to MODIS resolution, passing over information on the number of forest patches and area covered by forest per MODIS grid cell. Based on this information a heterogeneity index was created. The index was utilized to define three heterogeneity classes: homogenous forest, homogenous agriculture and heterogeneous agriculture and forest. This information was utilized to analyze land surface temperature between April 2003 until the beginning of November 2003. Thus, the temporal variations in land surface temperature were distinguished by the heterogeneity of the land cover structure. Figure 4 provides a visual interpretation of the workflow, which is explained in more detail in the following section.

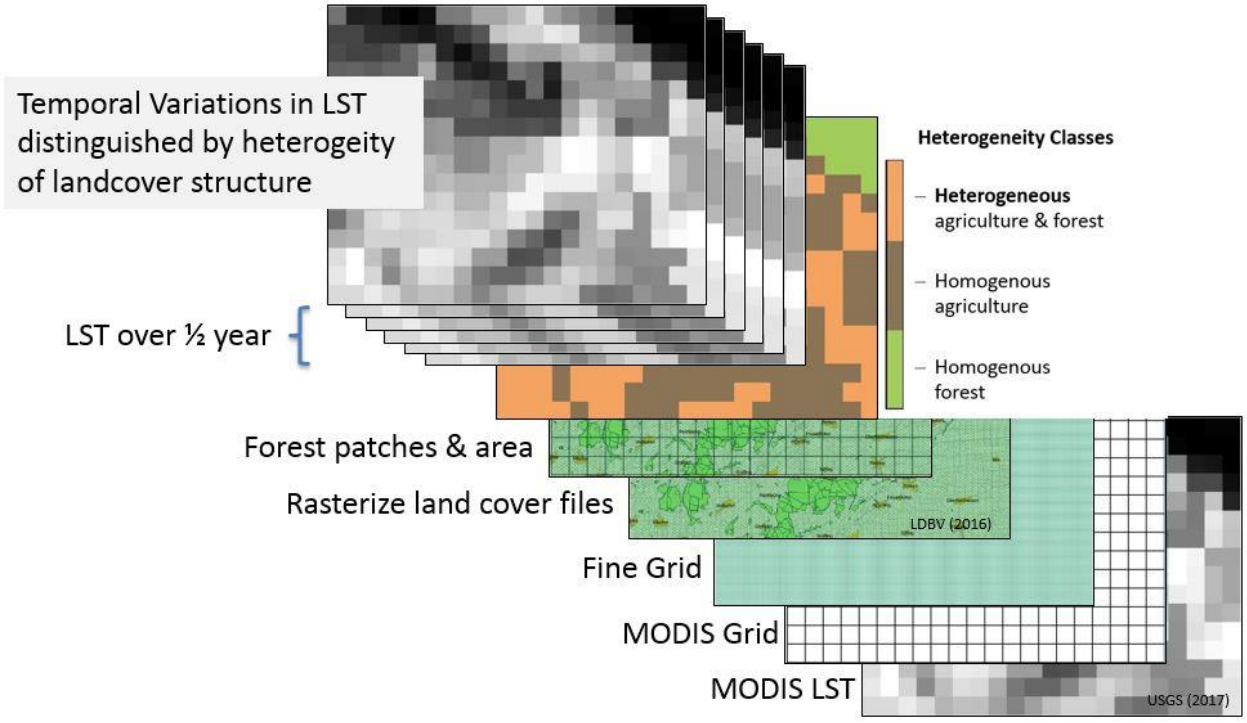

Figure 4: Workflow of the spatial analyses

5.3.1 Data Preparation

Extent of Study Area

The exact extent of the study area is based on slope and MODIS resolution. The average slope was aggregated to 25 km² grid cells. The slope was derived from ASTER gDEM v2 (NASA JPL, 2009). This data was utilized to determine the basic extent of the study area, involving 12 mean slope pixels, which amounts an areas of 300 km². The study area was cropped to those 12 pixels. For a smooth workflow, the area was further cropped to fit MODIS resolution. This simplifies the following workflow, because MODIS pixels fit exactly into the study area. Data representing the exact extent of the study area was created as raster data (from MODIS data) and as a vector file.

Preparation of Land Cover Data

Although only the land cover classes forest and agriculture entered the final analysis, initially, urban areas and water were included in the process. This was done for better

visual display. The four shape files containing information on land cover were cropped to the extent of the study area. Subsequently, the files were merged into one vector file.

Rasterization of Land Cover File

For the rasterization of the merged land cover shape file, a fine raster grid was created, which fits perfectly into the MODIS grid. A sample MODIS land surface temperature file was disaggregated. The MODIS data comes at a resolution of 926.6254 m * 926.6254 m. The disaggregation factor was set to 93, generating a resolution of 9.963714 m * 9.963714 m. the factor was set to be an integer for re-aggregation at a later step in the workflow. The merged land cover file was rasterized based on this newly created grid.

The disaggregation factor was determined by trial and error, creating raster layers of resolutions between 5 m and 20 m. These were used for the rasterization of land cover files. Visual inspection revealed, that a resolution of 10 m delivers a good result, where the number of forest patches in the raster file corresponds well to the number of forest patches in the shape file, however, with less computational requirements than at 5 m resolution.

Determination of Forest Patches

In order to create a heterogeneity index, forest patches were created, assigning an individual ID to each patch. The rasterized land cover data was turned into a binary file, assigning values of 1 to land cover class forest and values of 0 to all other land cover classes. Forest patches were created, utilizing the four neighbor rule. It was defined, that if any of the four adjacent neighbors of a forest grid cell was also of type forest, both cells would belong to the same patch. The result is a raster layer with 355 individual forest patches in the whole study are.

Number of Forest Patches per MODIS Grid Cells

The raster layer displaying forest patches was re-aggregated to MODIS resolution (aggregation factor 93). The information passed over to the generated raster file, was the number of patches. Thus, the resulting raster layer contained information of the number of forest patches per grid cell. Grid cells have the same resolution as MODIS land surface data (ca. 1km^2). The maximum number of patches per grid cell is 15.

Forest Area per MODIS Grid Cells

In order to calculate the area per MODIS grid cell covered by forest, the raster layer containing information on forest patches was re-aggregated to MODIS resolution. As the aggregation function, the number of forest pixels were counted. From the resolution of the fine raster grid (9.963714 * 9.963714 m), and the number of forest pixels, the area of forest per MODIS grid cell was calculated. The maximum area covered by forest corresponds to the area of a MODIS pixel.

5.3.2 Heterogeneity Index

Most heterogeneity indexes, common in the remote sensing community, come from island biogeography or animal movement analysis. Therefore, variables such as connectivity and distance are very important (Díaz-Varela et al., 2016; Ali et al., 2014). For the study at hand, a heterogeneity index was created from two individual indexes. One index was created, giving information about the amount of forest patches per MODIS resolution pixel (patch index). The area index corresponds to the area covered by forest per MODIS grid cell. The heterogeneity index is the sum of the patch index in the area index.

Patch Index

The maximum amount of forest patches found in one pixel over the whole research area is 15. However, only one pixel displays this many patches.
The next maximum is 10 patches. The pixel with 15 patches was treated as a pixel with 10 patches, because for the definition of heterogeneity in next, this one pixel would only distort the index as an outlier. There were no pixels displaying a number of 11 to 14 patches, all cells, except the one with 15 patches, were covered by a range of 0 to 10 patches. The patch index displays values of 0 to 1, with zero corresponding to 0 patch cover and 1 corresponding to the maximum amount of patches.

Area index

The area index also has a range of 0 to 1. It was created, so that a 50% forest coverage corresponds to an index value of 1. For the study at hand, an even mixing of land cover types can be considered the most heterogenic because the influence of forest and

agriculture are considered equal. Forest coverage of 0% corresponds to an index value of 0. For the level of landscape heterogeneity, it is specified that 20% forest coverage are equal to 80%, 30% are equal to 70% and 40% are equal to 60%, respectively. Forest cover of 90% was also assigned an index value of 0, because otherwise, these pixels distort the in the final heterogeneity index. However, for the definition of heterogeneity classes, all pixels with 90% and 100% forest cover were assigned a value of 20, to make them recognizable.

Patch index and area index were analyzed by the distribution, to make sure that both indexes are visible and the final index (Fig. 5). This was done before, to forest pixels were assigned a value of 20 to make them distinguishable.

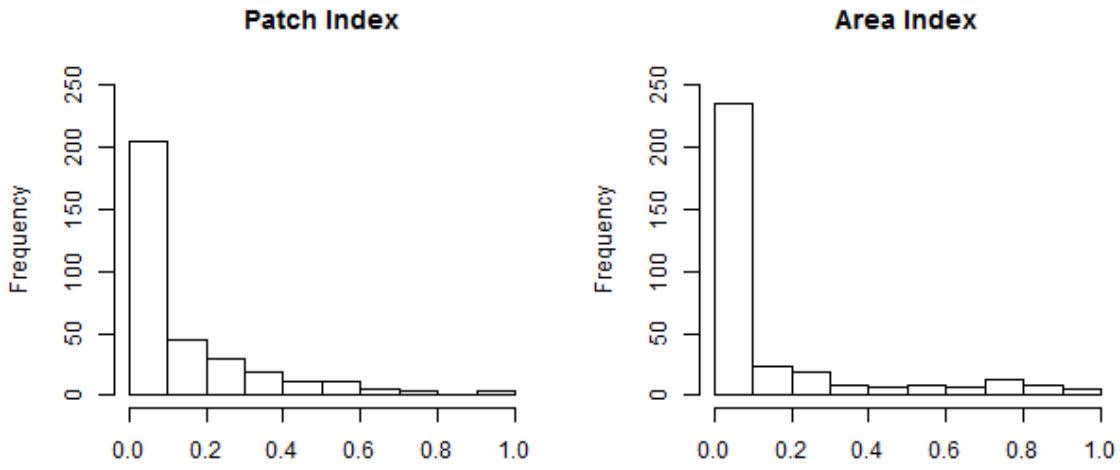

Figure 5: Histograms displaying the distribution of Area Index and Patch Index

Heterogeneity Index

The heterogeneity index is the sum of the patch index and the area index. Thus, it has a range of 0 to 2, with 0 displaying no heterogeneity. The higher the index value, the more heterogeneous the area.

Heterogeneity Classes

Based on the heterogeneity index, three heterogeneity classes were defined: homogenous agriculture, homogenous forest and heterogeneous land cover (agriculture and forest).

Homogenous forest was recognizable by an individually assigned value (see above). Homogenous agriculture was defined for all index values between zero and 0.2. Heterogeneous land cover was defined as all pixels with a heterogeneity index value between 0.3 and 1.8. The maximum index value that occurs is 1.8. Figure 6 shows the raster layer displaying the spatial distribution of the three heterogeneity classes and the forest patches for reference.

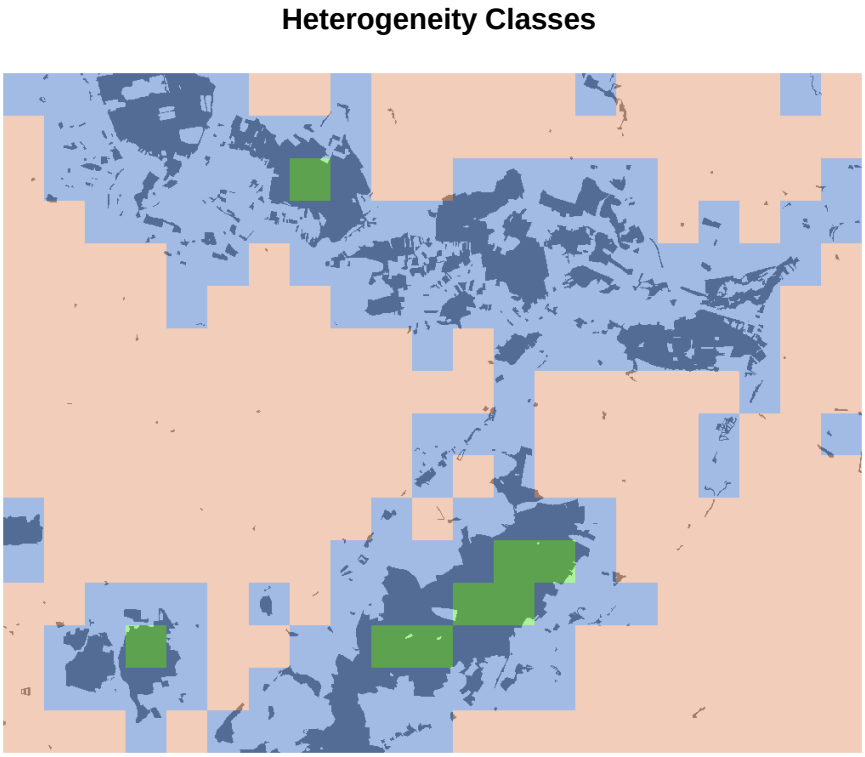

Figure 6: Map of the spatial distribution of heterogeneity classes with forest patches. Blue: heterogeneous land cover, brown: homogenous agriculture, green: homogenous forest

5.3.3 Time Series of Land Surface Temperature

MODIS land surface data was cropped to the study area and stacked, together with the raster file containing heterogeneity classes. MODIS data was provided in Kelvin, these were converted into degrees Celsius.

Each LST raster file in the stack corresponds to a time period of eight days. In each of these files, the pixels were grouped according to their corresponding heterogeneity class of the land cover. Subsequently, mean, minimum and maximum value ranges of land surface temperature were calculated.

6. Results from Model Evaluation

6.1 Statistical Measures for Model Evaluation

In the process of model calibration, simulated heat fluxes and land surface temperature over agricultural land and over forest were evaluated. The statistical tools utilized in this step include two standard regression tools, one dimensionless measure, one error index and two graphical representations. A mix of statistical measures was implemented to profit from their different strengths. The chosen statistics are common measures accepted within the scientific community and are recommended in literature. They are robust in the sense that they can be applied to different models and environmental conditions (Moriasi et al., 2007).

The coefficient of determination (R^2) and the Pearson correlation coefficient (r) are utilized as standard regression techniques. Both coefficients describe the level of collinearity between simulated and observed values. R^2 gives information about how much of the variance in the observed values is explained by the model, in this context by the linear model fitted to observations and simulations. The coefficient of determination ranges from 0 to 1 (0 indicating maximum error variance). Values above 0.5 may be considered a good model fit (Van Liew et al., 2003; Moriasi et al., 2007). Pearson's correlation coefficient is a measure for the strength and direction of linear relation. A perfect positive linear relationship is indicated by r = 1, and negative linear relation by r = -1, respectively. If r = 0 the variables are not linearly related (Moriasi et al., 2007).

The Nash Sutcliffe efficiency (NSE) is a normalized measure comparing the degree of variance of the observation and simulation residuals with the magnitude of variance of the residuals between observations and their mean (Equation 3).

$$NSE = 1 - \left[\frac{\sum_{i=1}^{n}\left(Y_i^{obs} - Y_i^{sim}\right)^2}{\sum_{i=1}^{n}\left(Y_i^{obs} - Y_i^{mean\,(obs)}\right)^2}\right] \qquad (3)$$ modified from Moriasi et al. (2007)

The dimensionless statistic has a range of -∞ to 1, with NSE = 1 indicating an optimal fit between observations and simulations. According to Moriasi et al. (2007) an NSE ≥ 0 may be considered acceptable. However, this depends on the data under investigation. Considering turbulent fluxes, average observation values are not well suited for capturing the dynamics. Furthermore, the NSE is highly sensitive to bias. In the context of this study, this limitation is important when Eddy-covariance fluxes are compared,

where a residual has to be expected from the energy balance closure. Likewise, simulations from SEWAB are based on a closed energy balance. If the NSE is smaller than zero, the mean of the observations is a better fit than model simulation values (Moriasi et al., 2007).

The root mean squared error (RMSE) was chosen as an error index. It provides information about the variance between observations and simulations. Values of zero indicate a perfect fit. RMSE values smaller than half the standard deviation may be considered a good model fit (Moriasi et al., 2007; Singh et al., 2004).

Graphical representations are provided by scatter plots of observations and simulations. Time series plots give further insights into model performance (see below).

6.2 Model Evaluation for Land Cover Type Agriculture

SEWAB was evaluated for its ability to simulate land surface temperature, sensible and latent heat flux over agricultural land, at the research site Scheyern. Evaluation data was made available for the timeframe from 15th of January to 9th of August 2014. The data was calculated by a so-called "Turbulenzknecht". The results were delivered together with flag information, with values of 0 and 1 indicating high quality data (Mauder & Foken, 2015).

Sensible heat flux

A correlation coefficient value of r = 0.71 indicates fairly high linear correlation between observed and simulated values for sensible heat flux. The coefficient of determination also indicates a good model fit. However, a value of R^2 = 0.51 is only just sufficient to make this assumption.

A negative Nash Sutcliffe efficiency of -0.03 reveals that the variance between the residuals of observations and simulations is of the same magnitude as the variance of the residuals of observations and their mean. The root mean squared error amounts to 51.09 Wm^{-2}. The combination of an acceptable R^2 value, but an unacceptable NSE shows that the error is caused by a model bias. Simulated values are on average higher than observations.

The scatter plot of observations and simulations shows that, while the bulk of data is in the same range, there are occurrences of sensible heat flux overestimation and underestimation (Fig.7). Further inspection of the range and distribution reveals disagreement where SEWAB suggests values above 400 Wm^{-2} (see Appendix Fig.1 and Fig.2). However, this also shows that the simulations of sensible heat principally reflect the variability above crop land, but the dynamics are exaggerated. Model performance is influenced by the residuals from the energy balance closure.

The time series plot for the whole evaluation period shows sporadic disagreement between observed and simulated values and a peak of modeled sensible heat flux in the month of June (Appendix Fig.5). Figure 8 is the same time series plot, considering only the months from May to August. Model overestimation starts in May, peaks in June with overestimations of more than 200 Wm^{-2}, and turns into underestimation of sensible heat between mid-July until mid-August. Please note that time series plots contain data gaps, where missing values occurred in the evaluation data. The gaps are present in simulations, because the data is a fusion from both crop fields (winter wheat and potato), based on wind direction. Wind direction is available in the evaluation data and is responsible for missing values in simulation data (Fig. 8, Fig.10 and Appendix Fig.5 and Fig.6).

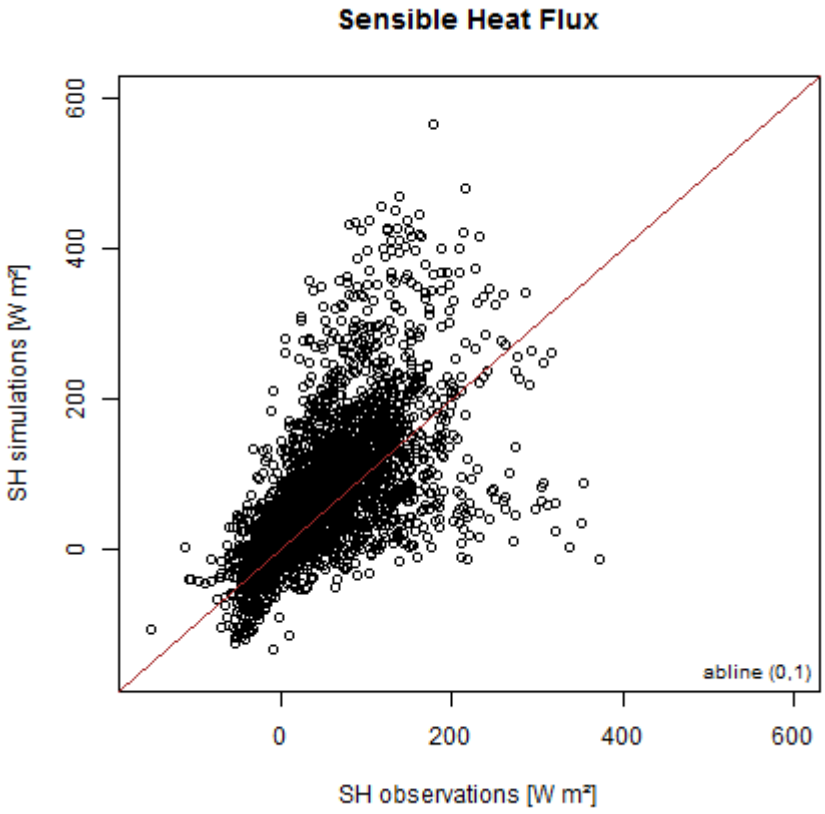

Figure 7: Scatter plot of sensible heat flux observations and simulations at Scheyern

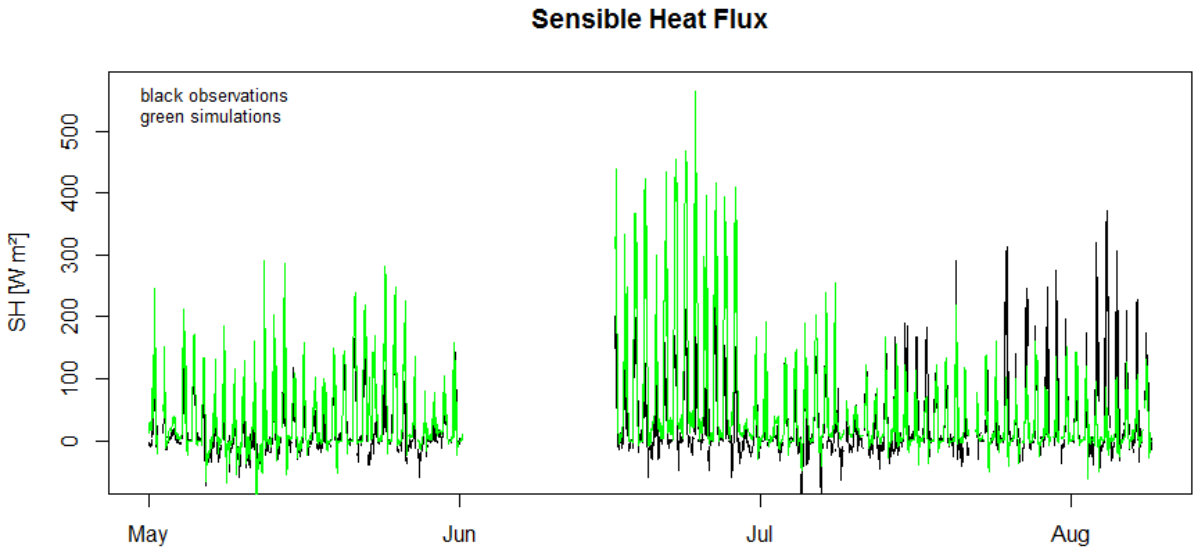

Figure 8: Time series plot from May to August for sensible heat flux at Scheyern

Latent heat flux

The simulations of the latent heat flux are in overall better agreement with observed values than sensible heat flux simulations. A higher correlation coefficient, of r = 0.81, indicates strong linear correlation, and an R^2 value of 0.66 reveals a better fit than for sensible heat flux.

The Nash Sutcliffe efficiency has a value of 0.46, which allows for the assumption that simulated values are clearly better predictors than the mean of observations. However, the root mean squared error differs only by roughly 8 Wm^{-2} to the RMSE of sensible heat flux (RMSE (latent heat flux) = 59.52 Wm^{-2}).

The scatter plot shows frequent disagreement between observations and simulations, particularly for the range of latent heat flux greater between 300 - 600 Wm^{-2} (Fig.9). Histograms reveal fairly similar distribution of observations and simulations (Appendix Fig.4). The differences between observations and simulations are owed mainly to outliers of simulations in high LH ranges compared to observations. However, observed values also include outliers for high LH values, although their range is slightly smaller (Appendix Fig.3).

The time series plot for the whole evaluation period shows that latent heat flux is generally underestimated when sensible heat flux is overestimated and vice versa (Appendix Fig.5 and Fig.6). In June, latent heat flux is clearly underestimated, which turns into overestimation in July and August and amounts to a strong overestimations of latent heat flux in a range of up to 200 Wm^{-2} (Fig.10).

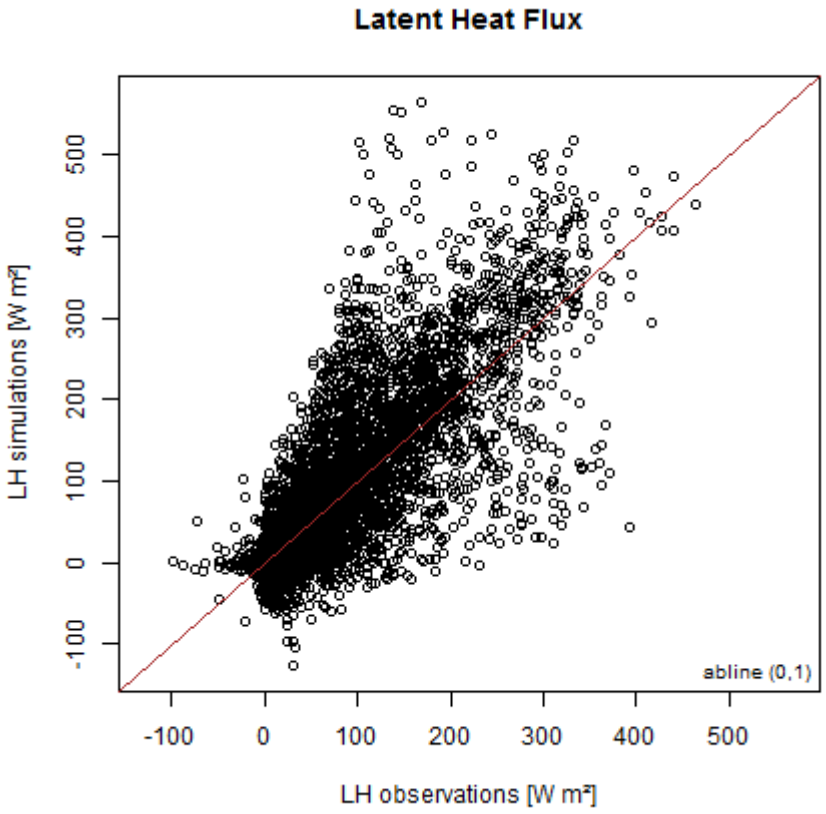

Figure 9: Scatter plot of latent heat flux observations and simulations at Scheyern

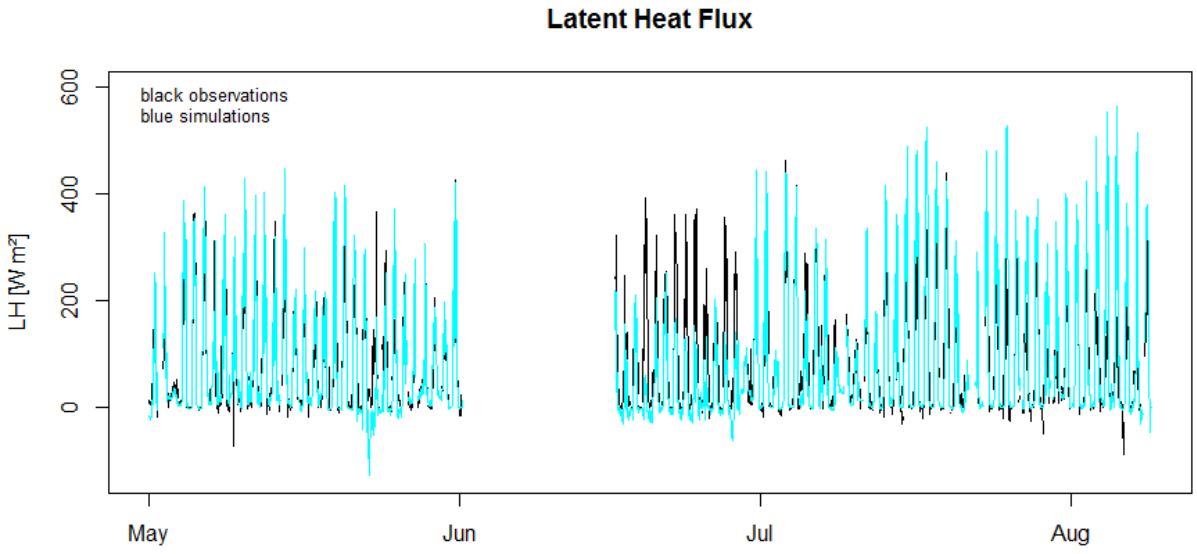

Figure 10: Time series plot from May to August for latent heat flux at Scheyern

Land Surface Temperature

No evaluation data for land surface temperature was available. The simulated values were investigated for their range and distribution. Surface temperature ranges from 6.06°C to 43.09°C. Temperature for simulated values over field 17 (potato) and over field 18 (winter wheat) was investigated separately. They hardly differ from the temperature range of land surface temperature that was created from both simulation runs, and combined depending on the wind direction. Land surface temperature simulations over the field on which potato was grown, ranges from -6.06°C to 43.42°C, the range over field 18 is -5.67°C to 39.87°C.

Boxplots reveal that very high temperature values, circa 40°C, are statistical outliers. However, such high surface temperatures are realistic during hot summer periods (Appendix Fig.7). The time series plot shows reasonable temperature development over the whole year (Fig. 11).

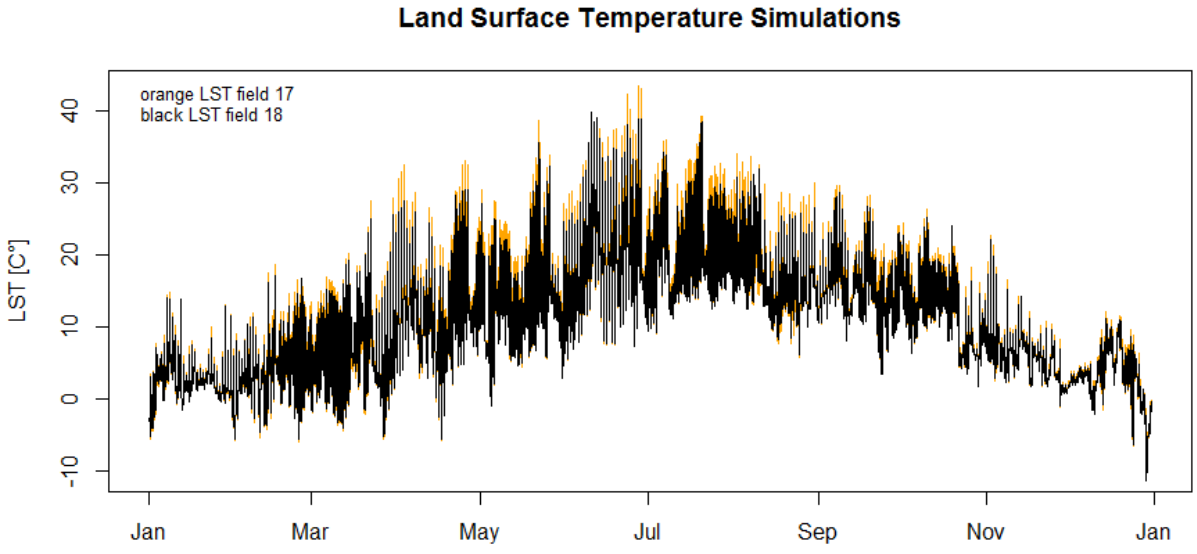

Figure 11: Time series plot for the whole year for land surface temperature simulations at Scheyern

6.3 Model Evaluation for Land Cover Type Forest

Simulations of turbulent fluxes and land surface temperature by the SVAT model were evaluated against flux tower measurements at the research site Waldstein. Evaluation data was made available for the whole year 2014 by the Micrometeorology Department of the University of Bayreuth.

Sensible heat flux

Standard regression analysis shows high linear correlation (r = 0.85) and also a good model fit between observations and simulations ($R^2 = 0.73$).

Compared to sensible heat flux simulations at the research site Scheyern, the Nash Sutcliffe efficiency reveals less residual variance between simulations and observations compared to residual variance of observations and their mean (NSE = 0.67). However, the root mean squared error is in a similar range as observed at Scheyern (RMSE = 56.89).

The scatter plot and the time series plot for the year 2014 show overall good agreement between simulations and observations (Fig.12 and Fig.13). Monthly time series plots confirm this result (please see the R script in supplementary materials for this section).

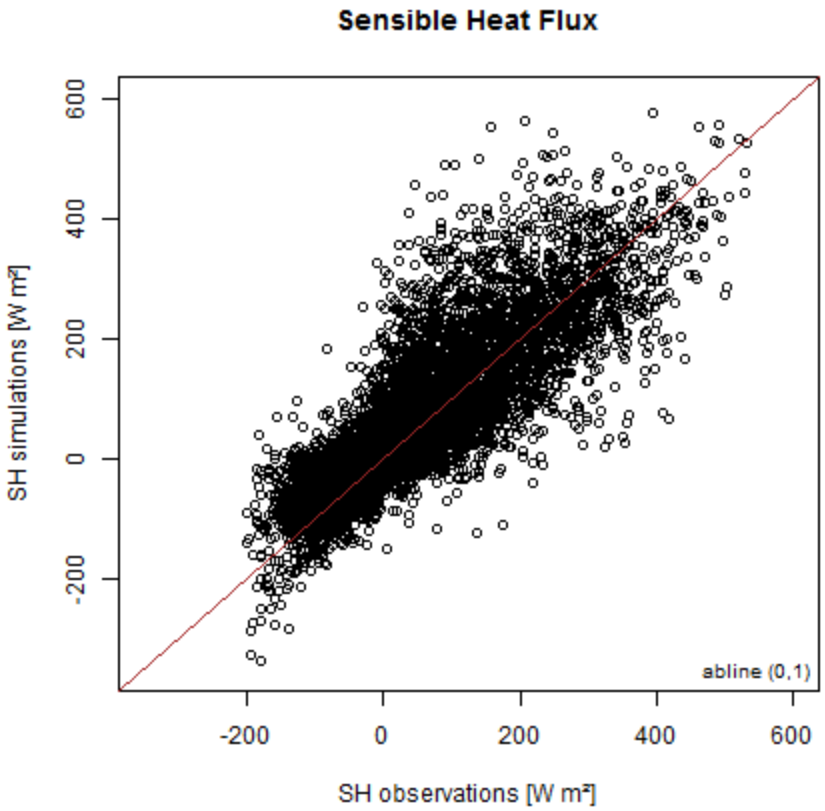

Figure 12: Scatter plot of sensible heat flux observations and simulations at Waldstein

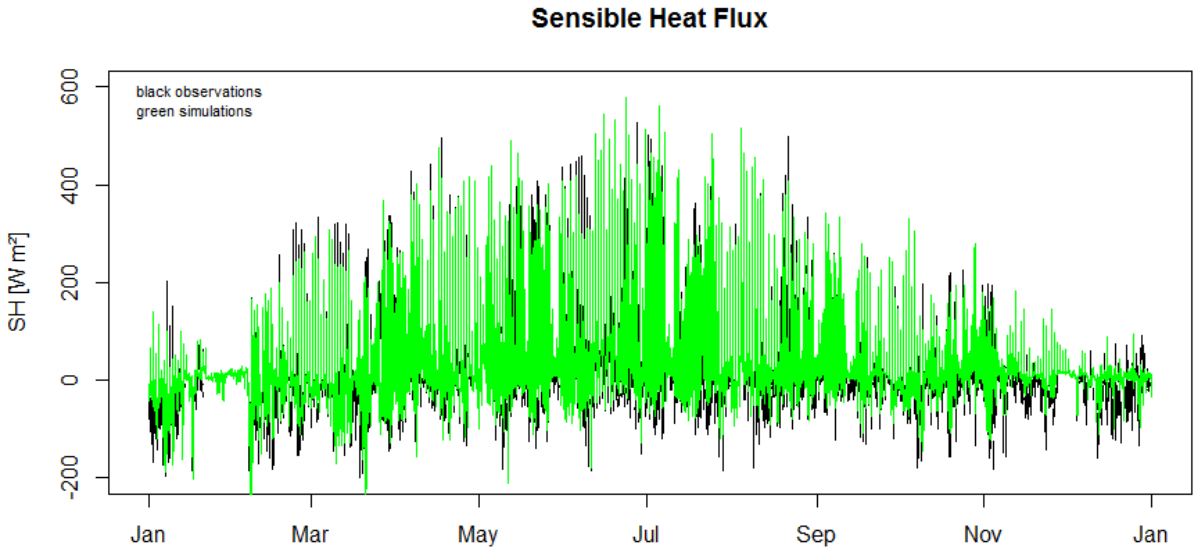

Figure 13: Time series plot (year 2014) for sensible heat flux at Waldstein

Latent heat flux

Evaluation data for latent heat flux contained many missing values. Of a total 17,520 data entries, 7,372 values were missing. For data inspection, latent heat flux simulations were set to NA wherever observation values were missing.

While linear correlation between simulations and observations for the latent heat flux is relatively high (r = 0.68), the coefficient of determination indicates a less optimal model fit than for sensible heat flux observations (R^2(LH)= 0.47).

The Nash Sutcliffe efficiency confirms this finding although with an NSE value of 0.33, simulations are still in an acceptable range. The root mean squared error amounts to 71.61 Wm^{-2}.

A wider division between simulations and observations is visible in the scatter plot, compared to sensible heat (Fig.14). The yearly time series plot reveals some disagreement (Fig.15). However, box plots and histograms reveal similar data distributions (Appendix Fig.11 and Fig.12).

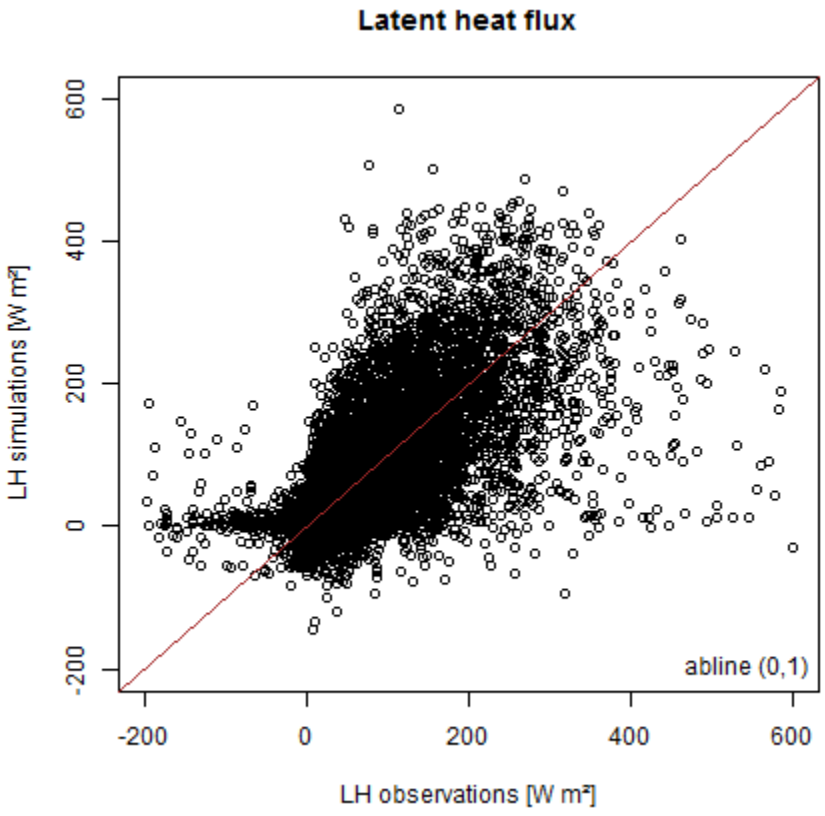

Figure 14: Scatter plot of latent heat flux observations and simulations at Waldstein

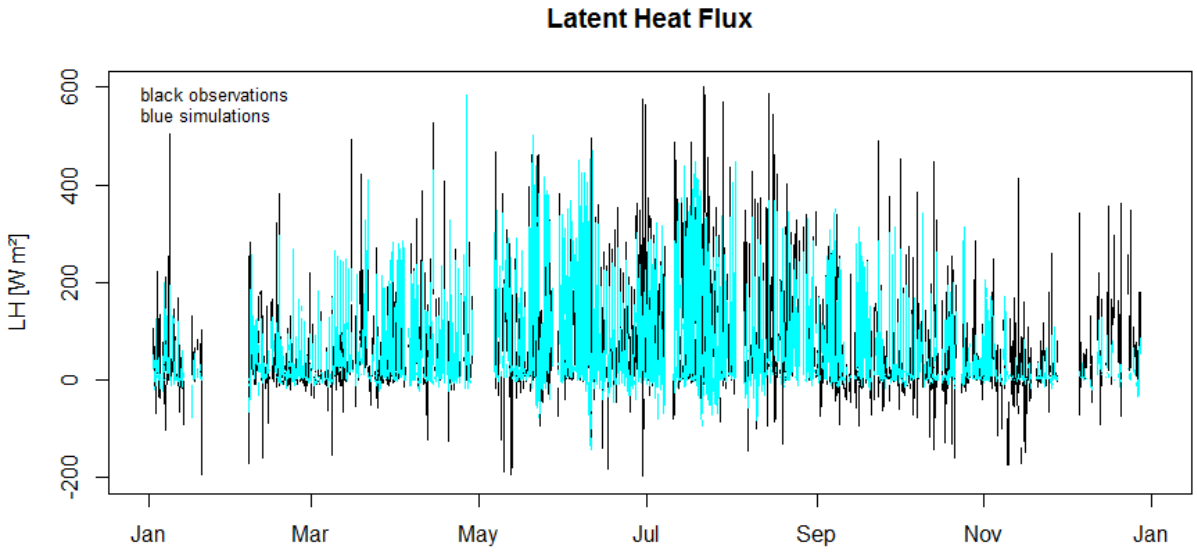

Figure 15: Time series plot (year 2014) for latent heat flux at Waldstein

Land Surface Temperature

Land surface temperature simulations are in a reasonable range and distribution (Appendix Fig.13). Over the whole 2014 year, land surface temperature ranges between -9.35°C and 32.57°C. The time series plot displays reasonable behavior (Fig. 16).

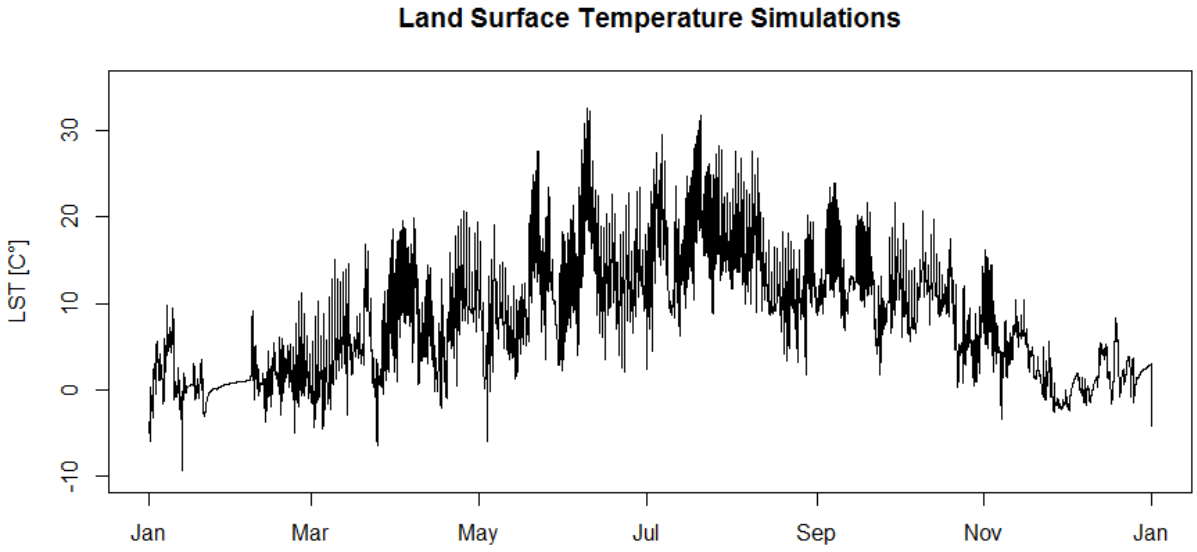

Figure 16: Time series (year 2014) for land surface temperature simulations at Waldstein

7. Results

7.1 SVAT Model Results

7.1.1 Latent Heat Flux

Simulated turbulent fluxes and land surface temperature were investigated during the years 2003 and 2004. Temporal aggregations are eight-day timeslots based on the remote sensing data. Only daytime values were investigated. This is based on the remote sensing data, which comes as daytime averages. The following statistical results will be presented here: mean values, value range, and standard deviation. Please note that the standard deviation represents the variance of daytime values within the eight-day timeslots to the mean of the respective eight-day timeframe. The Bowen ratio was calculated from the mean turbulent fluxes of eight-day timeslots.

Latent Heat Flux over Homogenous Agricultural Land Cover 2003

The average latent heat flux of daytime eight-day aggregations over the year 2003 has a range of 25.70 Wm^{-2} to 251.30 Wm^{-2}. Minimum values vary around -87 Wm^{-2} and 54.95 Wm^{-2}, with the absolute minimum between the 7th and 14th of April 2003, and highest minimum values between the 9th and the 16th of May. The maximum latent heat flux simulations range from 52.77 Wm^{-2} (Aug 5th– 12th) to an absolute maximum of 472.17 Wm^{-2} between the 10th and 17th of June. In the latter timeframe, the standard deviation peaks with a value of 123.90 Wm^{-2}. The lower end of the range is margined with a minimum of 15.71 Wm^{-2} between the 5th and 12th of August. Figure 17 displays the time series plot for mean, minimum, and maximum latent heat flux values together with precipitation information. In the supplementary materials an extensive list of the above-described statistics is provided in the Excel sheet "Statistics Latent Heat Flux Homogenous Agriculture 2003".

Latent Heat Flux over Heterogeneous Agricultural Land Cover 2003

Over heterogeneous agricultural land cover, mean latent heat flux simulations vary between 45.75 Wm^{-2} and 245.90 Wm^{-2} over the year 2003. Minimum latent heat flux ranges between -110.23 Wm^{-2} (July 20th – 27th) and 54.52 Wm^{-2} (July 4th – 11th). The lowest maximum value of 94.26 Wm^{-2} is simulated between the 5th and 12th of August. The absolute maximum is reached between the 10th and 17th of June, with 499.74 Wm^{-2}. The standard deviation varies between 29.10 Wm^{-2}(June 10th – 17th) and 126.61 Wm^{-2} (Aug

5th – 12th). Figure 18 displays the time series plot for 2003; and in the supplementary materials a list of statistical measures can be found ("Statistics Latent Heat Flux Heterogeneous Agriculture 2003").

The lowest value of average latent heat and the highest value of the mean sensible heat flux both occur at the same time, over homogenous and over heterogeneous agricultural area in 2003 (Aug 5th – 12th). Furthermore, the highest average and maximum values for sensible heat flux are higher over heterogeneous agriculture (mean 341.17 Wm^{-2}, max 464.95 Wm^{-2}). In comparison, the absolute maximum value over homogenous agriculture is about 15 Wm^{-2} lower. The highest mean values are about 20 Wm^{-2} lower than over heterogeneous agriculture (mean 322.45 Wm^{-2}, max 449.26 Wm^{-2}).

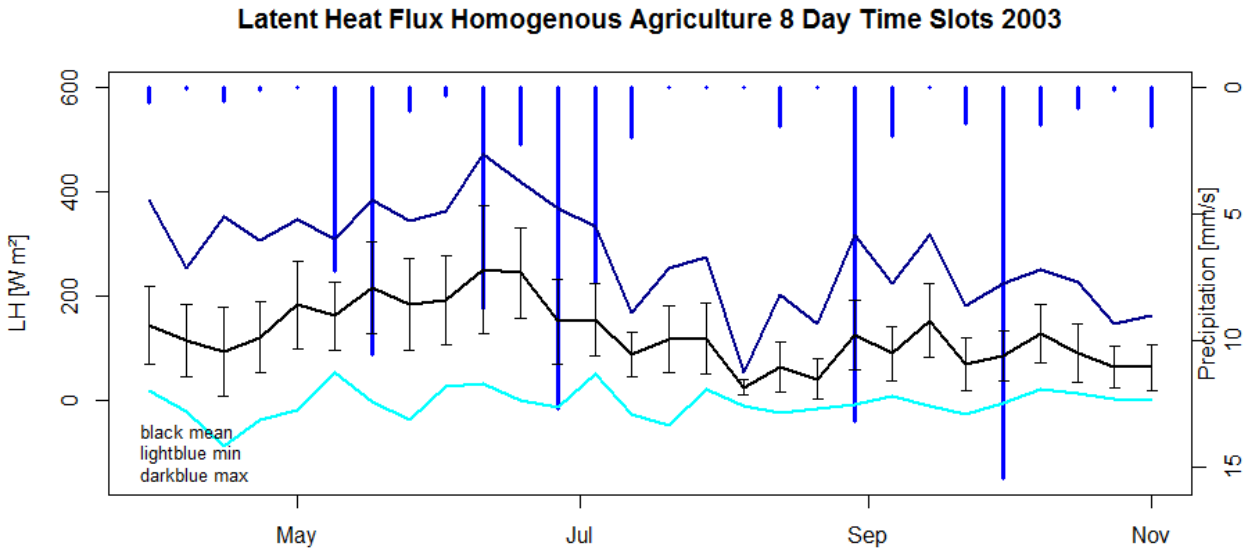

Figure 17: Latent heat flux aggregated to 8-day time slots (April – Nov 2003) and precipitation.

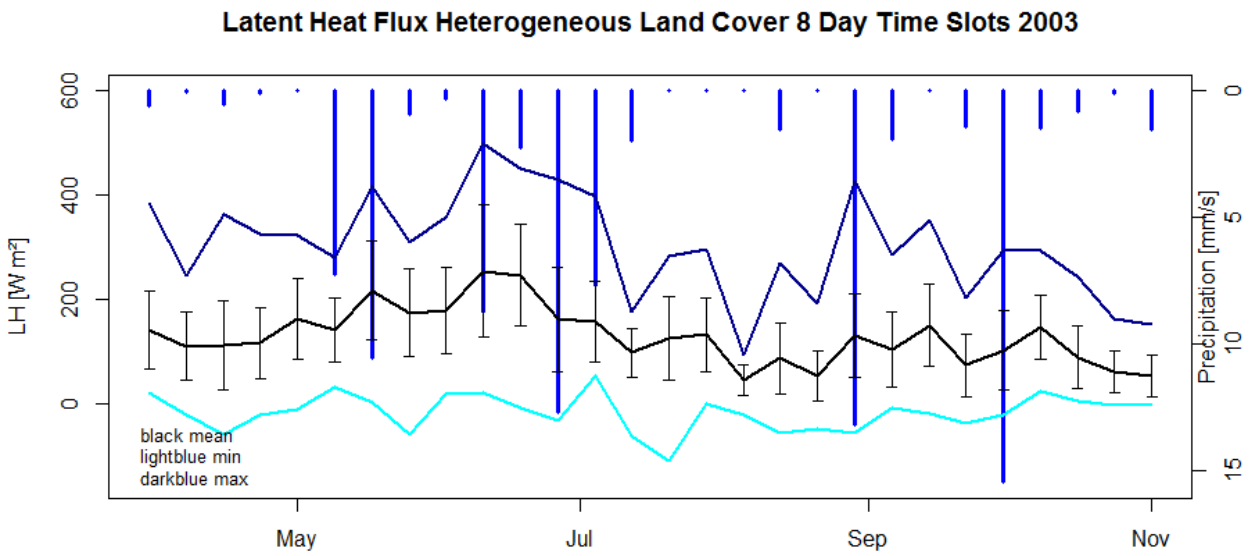

Figure 18: Latent heat flux over heterogeneous agricultural areas aggregated to 8-day time slots (April – Nov 2003) and precipitation.

Latent Heat Flux over Homogenous Agricultural Land Cover 2004

Mean values increase in the year 2004, where the average latent heat flux ranges between 31.33 Wm^{-2} and 268.35 Wm^{-2}. The absolute minimum value is reached between the 25th of May and the 1st of June, with -101.57 Wm^{-2}. Between the 2nd and the 9th of June, the highest minimum latent heat flux values are simulated (110.79 Wm^{-2}). The lowest maximum is reached between the 5th and the 12th of August (85.23 Wm^{-2}); the absolute maximum latent heat flux is simulated between the 30th of March and the 6th of April, with 534.42 Wm^{-2}. The standard deviation ranges between 24.20 Wm^{-2} (Aug 5th -12th), and 114.92 Wm^{-2} between the 30th of March and the 6th of April. The time series plot is provided in Figure 19. A list of statistical measures is provided in the supplementary materials ("Statistics Latent Heat Flux Homogenous Agriculture 2004").

Latent Heat Flux over Heterogeneous Agricultural Land Cover 2004

In the year 2004, the average latent heat flux is between 52.20 Wm^{-2} and 276.72 Wm^{-2}. The absolute minimum of -119.53 Wm^{-2} is simulated between the 25th and the 31st of May, the upper limit of minimum latent heat flux is reached between the 2nd and the 9th of June, with 164.46 Wm^{-2}. Maximum latent heat flux ranges between 135.31 Wm^{-2} (Oct 24th – 31st)

and 574.30 Wm^{-2} (Aug 29th – Sept 5th). The standard deviation fluctuates between 36.78 Wm^{-2} (Oct 24th - 31st) and 118.43 Wm^{-2} (March 30th – April 6th). The time series plot for the year 2004 is displayed in Figure 20. A list of statistical measures can be found in the supplementary materials ("Statistics Latent Heat Flux Heterogeneous Agriculture 2004").

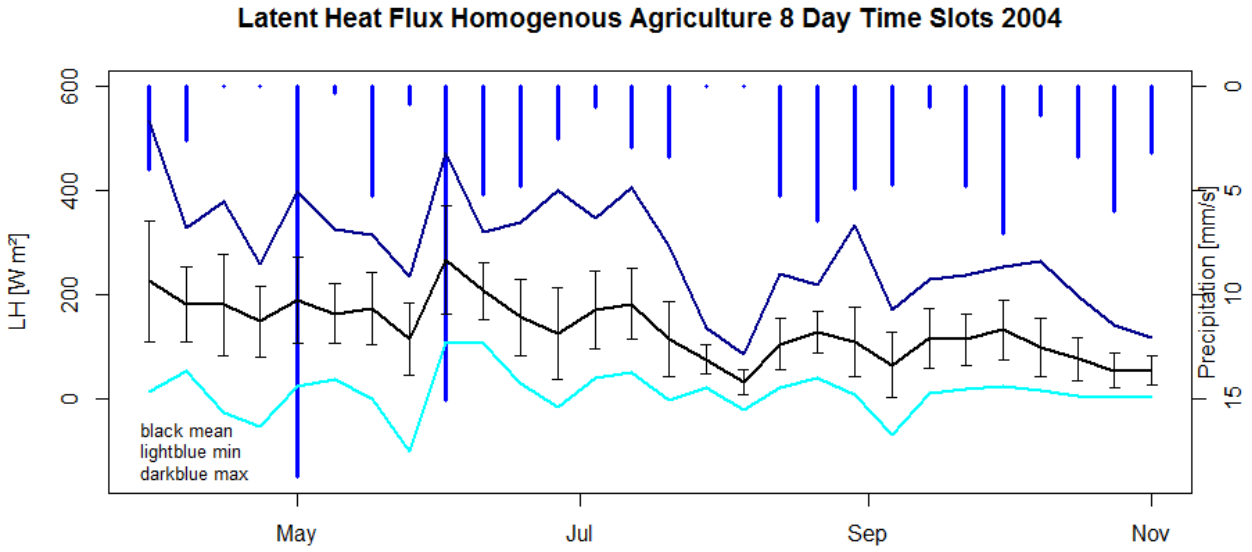

Figure 19: Latent heat flux aggregated to 8-day time slots (April – Nov 2004) and precipitation.

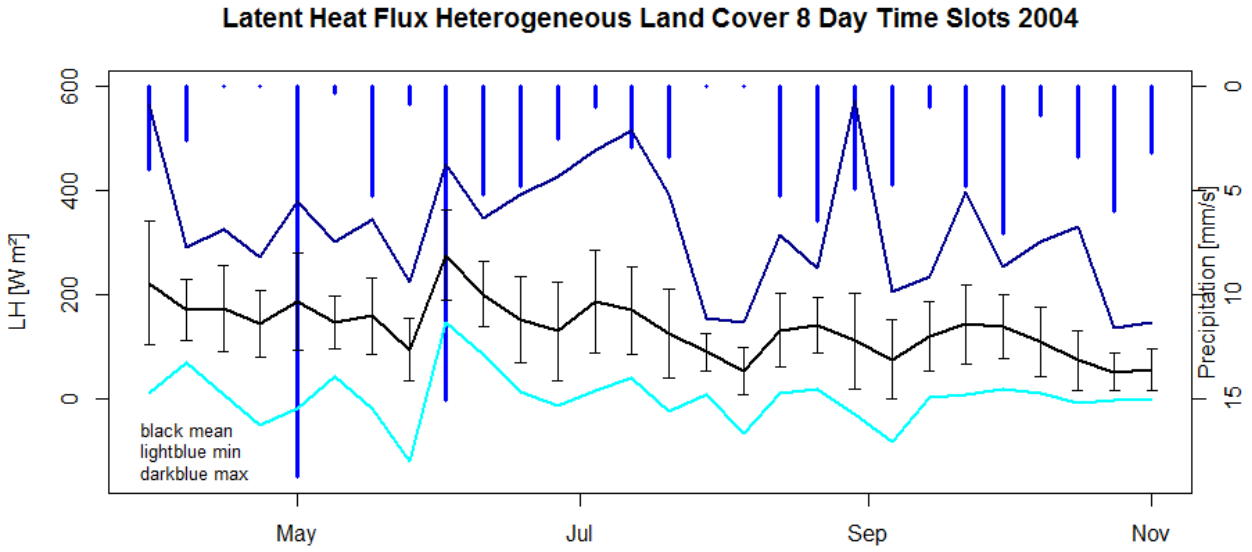

Figure 20: Latent heat flux over heterogeneous agricultural areas aggregated to 8-day time slots (April – Nov 2004) and precipitation.

7.1.2 Sensible Heat Flux

Sensible Heat Flux over Homogenous Agricultural Land Cover 2003

Average sensible heat flux values in the simulation period 2003 range between 29.73 Wm^{-2} and 322.45 Wm^{-2}. The absolute minimum value of -23.39 Wm^{-2} is reached between the 24th and the 31st of October; the upper end of the minimum value range is marked by 146.03 Wm^{-2} (Aug 5th – 12th). The lowest maximum sensible heat flux is simulated between the 8th and the 15th of October (74.44 Wm^{-2}). The absolute maximum is reached in the period of the 5th and the 12th of August with 449.26 Wm^{-2}. The standard deviation fluctuates around 21.60 Wm^{-2} (June 10th – 17th) and 94.36 Wm^{-2} between the 1st and the 8th of November. Figure 21 provides the time series plot for sensible heat flux simulations aggregated over 8-day averages 2003. A list of statistical measures can be found in the supplementary materials ("Statistics Sensible Heat Flux Homogenous Agriculture 2003").

Sensible Heat Flux over Heterogeneous Agricultural Land Cover 2003

In 2003, the average sensible heat flux varies around 13.21 Wm^{-2} and 341.17 Wm^{-2} over heterogeneous land cover. Minimum values range around -190.78 Wm^{-2} (Sept 30th – Oct 7th), and 144.67 Wm^{-2} (Aug 5th – 12th). The lowest maximum value for sensible heat flux is simulated between the 8th and the 15th of October (84.74 Wm^{-2}). The absolute maximum is reached between the 5th and the 12th of August, with 464.95 Wm^{-2}. The standard deviation fluctuates around 30.67 Wm^{-2} (June 18th – 25th), and 127.34 Wm^{-2} (Nov 1st – 8th). Figure 22 displays the time series plot for the year 2003. A statistical summary is provided in the supplementary materials ("Statistics Sensible Heat Flux Heterogeneous Agriculture 2003").

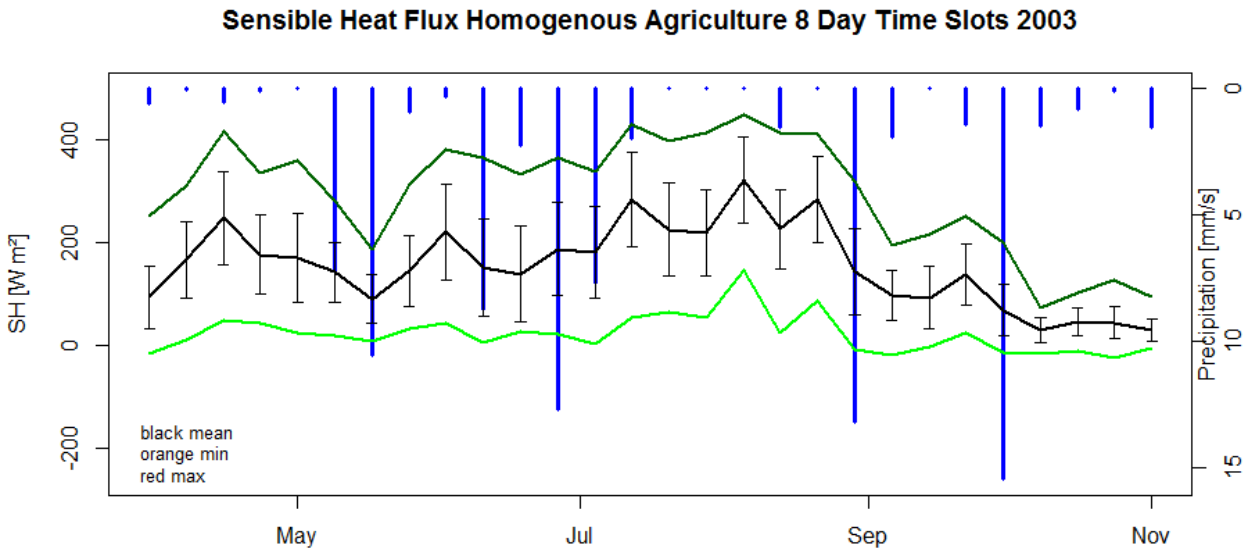

Figure 21: Sensible heat flux aggregated to 8-day time slots (April – Nov 2003) and precipitation.

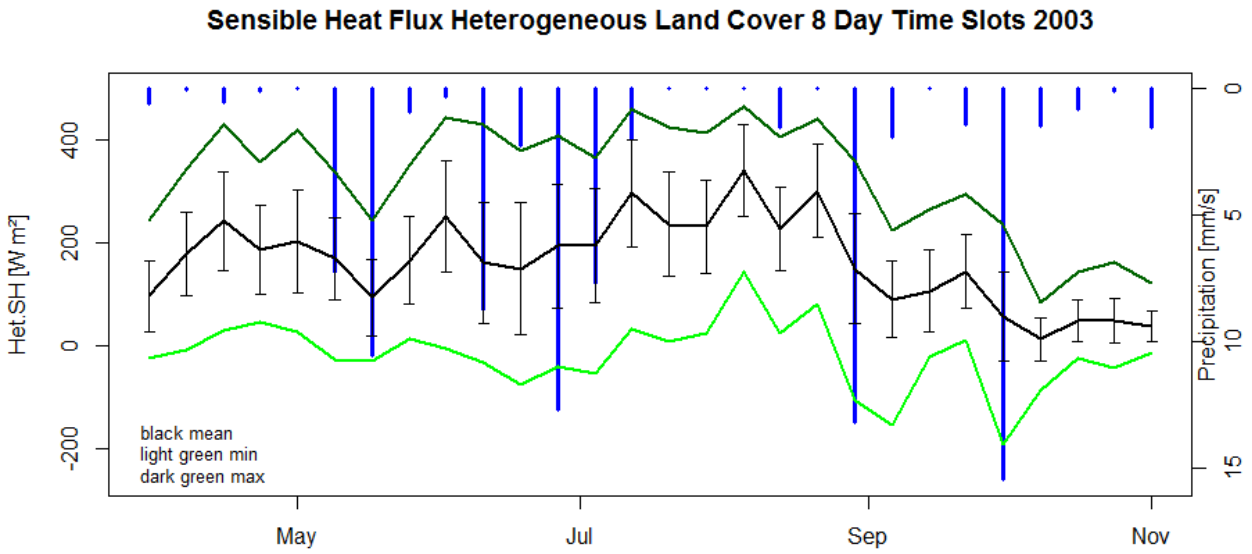

Figure 22: Sensible heat flux over heterogeneous agricultural areas aggregated to 8-day time slots (April – Nov 2003) and precipitation.

Sensible Heat Flux over Homogenous Agricultural Land Cover 2004

In the year 2004, mean values for sensible heat flux simulations over homogenous crop fields vary between 29.15 Wm^{-2} and 324.51 Wm^{-2}. The absolute minimum value of -58.55 Wm^{-2} is simulated between the 30th of March and the 6th of April. Minimum values reach

up to 136.99 Wm^{-2} (Aug 5th – 12th). The lowest maximum sensible heat flux occurs between the 1st and 8th of November. The absolute maximum is simulated between the 5th and the 12th of August with 442.32 Wm^{-2}. The standard deviation modulates around 14.84 Wm^{-2} (Nov 1st – 8th), and 92.02 Wm^{-2}(Sept 6th – 13th). Please find the time series plot and Figure 23 and a list of statistical measures in the supplementary materials ("Statistics Sensible Heat Flux Homogenous Agriculture 2004").

Sensible Heat Flux over Heterogeneous Agricultural Land Cover 2004

Mean sensible heat flux simulations over the year 2004 range between 12.48 Wm^{-2} and 330.70 Wm^{-2}. The absolute minimum of -259.99 Wm^{-2} is simulated between the 29th of August and the 5th of September. The highest minimum value amounts to 156.470 Wm^{-2} (Aug 5th – 12th). Maximum sensible heat flux simulations vary between 70.86 Wm^{-2} (Nov 1st – 8th) and an absolute maximum of 457.76 Wm^{-2} (June 26th – July 3rd). The standard deviation fluctuates between 25.43 Wm^{-2} (Oct 24th – 31st) and 114.71 Wm^{-2} (Aug 29th – Sept 5th). Please see Figure 24 for the time series plot and the supplementary materials for a statistical summary ("Statistics Sensible Heat Flux Heterogeneous Agriculture 2004").

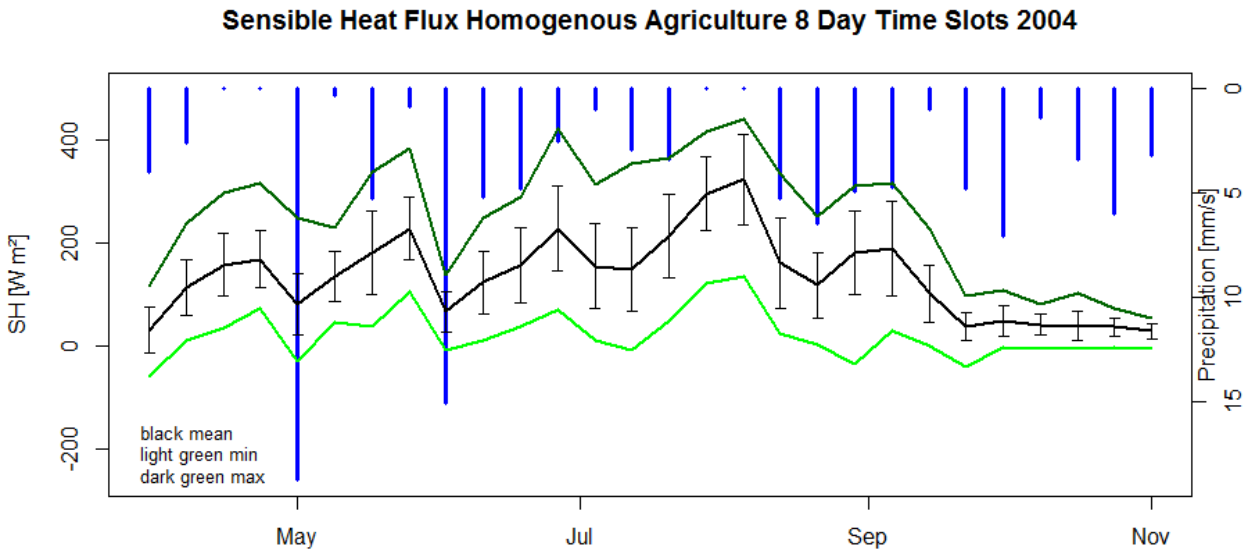

Figure 23: Sensible heat flux aggregated to 8-day time slots (April – Nov 2004) and precipitation.

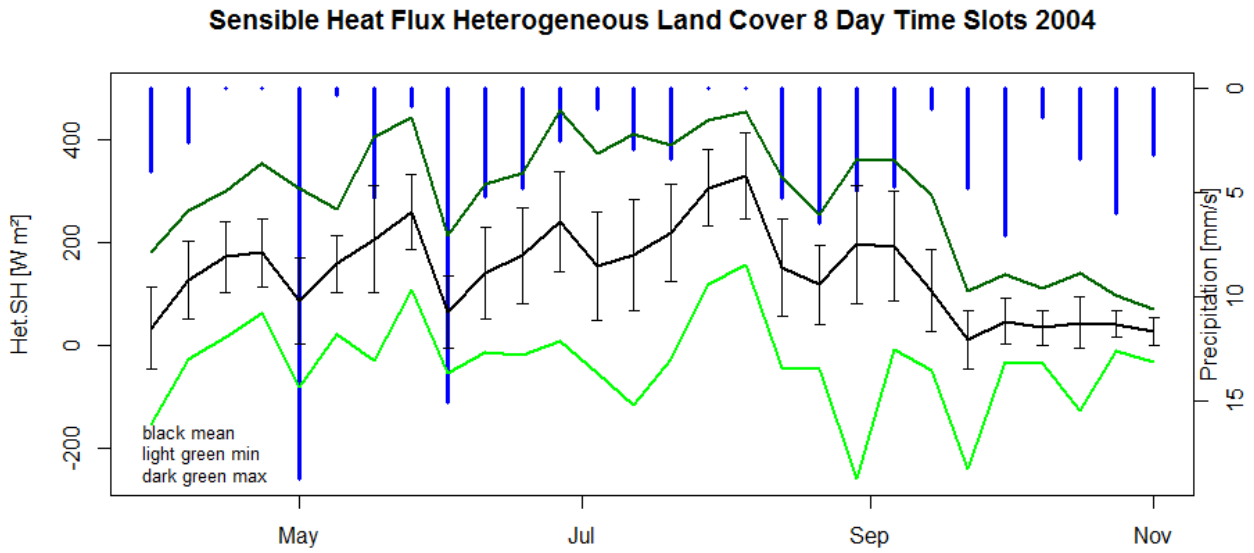

Figure 24: Sensible heat flux over heterogeneous agricultural areas aggregated to 8-day time slots (April – Nov 2004) and precipitation.

7.1.3 Bowen Ratio

Bowen Ratio over Homogenous Agricultural Land Cover 2003

The Bowen ratio, calculated from the mean sensible and latent heat fluxes (eight-day time slots), ranges between 0.23 and 12.55 in the year 2003. It reaches its minimum between the 8th and 15th of October. The Bowen ratio peaks between the 5th and the 12th of August, which is the same timeframe during which the maximum sensible heat flux peaks. Figure 25 displays the Bowen ratio, the sensible and latent heat flux of the year 2003. Please see the supplementary materials for a statistical summary ("Statistics Bowen Ratio Homogenous Agriculture 2003").

Bowen Ratio over Heterogeneous Agricultural Land Cover 2003

The Bowen ratio varies between 0.09 and 7.46 in the year 2003 over heterogeneous agricultural landscapes. Minimum values occur between the 8th and the 15th of October. A maximum Bowen ratio is reached between the 5th and the 12th of August. Figure 26 provides the time series plot of the Bowen ratio, the sensible and latent heat flux for the year 2003 over heterogeneous landscapes. Statistical measures can be found in the supplementary materials ("Statistics Bowen Ratio Heterogeneous Agriculture 2003").

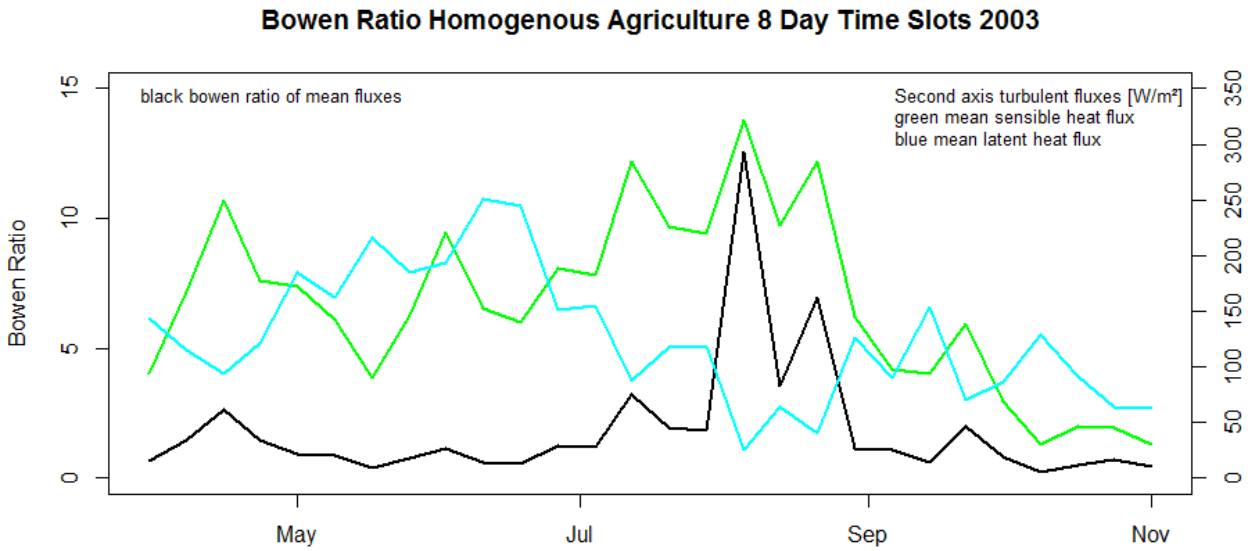

Figure 25: Bowen ratio, sensible and latent heat flux (April – Nov 2003)

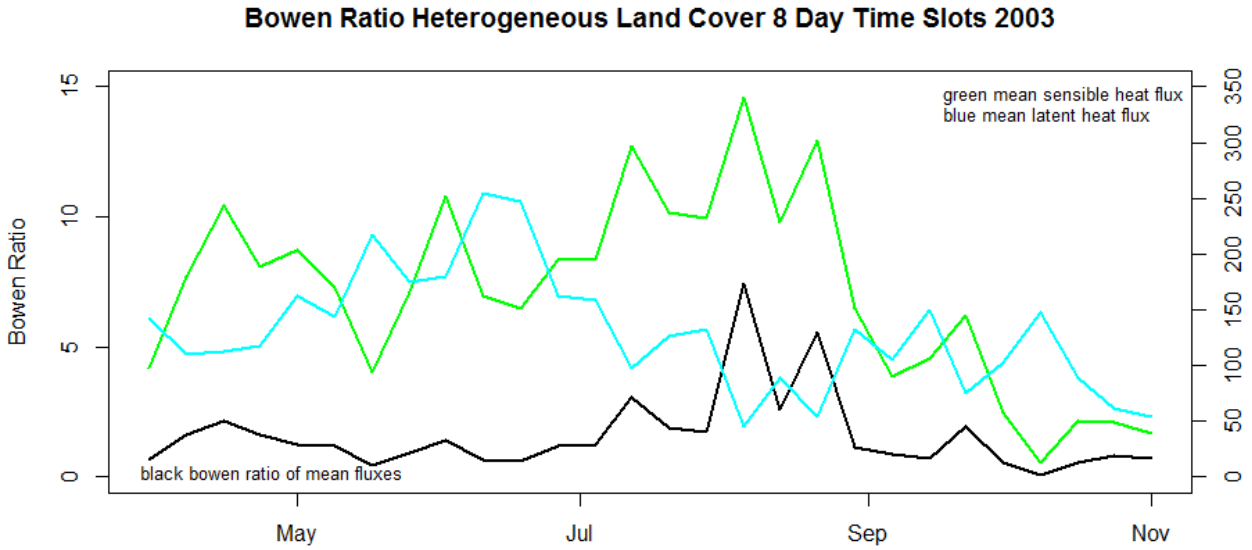

Figure 26: Bowen ratio, sensible and latent heat flux (April – Nov 2003)

Bowen Ratio over Homogenous Agricultural Land Cover 2004

In 2004, the Bowen ratio varies between 0.14 and 10.36. Minimum values occur between 30th of March and the 6th of April. Maximum values a calculated for the 5th to the 12th of August. Figure 27 displays the time series plot of the Bowen ratio, and the sensible and

latent heat flux for the year 2004. Please see supplementary materials for a statistical summary ("Statistics Bowen Ratio Homogenous Agriculture 2004").

Bowen Ratio over Heterogeneous Agricultural Land Cover 2004

In 2004, the Bowen ratio fluctuates between 0.09 and 6.2. Between the 22nd and the 28th of September a minimum is reached. Maximum values occur between the 5th and the 12th of August. Figure 28 displays the time series plot of the Bowen ratio, the sensible and latent heat flux for the year 2004. Statistical measures can be found in the supplementary materials ("Statistics Bowen Ratio Heterogeneous Agriculture 2004").

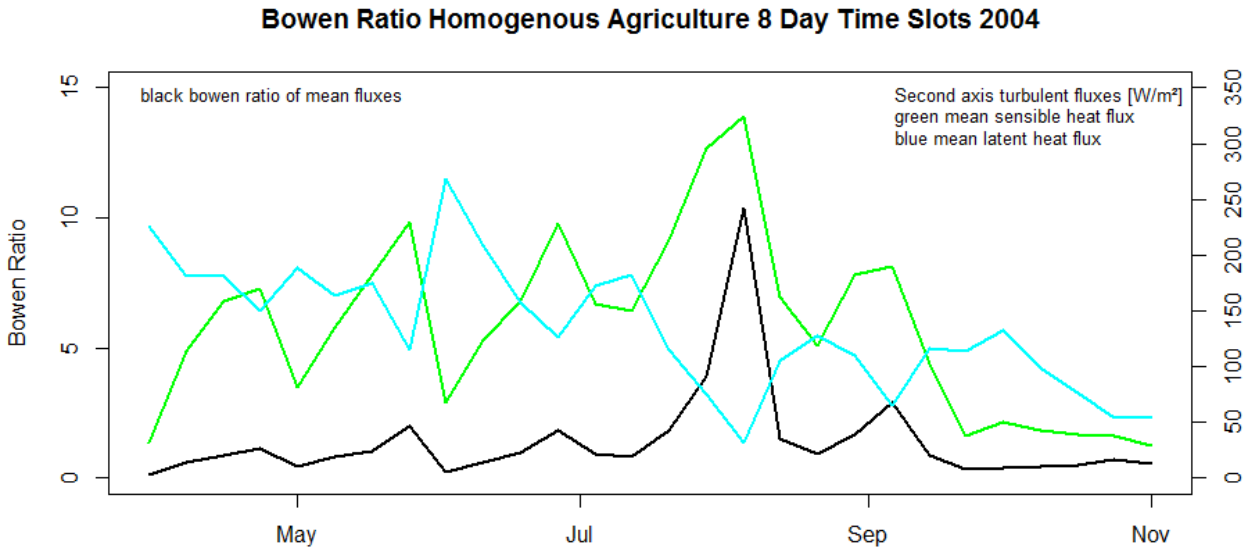

Figure 27: Bowen ratio, sensible and latent heat flux (April – Nov 2004)

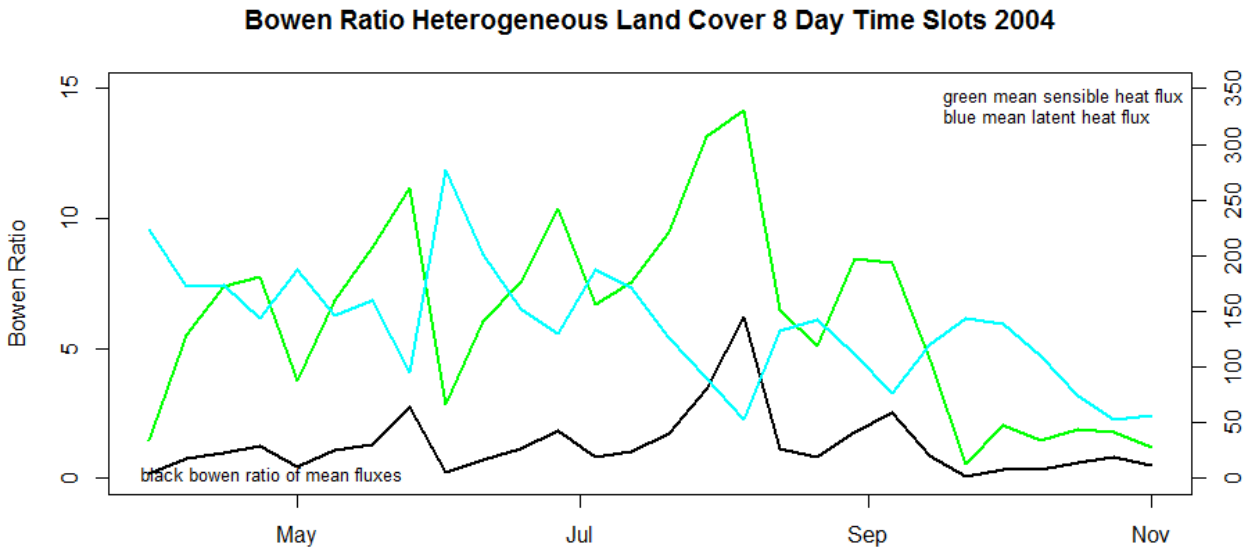

Figure 28: Bowen ratio, sensible and latent heat flux (April – Nov 2004)

7.1.4 Land Surface Temperature

Land Surface Temperature over Homogenous Agricultural Land Cover 2003

Average land surface temperature in the year 2003 ranges between 6.67°C and 41.46°C. The overall lowest value is simulated between the 24th and the 31st of October with -1.79°C; the highest minimum occurs between the 5th and the 21st of August (33.92°C). Maximum values fluctuate between 12.4°C (Oct 24th – 31st) and 59.52°C between the 28th of July and the 4th of August. The standard deviation varies between 2.16°C (Nov 1st – 8th) and 6.94°C (July 28th – Aug 4th). Figure 29 displays the time series plot for 2003. Statistical measures are listed in the supplementary materials ("Statistics Land Surface Temperature Homogenous Agriculture 2003").

Land Surface Temperature over Heterogeneous Agricultural Land Cover 2003

Over heterogeneous agricultural landscapes, land surface temperature was simulated with mean values ranging between 6.16°C and 37.61°C. Minimum values vary between -2.1°C (October 24th – 31st) and 32.3°C (Aug 5th – 12th). The lowest maximum value is simulated between October 24th and 31st with 11.73°C. The absolute maximum land surface temperature simulated occurs between July the 28th and August the 4th and

amounts to 50.7°C. The standard deviation fluctuates around 2.10°C (Nov 1st – 8th) and 6.28°C (April 7th – 14th). Figure 30 shows the time series plot for 2003, an excel sheet is provided in the supplementary material ("Statistics Land Surface Temperature Heterogeneous Agriculture 2003").

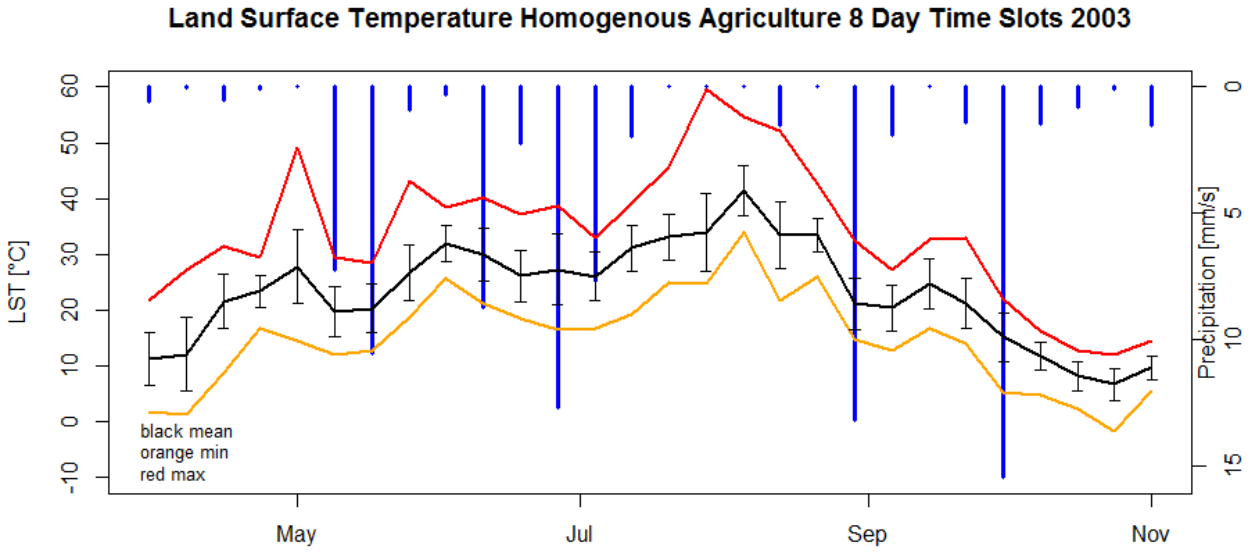

Figure 29: Land Surface Temperature aggregated to 8-day time slots (April – Nov 2003) and precipitation.

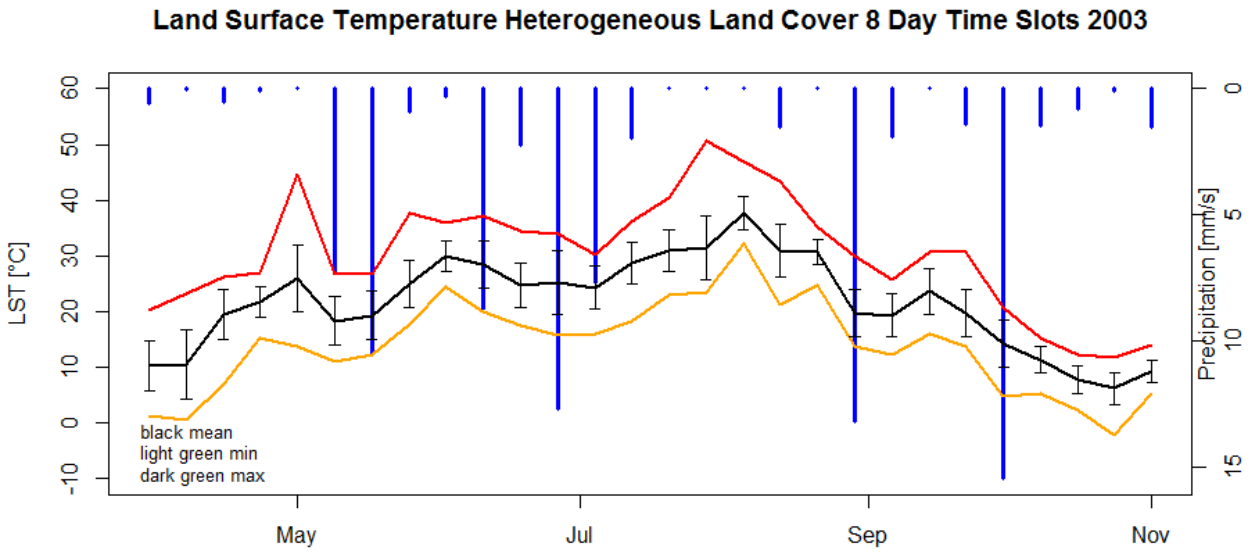

Figure 30: Land Surface Temperature over heterogeneous agricultural areas aggregated to 8-day time slots (April – Nov 2003) and precipitation.

Land Surface Temperature over Homogenous Agricultural Land Cover 2004

Mean values for land surface temperature simulations over the year 2004 vary between 10.82°C and 34.40°C. Minimum land surface temperatures range between 2.28°C (March 30th – April 6th), and 29.54°C (Aug 5th – 12th). The lowest maximum land surface temperature of 14.49°C is simulated between the 1st and the 8th of November; the absolute maximum occurs between the 5th and the 12th of August. The standard deviation ranges between 1.96°C (Sept 22nd – 29th) and 5.59°C (Aug 13th – 20th). Please see Figure 31 for the time series plot 2004 and listed statistical measures in the supplementary materials ("Statistics Land Surface Temperature Homogenous Agriculture 2004").

Land Surface Temperature over Heterogeneous Agricultural Land Cover 2004

Average land surface temperature is simulated between 10.35°C and 31.70°C during the year 2004. Minimum values range between 2.29°C (March 30th – April 6th) and 27.32°C (Aug 5th – 12th). The lowest maximum land surface temperature is simulated between the 1st and the 8th of November and amounts to 13.92°C. The absolute maximum temperature reaches 34.99°C between the 5th and the 12th of August. The standard deviation fluctuates around 1.80°C (Aug. 5th – 12th) and 5.61°C (June 2nd – 9th). Please see Figure 32 for the time series plot 2004 and supplementary materials for statistical listing ("Statistics Land Surface Temperature Heterogeneous Agriculture 2004").

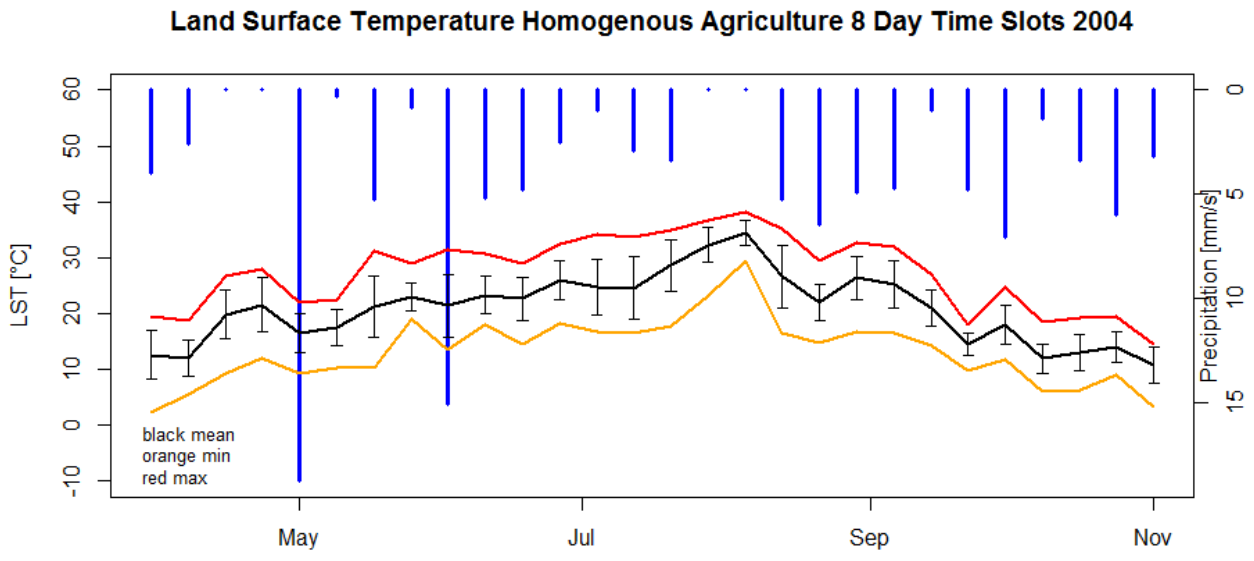

Figure 31: Land Surface Temperature aggregated to 8-day time slots (April – Nov 2004) and precipitation.

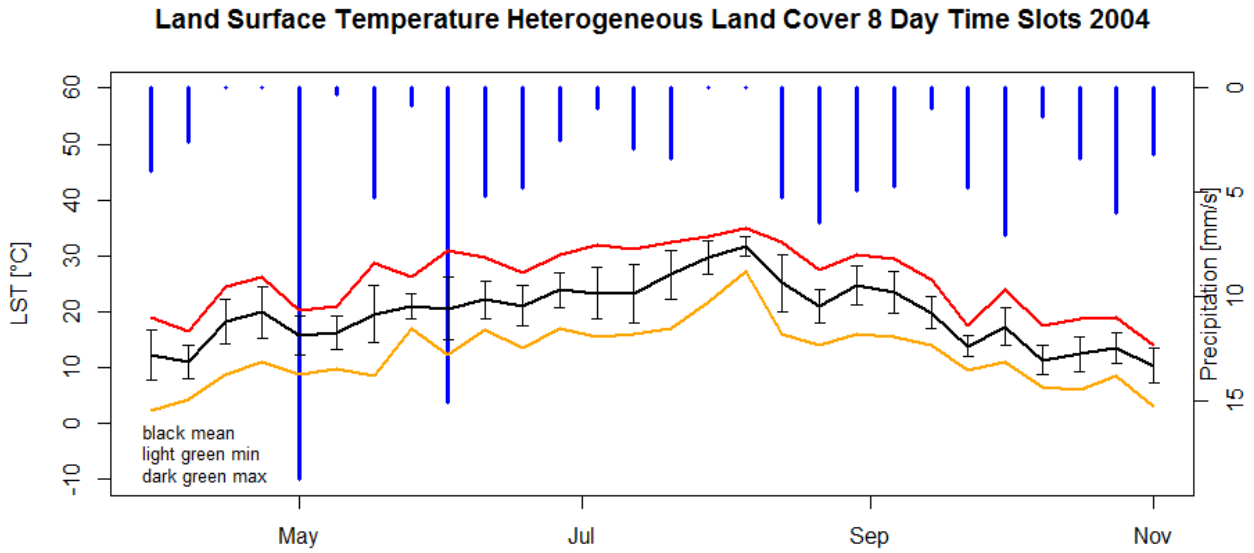

Figure 32: Land Surface Temperature over heterogeneous agricultural areas aggregated to 8-day time slots (April – Nov 2004) and precipitation.

7.2 Results from Spatial Analyses

Land Surface Temperature 2003

Land surface temperature from MODIS data is presented via time series plots, as in the results from SEWAB simulations. However, the variability in the SVAT model results is attributed to time (temporal variability). Land surface temperature from remote sensing products gives information on the spatial variability. The spatial variability of land surface temperature involves a value range of 7.34°C to 41.71°C over the whole study area and all land cover types.

7.2.1 Homogenous Agriculture

Land surface temperature retrieved from remote sensing products ranges between 8.93°C and 39.19°C over homogenous agricultural land cover. Minimum values fluctuate between an absolute minimum of 7.34°C between the 24th and 31st of October and 35.13°C between the 5th and the 12th of August. The lowest maximum value of 10.27°C occurs in the same timeframe as the lowest minimum value. The maximum land surface

temperature is 42.17°C, occurring in the same timeframe as the highest minimum value. The standard deviation fluctuates between 0.54°C (Oct 16th – 23rd) and 3.74°C (Sept 22nd – 29th). Figure 33 provides a time series plot of minimum, mean and maximum land surface temperature of all pixels with underlying homogenous agricultural land cover over the timeframe under investigation.

7.2.2 Heterogeneous Agricultural Land Cover

Average land surface temperature over heterogeneous agricultural land cover ranges between 8.49°C and 37.24°C. The lowest minimum and the lowest maximum values occur in the same timeframes as over homogenous agriculture. Likewise, the highest minimum and maximum values occur in the same time frames as over homogenous agricultural land cover. Minimum land surface temperatures vary between 6.37°C and 33.92°C. Maximum values range between 9.70°C and an absolute maximum of 40.10°C in August. The standard deviation varies between 0.63°C (Oct 16th – 23rd) and 3.12°C (Sept 22nd – 29th). Figure 34 shows the time series plot of land surface temperature over heterogeneous agricultural landscapes in 2003.

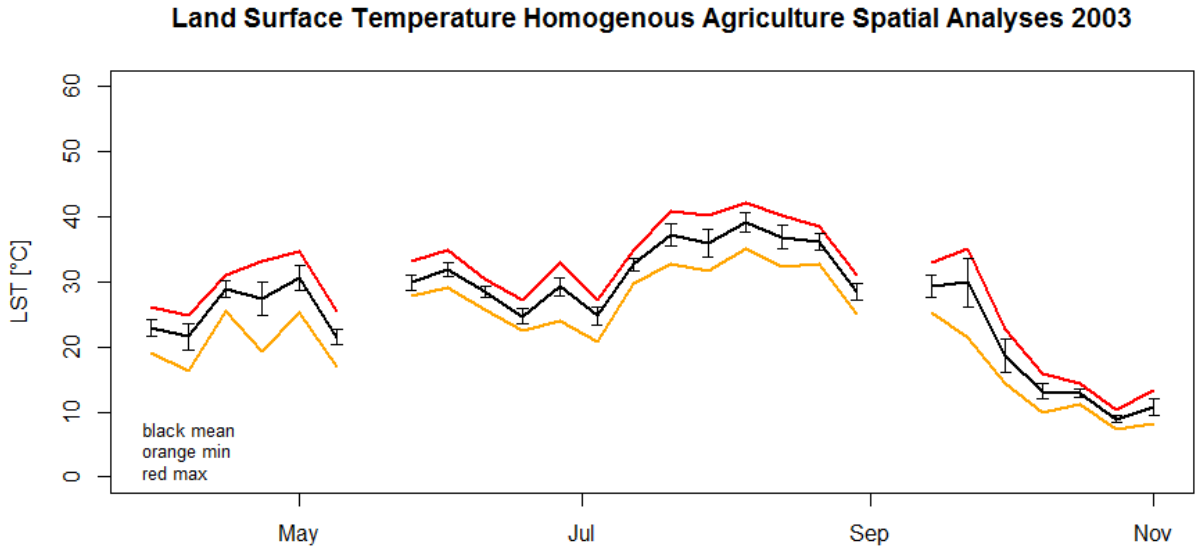

Figure 33: Land surface temperature over homogenous agricultural land cover.

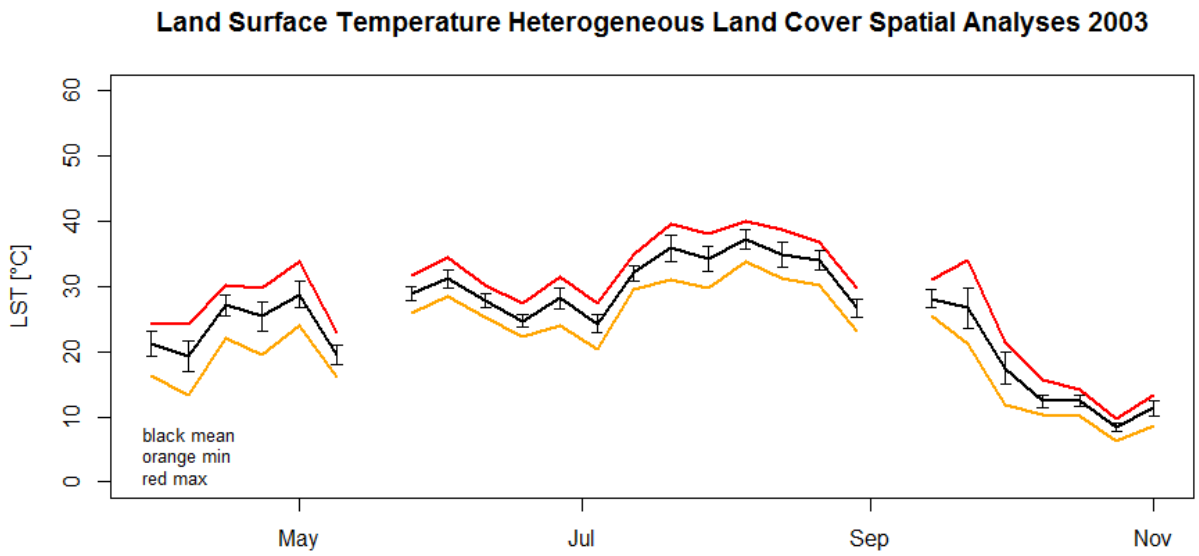

Figure 34: Land surface temperature over heterogeneous agricultural land cover.

8. Discussion

8.1 Comparison of Homogenous and Heterogeneous Land Cover

Homogenous and heterogeneous agricultural land cover structures were compared for their effect on the turbulent fluxes and the land surface temperature. In the following section, the plots presented in the results will be discussed and compared. Furthermore, scatterplots are provided along with RMSE calculations where appropriate. For the latter two computations, hourly values from daytime and nighttime were utilized, between April and the beginning of November. Additionally, Table 1 in the supplementary material provides an overview of the temporal occurrences of lowest and highest mean values, and minimum and maximum values for the main climate variables in model results and spatial analyses.

8.1.1 SVAT Model Simulations

Latent Heat Flux

The scatter plot reveals a good fit between latent heat flux simulations for heterogeneous and homogeneous land cover type during the year 2003 (Fig.35). This is in line with the general similarity of the time series plots (Fig.17 and Fig.18). The root mean squared error

between homogenous agricultural landscapes and heterogeneous land cover for latent heat amounts to 21.98 Wm^{-2}, which is only about 2 Wm^{-2} less than in the year 2004.

Latent heat flux simulations for 2003 over both, homogenous and heterogeneous agricultural landscapes show their maximum values between the 25th of May and the 1st of June. Figure 17 and Figure 18 reveal that latent heat simulations in general, and especially maximum values, react strongly to precipitation. Minimum values fluctuate less than maximum values. However, more irregularities in minima are visible over heterogeneous land cover (Fig.17 and Fig.18). This is likely due to strong fluctuation of turbulent fluxes early in the day and in the late afternoon and to occasional extreme values.

In June, July and August 2003 the latent heat flux diminishes over both land cover types. This can be attributed to a lack of precipitation and high temperatures during the summer months. Figure 17 and Figure 18 show that the latent heat flux reacts strongly to precipitation. The highest mean values for evapotranspiration are simulated between June the 10th and 17th, during a period of heavy precipitation.

Even more rain fell between June 26th and July 3rd. However, under both land cover scenarios latent heat flux diminishes nevertheless. While 16 days earlier, the latent heat flux peaks during rainfall, at the end of June and the beginning of July, evapotranspiration declines even though water is available. This indicates that the soil and the vegetation had a higher water demand than the atmosphere. Constantly low precipitation levels are reported from February 2003 onwards (Fink 2004). Figure 17 and Figure 18 reveal very little rainfall in April, with slightly more precipitation in May and June. In the model simulations the ground must have already been in a state of drying out by the end of June, limiting the availability of water for evaporation.

Under both land cover scenarios, the latent heat flux collapses during summer, showing lowest mean values between August 5th and 12th, which corresponds to the longest dry period. However, the lowest mean value for homogenous agriculture amounts to 25.70 Wm^{-2}. Over heterogeneous land cover average latent heat does not drop below 45.90 Wm^{-2}. These findings partly confirm hypothesis 1, expecting lowest average latent heat flux values to be higher and delayed over heterogeneous landscapes. Lowest mean values occur in the same time period over both land cover types. However, over heterogeneous

agricultural landscapes the lowest mean values remain higher than over homogenous crop fields.

In 2004, maximum values are overall higher over heterogeneous land cover. An explanation would be the capacity of trees to retrieve water from lower ground levels and to regulate water uptake and release (Teuling et al., 2010). This in return would allow for higher maximum values and latent heat flux compared to the treeless homogenous areas.

In the reference year, latent heat simulations are also very similar to each other, over both land cover types (Fig.19, Fig.20, Fig.36). However, the spread for high values is slightly larger than in 2003 (Fig.36). Comparing homogenous and heterogeneous land cover, the RMSE amounts to 23.9 Wm^{-2}. Precipitation was sustained over most of the year, with a rainfall deficit in early August. Average latent heat flux over both land cover types fluctuates throughout the period under investigation, however, lowest mean values do not occur at the same type. Over homogenous crop fields, lowest mean values occur during the same period as in 2003 (Aug 5^{th} – 12^{th}). Over heterogeneous structures, lowest average evapotranspiration is simulated in October. This does not entirely confirm hypothesis 1, because the delay would still be expected within the hot summer period. The lowest mean values differ by 6.3 Wm^{-2} with lower minimum average evapotranspiration over homogenous agriculture, as expected according to hypothesis 1.

Over both land cover types, lowest averages were overall lower during the 2003 summer heat wave, as compared to the reference year. In both years, temporal delay of minimum average latent heat is either not present, or too late in the year to support hypothesis 1. However, it is also possible that the delay falls within one 8-day aggregation period. In support of hypothesis 1 are higher mean evaporation levels over heterogeneous land cover, during the period of lowest average latent heat flux.

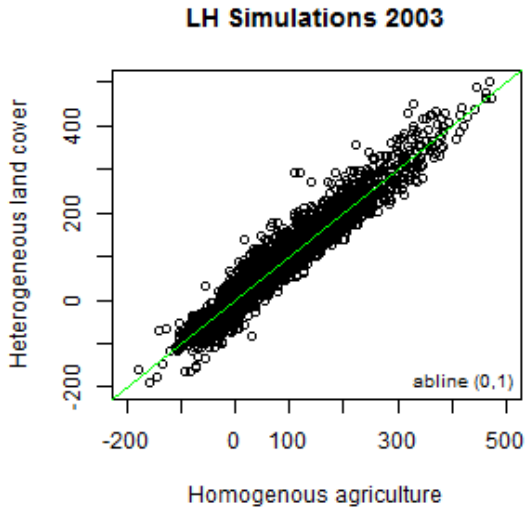

Figure 35: Scatter plot of latent heat flux simulations over homogenous and heterogeneous land cover 2003

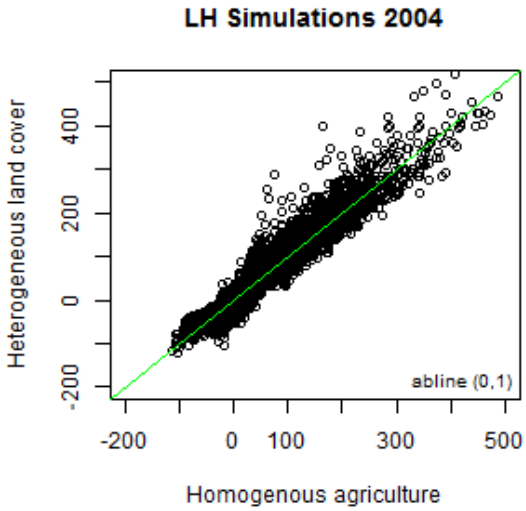

Figure 36: Scatter plot of latent heat flux simulations over homogenous and heterogeneous land cover 2004

Sensible Heat Flux

Over homogenous agricultural landscapes, minimum values fluctuate around 0 Wm^{-2}, while, over heterogeneous landscapes minimum sensible heat flux values drop to less than -200 Wm^{-2}. It is important to keep in mind that scatter plots include daytime and nighttime values (Fig.37 and Fig.38). However, like for latent heat, fluctuations of minimum and maximum values are not surprising.

Comparing sensible heat flux simulations over homogenous and heterogenous agricultural landscapes during the snow free period of 2003 and 2004 shows almost the same error variance for both years (RMSE (2003) = 24.31 Wm^{-2} and RMSE (2004) = 24.94 Wm^{-2}). Scatter plots reveal very similar values of sensible heat flux simulations over heterogeneous and homogenous agriculture during the heat wave and the reference year (Fig.37 and Fig.38). In the lower value range a wider spread of data is visible in 2004.

Furthermore, generally SH values are slightly higher over heterogenous agriculture (Fig.37 and Fig.38). A wider range of senible heat of heterogeneous land cover is reflected in averages of daytime values of 8-day time slots (Appendix Table 1).

These differences are within expectations, as sensible heat flux over forest landscapes can be expected to be higher, compared to lower vegetation (Teuling et al., 2010). Particularly in the occurrence of drought and heat waves, the sensible heat flux over forest is expected

to increase. However, according to Teuling et al. (2010), sensible heat flux is initially higher over forest than over grassland, but this trend may reverse in the course of the summer drought (Teuling et al., 2010). Sensible heat flux simulations of the study at hand to not show a reversing of SH magnitudes depending on the presence of forest patches. This is likely due to the energy balance closure by the model, leading to a larger share of available energy being assigned to SH, when LH is restricted by water availability. This, together with a prologued precipitation deficit, may outweigh the balancing effect of forest on sensible heat druing the heat wave.

Furthermore, The highest mean values of sensible heat occur in the same time period in both years and over both land cover types (Aug 5th – 12th). In both years, homogenous agriculture shows higher SH values during the timeframe, when mean sensible heat flux peaks. In comparison to latent heat, this is the same time frame, during which latent heat reaches its lowest average values (except in 2004 over heterogeneous land cover) (see above). Therefore, sensible heat flux simulations do not support hypothesis 1. The reason is likely the same as described above. Stage 2 and 3 (Teuling et al. 2010) in the process of surface drying are reached. Thus, the unavailability of water heavily restricts evapotranspiration. According to the energy balance closure, excess energy is allocated to the sensible heat flux.

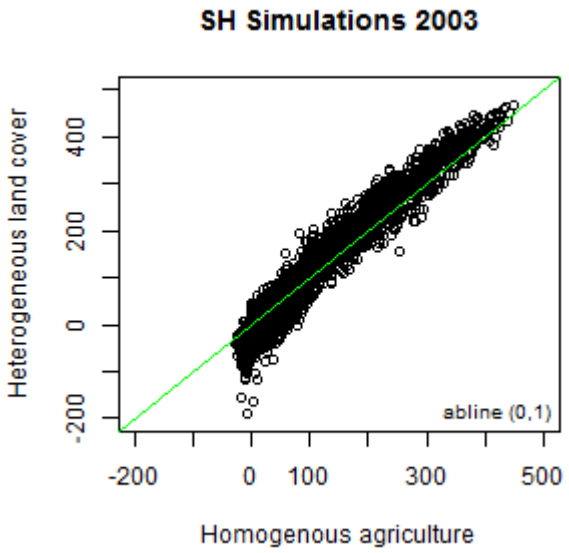

Figure 37: Scatter plot of sensible heat flux simulations over homogenous and heterogeneous land cover 2003.

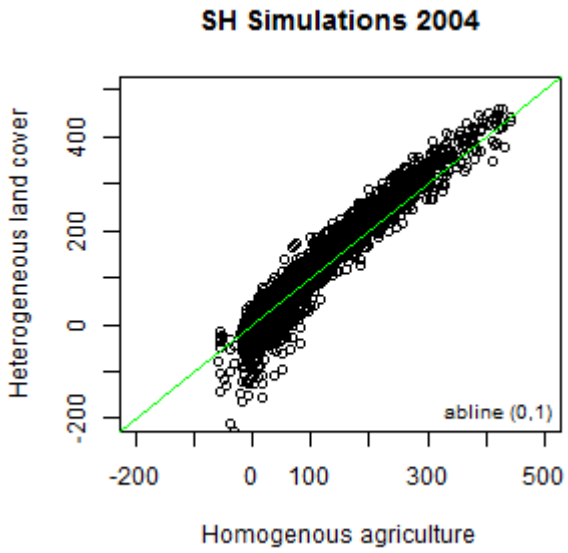

Figure 38: Scatter plot of sensible heat flux simulations over homogenous and heterogeneous land cover 2004.

Bowen Ratio

The Bowen ratio gives further insight into the division of energy and water. In the year 2003 heterogeneous land cover reveals a lower and narrower range of the Bowen ratio (0.09 – 7.46), compared to homogenous agriculture. Over homogenous crop fields, the ratio only drops to a minimum of 0.23 and reaches a maximum of 12.55. The Bowen ratio peaks in August 2003 (Fig.25 and Fig.26). This is not unexpected, because August was the month when the heat wave, and simultaneously the drought, hit the hardest (Miralles et al., 1012; Fischer et al., 2007). However, the maximum peak is clearly more pronounced over homogenous agriculture. Thus, the sensible heat flux received a larger share of the available energy over homogenous crop fields. These results confirm the expectation of a more stable Bowen ratio over heterogeneous landscapes than over homogenous agricultural areas (hypothesis 2).

A similar pattern is observable in the year 2004. Under both land cover scenarios, the Bowen ratio peaks during the same period when maximum average sensible heat flux is simulated (Aug 5th – 12th). However, over heterogeneous landscape, this peak is less pronounced than over homogenous crop areas, and only reaches a maximum of 6.2. Over homogenous agriculture, the maximum Bowen Ratio amounts to 10.36. The minimum is 0.14, as compared to 0.09 over heterogeneous land cover. Over the rest of the timeframe, the Bowen ratio of both land cover types is relatively stable, however slightly more stable over heterogeneous areas.

Thus, in both years, the Bowen ratio indicates that the sensible heat flux gets a larger share of the available energy over homogenous crop fields during hot and dry summer periods, compared to heterogeneous agricultural landscapes. This supports hypothesis 2 and indicates that forest patches provide regulating ecosystem services in agricultural landscapes. Namely, the partitioning of the available energy is regulated by forest patches, leading to a more balanced behavior of the turbulent fluxes.

Land Surface Temperature

In 2003 mean land surface temperature over homogenous crop fields varies between 6.67°C and 41.46°C, as compared to a range of 6.16°C to 37.61°C over heterogeneous landscapes. While lower mean values differ only slightly between LC structures, the highest average LST value is about 4°C lower of heterogeneous land cover. This trend is even more pronounced for maximum land surface temperatures, which differ by almost

10°C. While homogenous agriculture reaches values of 59.52°C, heterogeneous land cover only heats up to 50.70°C maximum. Thus, hypothesis 3 is strongly supported.

A distinction of land cover structures by high land surface temperature values is also visible in the scatter plots. While surface temperature of homogenous land cover keeps rising, simulations for heterogeneous land cover flatten out at the top end of the value range (Fig.39, Fig.40). This pattern is visible in both years, however, more pronounced in 2003, when overall land surface temperature values reach higher levels than in 2004. Forest patches thus show a regulating effect on surface temperatures. Particularly during the 2003 summer heat wave, the occurrence of forest islands in agricultural landscapes leads to lower average and less intense maximum temperatures.

The RMSE, comparing day time and night-time values of the timeframe under investigation, amounts to 1.34°C in the year 2003. A slightly lower RMSE of 1.07°C is computed for the year 2004. Thus, in the year of drought and heat wave, the difference between homogenous and heterogeneous agricultural structures in their influence on surface temperature is greater than in the reference year.

The time series plots show that over both land cover structures, surface temperature peaks in the same timeframe, namely between July 28th and August 4th 2003. In July and August, land surface temperatures are the highest, which is within expectation as these are the months of drought and heat wave (Fig.29 und Fig.30) (Fink 2004). In 2004, July and August are also the months with the highest surface temperatures. However, average and maximum temperatures are lower than in 2003. The peak at the end of July/ beginning of August is less pronounced in 2004 than in 2003 (Fig.29 und Fig.30). This is likely due to less direct SWD reaching the surface in 2004, because higher precipitation levels indicate the presence of more clouds than in 2003.

In 2004, maximum surface temperature over homogenous agriculture (38.18°C) and heterogeneous agriculture (34.99°C) differ by approximately 4°C, which is only half as much difference as in the year 2003. This indicates a greater level of ecosystem services provisioning during drought and heat wave, as compared to what can be considered a normal year in climatic terms. While the reference year also confirms hypothesis 3, the regulation of maximum surface temperatures by forest patches is strongest during heat waves, according to the findings of this study. Thus, the supply of this ecosystem service reaches its maximum, when the demand is highest.

The ranges of mean values are lower than in the year 2003. Highest mean values differ by about 3°C between land cover structures, which is 1°C less than in 2003. Thus, average values confirm that surface temperature regulation by forest patches is stronger during the year of drought and heatwave than during the reference year (see above).

Lower land surface temperatures over heterogeneous agricultural landscapes than over homogenous crop fields confirm hypothesis 3, thus showing the relevance of forest patches in agricultural landscape structuring for temperature regulation, particularly during heat waves.

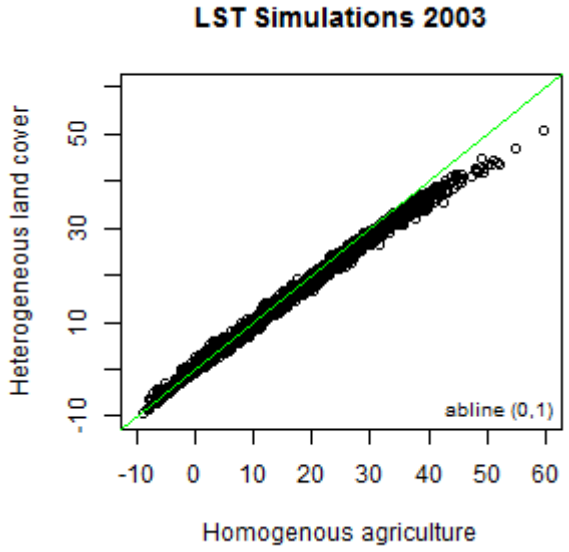

Figure 39: Scatter plot over land surface temperature simulations of homogenous and heterogeneous land cover 2003.

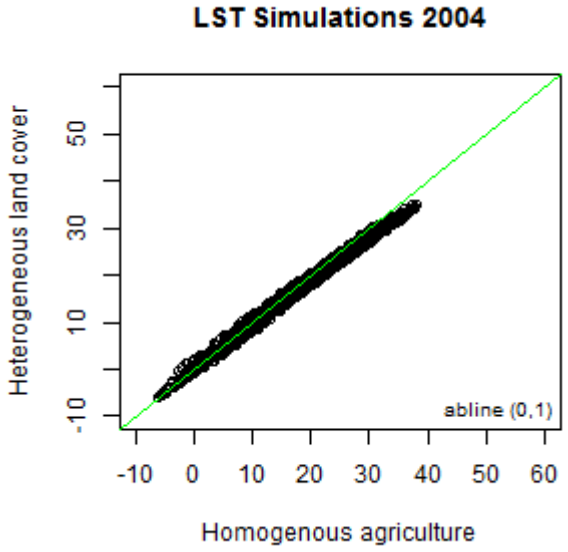

Figure 40: Scatter plot over land surface temperature simulations of homogenous and heterogeneous land cover 2004.

8.1.2 Land Surface Temperature from Spatial Analyses

The spatial analysis confirms the findings of model simulations. However, simulated mean values are temporal aggregations while the spatial analysis gives insight into spatial variations. The scatter plot reveals overall slightly lower temperatures over heterogeneous landscapes (Fig.41). An RMSE value of 1.53°C confirms that heterogeneous structuring of agricultural landscapes provides the ecosystem service of regional surface temperature regulation.

The range of land surface temperature over homogenous agriculture (8.93°C – 39.19°C) differs from values over heterogeneous land cover (9.49°C – 37.24°C), mainly in the higher range. Mean surface temperatures of homogenous areas peak at about 2°C higher than surface temperatures over heterogeneous land cover. This implies that heterogeneous land cover provides higher levels of the surface regulating ecosystem service than homogenous crop fields.

Over heterogeneous land cover, the higher end of the mean range is similar to model simulations (Appendix Table 1). Over homogenous agriculture, the highest mean values are about 2°C lower compared to model simulations. Continuing this trend, maximum land surface temperature values retrieved from remote sensing data remain below 43°C over both land cover structures, and maximum values are almost 10°C lower than maximum surface temperatures simulated by the SVAT model (Appendix Table 1).

The differences in mean and maximum values can be explained by the type of data being aggregated. Temporal aggregations from the micrometeorological model consider the whole range of temperature values during the day. The land surface temperature product provided from remote sensing data already comes as average daytime values aggregated to eight-day periods. This explains why the spatial data shows much lower maximum values of surface temperature than model simulations.

Furthermore, the overall variance of model simulations is higher than the variance observed in spatial aggregations. This is within expectation, as the temporal effect of temperature during the day is expected to be higher than the influence of land cover. In other words, the temperature differences between the morning and midday are higher than the differences between mean temperatures measured over different land cover types at the same time.

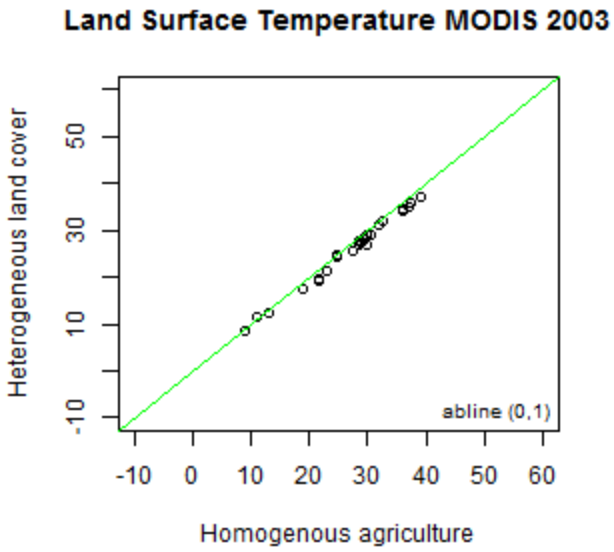

Figure 41: Scatter plot of MODIS land surface temperature over homogenous and heterogeneous land cover.

8.2 Limitations of the Study

8.2.1 Model Evaluation for Land Cover Type Agriculture

Despite several model calibration steps, the overestimation of sensible heat flux in June and correspondingly the underestimation of the latent heat flux, could not be eliminated. In July and August, the reverse simulation errors occur. Figure 42 displays sensible heat flux observations and simulations as well as precipitation and air temperature. Figure 43 displays latent heat flux observations and simulations together with precipitation and air temperature. Little precipitation throughout May and a lack thereof in the first half of June, together with very high air temperatures, may be responsible for the model's behavior. Consequently, it can be concluded that the model does not compute unreasonable turbulent fluxes in relation to air temperature and precipitation availability.

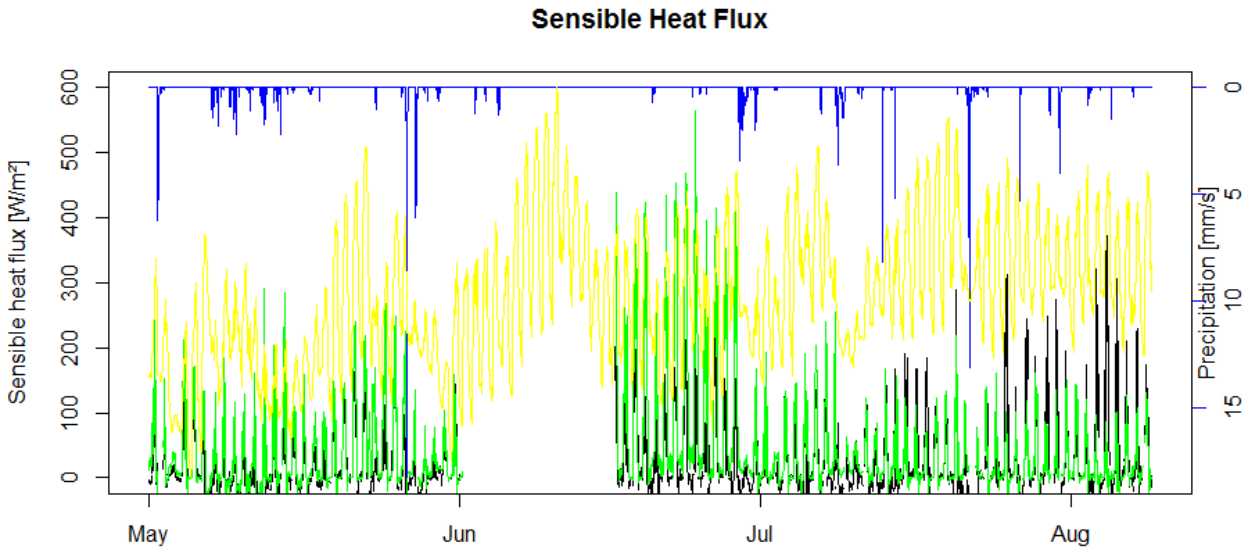

Figure 42: Time series plot from May to August for sensible heat flux at Scheyern. Black = sensible heat flux observations. Green = sensible heat flux simulations. Blue = precipitation. Yellow = air temperature. Please note that no axis for air temperature is available.

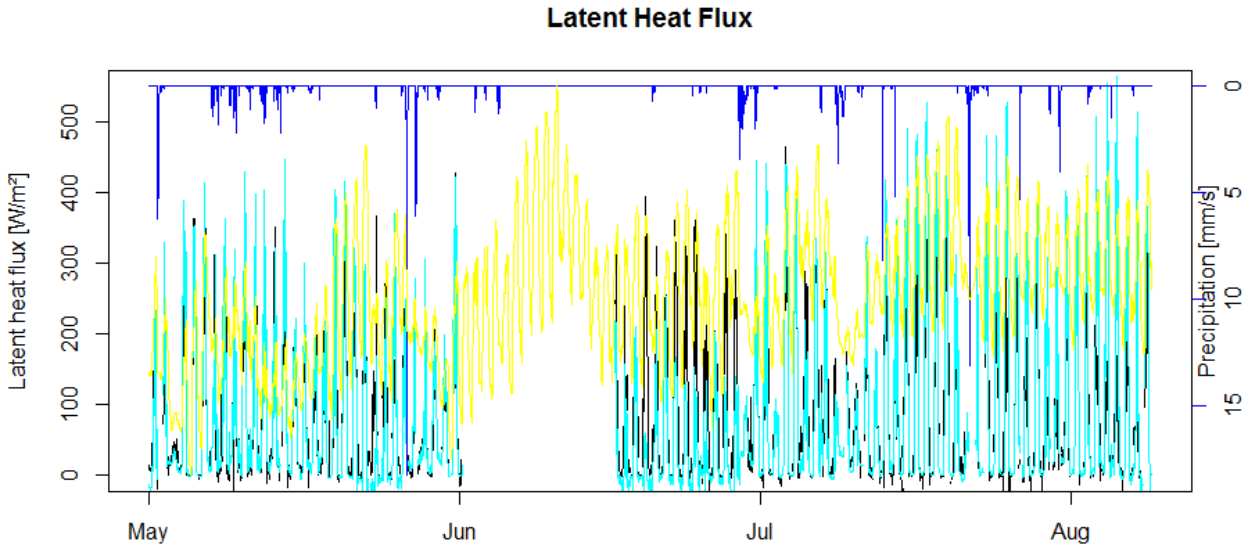

Figure 43: Time series plot from May to August for latent heat flux at Scheyern. Black = latent heat flux observations. Light blue = latent heat flux simulations. Blue = precipitation. Yellow = air temperature. Please note that no axis for air temperature is available.

When the forcing data for model calibration at Scheyern was created, down-welling longwave radiation had to be calculated. In the process, the temperature of the measurement device had to be substituted by air temperature. It is possible that these

compromises lead to distortions in the radiation budget, which may result in flawed flux simulations. However, inspection of the radiation budget shows continuous and intense down-welling short wave radiation and up welling longwave radiation in the month of June (Appendix Fig.8). This is reasonable, considering that a lack of precipitation and high air temperatures in the month of June indicate unlikeliness of cloud cover. Nevertheless, the above-mentioned potential error source does exist. Please note that Figure 8 in the Appendix shows the radiation budget for field 18 exemplary for both fields because differences are minor.

The development of soil moisture corresponds to the lack of precipitation and high temperatures (Appendix Fig.9). The water content in the top soil layer, but also the total soil column, decreases continuously with approaching summer. The month of June is distinguishable by its dryness. Please note that Figure 9 in the Appendix displays the soil moisture development over field 18 exemplary for both fields because differences are minor. The partitioning of water appears reasonable.

The components which comprise latent heat flux give further insight into model behavior (Appendix Fig.10). Please note that in Figure 10 in the Appendix field 18 is shown exemplary for both fields due to minor differences. In June levels of transpiration and evaporation drop to a minimum. This indicates that a general lack of water restricted the latent heat flux. Consequently, the sensible heat flux received a much higher share of energy in model simulations.

Simulations are not in agreement with the data calculated from the Turbulenzknecht. The data supplied for model evaluation, contains a large data gap in the first half of June and several data gaps throughout the evaluation period, which ends in August. It is possible that the data for the second half of June also contains errors. This suspicion is suggested by the closeness to a large data gap.

However, from the investigations above, the conclusion is drawn that in the simulation runs for the research site Scheyern, the month of June displays an imbalance in the turbulent fluxes due to persisting hot and dry conditions. The development of sensible and latent heat flux, the individual components comprising the latent heat flux, the development of soil moisture, precipitation, air and land surface temperature all follow the same pattern. Thus, the simulations are coherent.

The reason for this model behavior is likely the same reason as for unexpected patterns in the turbulent fluxes at the research area. A lasting lack of precipitation together with high levels of radiation cause SEWAB to allocate the largest share of the available energy to the latent heat flux

8.2.2 Model Application at the Research Area

For the application of the SVAT model at the research area, down-welling shortwave and longwave radiation had to be parameterized from information on cloud cover. While the radiation budget appears overall reasonable, sometimes overestimation of longwave radiation is suspected at nighttime. Periods of about 1 to 3 days occur, during which net longwave radiation is in the positive value range at night. This suggests that the sky reaches higher temperatures than the ground, which is rarely the case. However, such unrealistic simulations do not occur consistently. Figure 14 in the Appendix shows the radiation budget of October 2003 as a month when the supposedly wrong simulations occur frequently compared to most other months during the simulation period. However, this does not distort the results of this study, because nighttime values were not considered.

A limitation in the simulation of heterogeneous landscapes from model simulations arises from the tile approach (50% weighing of agriculture and forest, respectively). The role of forest as an air flow obstacle is not considered in the study at hand.

Regarding the spatial analysis, some distortion of land surface temperature may occur from water and urban land cover. However, the study area was chosen so that the share of those two land cover types is kept to a minimum. Furthermore, the heat increasing effect of urban areas and the temperature regulating effect of water would be expected to cancel each other out to a certain extent.

8.2.3 Extrapolation into the future

Another restriction should be mentioned, regarding the ability to draw conclusions for the future. In the future climate, we not only expect higher temperatures and an increase in extreme events, but also higher average moisture content in the atmosphere. While this does not distort the results of the study at hand, when extrapolating the results into the

future, caution must be paid to the fact that the interaction between the land surface and the atmosphere will be influenced also by a general increase of water vapor in the boundary layer (Pielke & Niyogi, 2013).

9. Conclusion

Regional climate regulation is a crucial aspect in the attempt to tackle climate change. Increasing the level of understanding for the processes involved in the interaction between the land surface and the atmosphere is one step towards improved mitigation and adaptation strategies. Applying this knowledge to landscape planning, the ecosystem service of regional climate regulation can be increased. As shown in this work, through the structuring of the landscape, agricultural areas can become more resilient to extreme events, such as summer droughts and heat waves.

The results of the study at hand confirm the hypotheses with few exceptions. According to hypothesis 1, during hot and dry summer months, a maximum in sensible heat and a minimum in latent heat flux is diminished and delayed over heterogeneous land cover. A delay cannot be detected in the turbulent fluxes. However, higher levels of evapotranspiration are sustained over heterogeneous land cover during the time, when average latent heat flux reaches a minimum. Thus hypothesis 1 is partly confirmed.

The reason why the results only partly confirm hypothesis 1 lies in the equations of the SVAT model. The closure of the energy balance leads to an increased share of energy being allocated to the sensible heat flux, when latent heat is restricted by water availability. Thus, in periods of very high radiation amounts reaching the ground, and a prolonged lack of precipitation, SEWAB tends to simulate extremely high levels of sensible heat flux. For future applications of SEWAB, this needs to be considered.

Nevertheless, the Bowen ratio between SEWAB simulation fluxes is more balanced over heterogeneous land cover. While it still peaks during the heatwave, the peak is lower over heterogeneous land cover. The supports hypothesis 2, which states that the Bowen ratio remains more stable over heterogeneous agricultural landscapes. It can be concluded, that heterogeneous agricultural landscapes balance the partitioning of energy between the sensible and the latent heat flux better than homogenous crop growing areas.

The strongest support of regional climate regulating ecosystem services being supplied by heterogeneous agricultural landscapes is provided by the simulations of land surface temperature and by the spatial analyses. Average land surface temperature has been found to be lower over heterogeneous landscapes. Therefore, hypothesis 3 is confirmed. Moreover, maximum surface temperatures are considerably higher over homogenous agriculture and the delivery of this regional climate regulating service is increased during summer extremes, when it is most demanded.

From the results of this study, the conclusion can be drawn that heterogeneous agricultural landscapes are more resilient to extremely hot and dry summer periods than homogenous landscapes. Thus, hypothesis 4 is affirmed. This can be attributed to the ecosystem service of regional climate regulation, provided by patches of forest in the agricultural landscape.

Under the premises of climate change projections of higher temperatures and more frequent summer heat waves and droughts, regional climate regulation through landscape structuring is a promising approach. It can increase the resilience of agricultural landscapes, and therefore increase the chances to achieve food security for a growing world population.

Furthermore, regional climate regulation through land cover structuring is effective locally, yet applicable on a global scale. This resource extensive intervention does not involve much technical expertise, which may not be available in some parts of the world. While the intensification of agriculture with heavy machinery is still leading to a reduction of landscape complexity, creating more heterogeneous landscapes may be an effective tool for sustainable development worldwide.

Returning to a patchier landscape structure is also promising in countries like Germany, where the history of intensive farming and attempts to "improve" the landscape (such as *Flurbereinigung*) have caused a depletion of ecosystem services in crop growing areas (Power, 2010; Kovacs-Hostyanszki et al., 2017; Grunewald et al., 2015). Increasing the share of forest patches is a feasible strategy to increase the adaptive capacity of agricultural landscapes to changing climatic conditions in the future. It can also be considered a premise to increase the resilience of these areas to climatic extreme events.

Furthermore, forest patches within agricultural lands would also provide other ecosystems services, such as erosion control, and higher levels of biodiversity, since they

break up the dominance of cultivated plants. Patches of permanent, natural vegetation provide habitat to insects, thus contributing to pollinating ecosystem services (Grunewald & Bastian, 2015). While not the focus of this work, these added benefits need to be taken into account in the process of landscape planning.

At the same time, this research could be expanded to include different climates and different regions. Annual and perennial crops need to be considered, as well as the agricultural and societal history of different places, and the underlying topography. Such factors shape the landscape structure, therefore setting the scene for planned interventions. To inform landscape planning and policy making alternative agricultural practices, such as permaculture, may provide prospects to increase climate change resilience. Techniques involving permanent vegetation cover, e.g. through cover crops, should be examined in more detail for their regional climate regulating potential.

The scientific field of land surface modelling holds great potential to generate knowledge about the interaction between land cover structure and the atmosphere. This provides a basis for aimed intervention in order to mitigate the development of droughts and heatwaves under changing environmental conditions. Furthermore, forest patches increase the resilience of agricultural landscapes to such extreme events. Heterogeneous structuring of agricultural lands provides the means to increases regional climate regulating ecosystem services and enhance the chances of a food secure world in the future.

References

Alavipanah, S., Wegmann, M., Qureshi, S., Weng, Q., & Koellner, T. (2015). The role of vegetation in mitigating urban land surface temperatures: a case study of Munich, Germany during the warm season. *Sustainability, 7*(4), 4689-4706. DOI: 10.3390/su7044689.

Aleixandre-Benavent, R., Aleixandre-Tudó, J. L., Castelló-Cogollos, L., & Aleixandre, J. L. (2017). Trends in scientific research on climate change in agriculture and forestry subject areas (2005–2014). *Journal of Cleaner Production, 147,* 406-418.DOI: 10.1016/j.jclepro.2017.01.112.

Ali, A., De Bie, C. A. J. M., Skidmore, A. K., Scarrott, R. G., & Lymberakis, P. (2014). Mapping the heterogeneity of natural and semi-natural landscapes. *International Journal of Applied Earth Observation and Geoinformation, 26*, 176-183. DOI: 10.1016/j.jag.2013.06.007.

Arya, S. Pal (1988). Introduction to micrometeorology. In J. Holton (Ed.), *International geophysics series* (42). San Diego, California: Academic Press.

Babel, W., Biermann, T., Coners, H., Falge, E., Seeber, E., Ingrisch, J., ... & Willinghöfer, S. (2014). Pasture degradation modifies the water and carbon cycles of the Tibetan highlands. *Biogeosciences, 11*(23), 6633-6656. DOI: 10.5194/bg-11-6633-2014.

Babel, W. (2017). *Models in Micrometeorology: Carbon and water budgets from ecosystem to landscape scale. Bottom-up modelling, model structures.* [Lecture slides]. Retrieved from https://elearning.uni-bayreuth.de/course/view.php?id=15431 [last access 24.05.2017].

Bahrenberg, G., Böhn, D., Köck, H., & Taubmann, W. (1999): Agrarwirtschaftliche und ländliche Räume. In W. Taubmann (Ed.), Handbuch des Geographieunterrichts (Band 5). Köln: Aulis-Verlag Deubner.

Baldocchi, D., Falge, E., Gu, L., Olson, R., Hollinger, D., Running, S., ... & Fuentes, J. (2001). FLUXNET: A new tool to study the temporal and spatial variability of ecosystem–scale carbon dioxide, water vapor, and energy flux densities. *Bulletin of the American Meteorological Society, 82*(11), 2415-2434.

Bayerische Vermessungsverwaltung (2017). AKTIS-Digitales Landschaftsmodell-DLM25.

Bayerisches Landesamt für Umwelt (LFU) (2012*). Klimabericht Bayern. Der Klimawandel in Bayern. Auswertung Regionaler Klimaprojektionen*. Retrieved from http://www.bestellen.bayern.de/shoplink/lfu_klima_00082.htm [last access 25.08.2017].

Bayerisches Landesamt für Umwelt & Bayerisches Landesamt für Wald und Forstwirtschaft (2010). *Handbuch der Lebensraumtypen nach Anhang I der Fauna-Flora-Habitat-Richtlinie in Bayern.* Augsburg & Freising-Weihenstephan. Retrieved from https://www.lfu.bayern.de/natur/biotopkartierung_flachland/kartieranleitungen/doc/lrt_handbuch_201003.pdf [last access 18.08.2017].

Bayerisches Landesamt für Wald und Fortwirtschaft (n.d.). *Die Waldkiefer (Pinus sylvestris L.).* Retrieved from http://www.lwf.bayern.de/waldbau-bergwald/waldbau/082195/index.php [last access 18.08.2017].

Biermann, T. (2014). *Eddy-covariance measurements as a tool for ecological and hydrological studies on the Tibetan Plateau.* Doctoral Dissertation, University of Bayreuth. Retrieved from https://epub.uni-bayreuth.de/1840/ [last access 26.08.2017].

Biermann, T., Babel, W., Ma, W., Chen, X., Thiem, E., Ma, Y., & Foken, T. (2014). Turbulent flux observations and modelling over a shallow lake and a wet grassland in the Nam Co basin, Tibetan Plateau. *Theoretical and applied climatology, 116*(1-2), 301-316. DOI: 10.1007/s00704-013-0953-6.

Black, E., Blackburn, M., Harrison, G., Hoskins, B., & Methven, J. (2004). Factors contributing to the summer 2003 European heatwave. *Weather, 59*(8), 217-223.

Bundesanstalt für Geowissenschaften und Rohstoffe, BGR (n.d.): Bodenatlas Deutschland. https://geoviewer.bgr.de/mapapps/resources/apps/bodenatlas/index.html?lang=en&tab=boedenDeutschlands [last access 25.08.2017].

Campbell Scientific, Inc. (2011): CNR1 Net Radiometer. Instruction Manual. Revision: 5/11.

Deshi, K.E., Obasi, M.O., Odiaka, N.I., Kalu, B.A., & Ifenkwe, O.P. (2015). Leaf Area Index Values of Potato (*Solanum tuberosum* L.) Stored For Different Periods in Different Kinds of Stores. *Journal of Agriculture and Veterinary Science, 8*(1), 09-19.

Díaz-Varela, E., Roces-Díaz, J. V., & Álvarez-Álvarez, P. (2016). Detection of landscape heterogeneity at multiple scales: Use of the Quadratic Entropy Index. *Landscape and Urban Planning, 153*, 149-159. DOI: 10.1016/j.landurbplan.2016.05.004.

DWD Climate Data Center (CDC) (2017a). Historische stündliche Stationsmessungen der Niederschlagshöhe für Deutschland, Version v005.

DWD Climate Data Center (CDC) (2017b). Historische stündliche Stationsmessungen des Luftdrucks für Deutschland, Version v004

DWD Climate Data Center (CDC) (2017c): Historische stündliche Stationsmessungen der Lufttemperatur und Luftfeuchte für Deutschland, Version v005.

DWD Climate Data Center (CDC) (2017d): Historische stündliche Stationsmessungen der Windgeschwindigkeit und Windrichtung für Deutschland, Version v005.

DWD Climate Data Center (CDC) (2017e): Historische stündliche Stationsmessungen der Wolkenbedeckung für Deutschland, Version v004.

Fink, A. H., Brücher, T., Krüger, A., Leckebusch, G. C., Pinto, J. G., & Ulbrich, U. (2004). The 2003 European summer heatwaves and drought–synoptic diagnosis and impacts. *Weather, 59*(8), 209-216.

Fischer, E. M., Seneviratne, S. I., Vidale, P. L., Lüthi, D., & Schär, C. (2007). Soil moisture–atmosphere interactions during the 2003 European summer heat wave. *Journal of Climate, 20*(20), 5081-5099. DOI: 10.1175/JCLI4288.1.

Foken, T. (2008). *Micrometeorology*. Berlin, Heidelberg: Springer-Verlag. DOI: 10.1007/978-3-642-25440-6.

Foken T., Leuning, R., Oncley, S.R., Mauder, M., & Aubinet, M. (2012). Corrections and Data Quality Control. In M. Aubinet, T. Vesala & D. Papale (Eds.), *Eddy Covariance: A Practical Guide to Measurement and Data Analysis* (pp.85-132). Dordrecht, Heidelberg, London, New York: Springer Atmospheric Sciences. DOI: 10.1007/978-94-007-2351-1_4.

Food and Agriculture Organisation (FAO) (2009). Global agriculture towards 2050. How to feed the world 2050. High level expert forum, Rome, 12-13 October 2009.

Gerber, J. F., & Decker, W. L. (1960). Estimates of Bowen's ratio by the heat budget measurements of a cornfield. *Journal of Geophysical Research, 65*(11), 3699-3702. DOI: 10.1029/JZ065i011p03699.

Gordon, R., Brown, D. M., & Dixon, M. A. (1997). Estimating potato leaf area index for specific cultivars. *Potato Research, 40*(3), 251-266. DOI: 10.1007/BF02358007.

Grunewald, K., & Bastian, O. (2015). *Ecosystem services – Concept, methods and case studies*. Berlin: Springer.

Helmholtz Zentrum München. Deutsches Forschungszentrum für Gesundheit und Umwelt (2005). *GSF pachtet Klostergut Scheyern. Klostergut Scheyern bleibt interdisziplinäre Forschungsstätte.* Retrieved from https://www.helmholtz-muenchen.de/aktuelles/uebersicht/pressemitteilungnews/article/18486/index.html [last access 04.05.2017].

Helmholtz Gemeinschaft (2011). *TERENO. Terrestrial Environmental Observatories. Bayrisches Alpen-Voralpen-Observatorium.* Retrieved from http://teodoor.icg.kfa-juelich.de/observatories-de/bayrisches-alpen-voralpen-observatorium/bavarian-alps-pre-alps-observatory-de [last access 04.05.2017].

Henderson-Sellers, A., McGuffie, K., & Pitman, A. J. (1996). The project for intercomparison of land-surface parametrization schemes (PILPS): 1992 to 1995. *Climate Dynamics, 12*(12), 849-859.

Herrmann, I., Pimstein, A., Karnieli, A., Cohen, Y., Alchanatis, V., & Bonfil, D. J. (2011). LAI assessment of wheat and potato crops by VENμS and Sentinel-2 bands. *Remote Sensing of Environment, 115*(8), 2141-2151. DOI: 10.1016/j.rse.2011.04.018.

Hutson, D. H., & Roberts, T. R. (1990). *Environmental fate of pesticides.* Chichester: Wiley.

IPCC - Intergovernmental Panel on Climate Change (2013). *Climate Change 2013. The Physical Science Basis*. Retrieved from https://www.ipcc.ch/publications_and_data/publications_and_data_reports.shtml [last access 27.05.2017].

Jarvis, P. G. (1976). The interpretation of the variations in leaf water potential and stomatal conductance found in canopies in the field. *Philosophical Transactions of the Royal Society of London, Series B*(273), 593–610.

Jury, W. A., Gardner, W. R., & Gardner, W. H. (1991). *Soil Physics* (5th Edition), 328pp. New York: John Wiley & Sons.

Koellner, T. (2013). *Ecosystem services and global trade of natural resources: ecology, economics and policies*. London: Taylor & Francis (Routledge explorations in environmental economics).

Koster, R. D., Dirmeyer, P. A., Guo, Z., Bonan, G., Chan, E., Cox, P., ... & Liu, P. (2004). Regions of strong coupling between soil moisture and precipitation. *Science, 305*(5687), 1138-1140. DOI: 10.1126/science.1100217.

Kovács-Hostyánszki, A., Espíndola, A., Vanbergen, A. J., Settele, J., Kremen, C., & Dicks, L. V. (2017). Ecological intensification to mitigate impacts of conventional intensive land use on pollinators and pollination. *Ecology Letters, 20*(5), 673-689. DOI: 10.1111/ele.12762.

Louis, J. F. (1979). A parametric model of vertical eddy fluxes in the atmosphere. *Boundary-Layer Meteorology, 17*(2), 187-202.

Manabe, S. (1969). Climate and the ocean circulation 1: i. The atmospheric circulation and the hydrology of the earth's surface. *Monthly Weather Review, 97*(11), 739-805.

Matzner, E. (Ed.). (2013). *Biogeochemistry of Forested Catchments in a Changing Environment, A German Case Study.* Berlin, Heidelberg: Springer Science & Business Media.

Mauder M., & Foken T. (2015). Documentation and instruction manual of the eddy-covariance software package TK3 (update). Work Report. University of Bayreuth, Department of Micrometeorology, ISSN 1614-8916, 62, 64pp. Retrieved from http://epub.uni-bayreuth.de/2130/.

McDonough, K., Hutchinson, S., Moore, T., & Hutchinson, J. S. (2017). Analysis of publication trends in ecosystem services research. *Ecosystem Services, 25*, 82-88. DOI: 10.1016/j.ecoser.2017.03.022.

Meehl, G. A., & Tebaldi, C. (2004). More intense, more frequent, and longer lasting heat waves in the 21st century. *Science, 305*(5686), 994-997. DOI: 10.1126/science.1098704.

Mengelkamp, H. T., Warrach, K., & Raschke, E. (1997). A land surface scheme for atmospheric and hydrologic models: SEWAB (Surface Energy and Water Balance). *GKSS – Forschungszentrum Geesthacht GmbH*.

Mengelkamp, H. T., Warrach, K., & Raschke, E. (1999). SEWAB–a parameterization of the surface energy and water balance for atmospheric and hydrologic models. *Advances in Water Resources, 23*(2), 165-175. DOI: 10.1016/S0309-1708(99)00020-2.

Mengelkamp, H. T., Kiely, G., & Warrach, K. (2001). Evaluation of the hydrological components added to an atmospheric land-surface scheme. *Theoretical and applied climatology, 69*(3), 199-212. DOI: 10.1007/s007040170025.

Millennium Ecosystem Assessment (MA) (2005). *Ecosystems and Human Well-being: Synthesis.* Washington DC: Island Press. Retrieved from http://www.millenniumassessment.org/documents/document.356.aspx.pdf.

Miralles, D. G., den Berg, M. V., Teuling, A. J., & Jeu, R. D. (2012). Soil moisture-temperature coupling: A multiscale observational analysis. *Geophysical Research Letters, 39*(21). n/a-n/a. DOI: 10.1029/2012GL053703.

Moeller, K. (2002). *Auswirkungen von Krautfäulebefall und N-Ernährung auf das Wachstumsverhalten von Kartoffeln* [Effect of Phytophthora and N-nutrition on the growth of potatoes]. Retrieved from http://orgprints.org/1046/1/moeller-2002-kartoffel-krautfaeule-n-ernaehrung.PDF [last access 04.05.2017].

Monteith, J. L., & Szeicz, G. (1962). Radiative temperature in the heat balance of natural surfaces. *Quarterly Journal of the Royal Meteorological Society, 88*(378), 496-507.

Moriasi, D. N., Arnold, J. G., Van Liew, M. W., Bingner, R. L., Harmel, R. D., & Veith, T. L. (2007). Model evaluation guidelines for systematic quantification of accuracy in watershed simulations. *Transactions of the ASABE, 50*(3), 885-900. DOI: 10.13031/2013.23153.

NASA LP DAAC (2015). MODIS MYD11A2 Land Surface Temperature & Emissivity 8-Day L3 Global Data. Version 6. NASA EOSDIS Land Processes DAAC, USGS Earth Resources Observation and Science (EROS) Center, Sioux Falls, South Dakota (https://lpdaac.usgs.gov), at http://dx.doi.org/10.5067/MODIS/MYD11_A2.006. [last access 29.06.2017].

NASA JPL (2009): Advanced Spaceborn Thermal Emission and Reflectance Radiometer Global Digital Elevation Model Version 2 (ASTER GDEM v2). https://lpdaac.usgs.gov/node/1079 [last access 17.10.2016]. ASTER GDEM is a product of METI and NASA.

Noilhan, J., & Planton, S. (1989). A simple parameterization of land surface processes for meteorological models. *Monthly Weather Review, 117*(3), 536-549. DOI: 10.1175/1520-0493(1989)117<0536:ASPOLS>2.0.CO;2.

Petropoulos, G., Carlson, T. N., & Wooster, M. J. (2009). An overview of the use of the SimSphere Soil Vegetation Atmosphere Transfer (SVAT) Model for the study of land-atmosphere interactions. *Sensors, 9*(6), 4286-4308. DOI: 10.3390/s90604286.

Pielke, R.A., Seastedt, T.R., & Suding, K. (2013). *Climate vulnerability. Understanding and Addressing Threats to Essential Resources. Volume 4: Vulnerability of Ecosystems to Climate.* Amsterdam [u.a.]: Academic Press.

Pielke, R.A., & Niyogi, D. (2013). *Climate Vulnerability. Understanding and Addressing Threats to Essential Resources. Volume 2: Vulnerability of Food Resources to Climate.* Amsterdam [u.a.]: Academic Press.

Pitman, A.J. (2003). The evolution of, and revolution in, land surface schemes designed for climate models. *International Journal of Climatology ,23*(5), pp. 479–510. DOI: 10.1002/joc.893., 23(5), 479-510.

Power, A. G. (2010). Ecosystem services and agriculture: tradeoffs and synergies. *Philosophical Transactions of the Royal Society of London B: Biological Sciences, 365*(1554), 2959-2971. DOI: 10.1098/rstb.2010.0143.

QGIS Development Team (2015). *QGIS Geographic Information System.* Open Source Geospatial Foundation. Retrieved from http://qgis.osgeo.org.

R Core Team (2017). *R: A language and environment for statistical computing*. R Foundation for Statistical Computing, Vienna, Austria. Retrieved from https://www.R-project.org/.

Renes, J. (2009). Agrarian Transformations. In R. Kitchin & N. J. Thrift (Eds.): *International encyclopedia of human geography* (58–64). Utrecht: Elsevier Science.

Richards, L. A. (1931). Capillary conduction of liquids through porous mediums. *Physics, 1*(5), 318-333. DOI: 10.1063/1.1745010.

Sato, H., Ito, A., Ito, A., Ise, T., & Kato, E. (2015). Current status and future of land surface models. *Soil science and plant nutrition, 61*(1), 34-47. DOI: 10.1080/00380768.2014.917593.

Sellers, P. J., Dickinson, R. E., Randall, D. A., Betts, A. K., Hall, F. G., Berry, J. A., ... & Sato, N. (1997). Modeling the exchanges of energy, water, and carbon between continents and the atmosphere. *Science, 275*(5299), 502-509.

Seneviratne, S. I., Corti, T., Davin, E. L., Hirschi, M., Jaeger, E. B., Lehner, I., ... & Teuling, A. J. (2010). Investigating soil moisture–climate interactions in a changing climate: A review. *Earth-Science Reviews, 99*(3), 125-161. DOI: 10.1016/j.earscirev.2010.02.004.

Serafimovich, A., Eder, F., Hübner, J., Falge, E., Voß, L., Sörgel, M., ... & Foken, T. (2011). *Exchange processes in mountainous Regions (EGER) Documentation of the Intensive Observation Period (IOP3) June, 13th to July, 26th 2011.* Retrieved from https://epub.uni-bayreuth.de/304/1/ARBERG47.pdf [last access 31.5.2017].

Singh, J., Knapp, H. V., Arnold, J. G., & Demissie, M. (2005). Hydrological modeling of the Iroquois River watershed using HSPF and SWAT. JAWRA Journal of the American Water Resources Association, 41(2), 343-360.

Teuling, A. J., Seneviratne, S. I., Stöckli, R., Reichstein, M., Moors, E., Ciais, P., ... & Dellwik, E. (2010). Contrasting response of European forest and grassland energy exchange to heatwaves. *Nature Geoscience, 3*(10), 722-727. DOI: 10.1038/ngeo950.

Thünen Institut (2014). *Thünen Atlas: Landwirtschaftliche Nutzung Version 2014.* Retrieved from https://gdi.thuenen.de/lr/agraratlas/indexMap.htm?LP=2 [last access 17.08.2017].

Van Liew, M. W., Arnold, J. G., & Garbrecht, J. D. (2003). Hydrologic simulation on agricultural watersheds: Choosing between two models. *Transactions of the ASAE, 46*(6), 1539-1551.

Viglizzo, E. F., Jobbágy, E. G., Ricard, M. F., & Paruelo, J. M. (2016). Partition of some key regulating services in terrestrial ecosystems: Meta-analysis and review. *Science of the Total Environment, 562*, 47-60. DOI: 10.1016/j.scitotenv.2016.03.201.

Vihervaara, P., Rönkä, M., & Walls, M. (2010). Trends in ecosystem service research: early steps and current drivers. *AMBIO: A Journal of the Human Environment, 39*(4), 314-324. DOI: 10.1007/s13280-010-0048-x.

Wetter online (n.d.): *Klima in der Region Straubing.* Retrieved from http://www.wetteronline.de/?pcid=pc_rueckblick_climate&gid=10788&pid=p_rueckblick_climatehistory&sid=Temperature&month=08&iid=10788 [last access 18.08.2017].

Xiaoyu, S., Bei, C., Guijun, Y., & Haikuan, F. (2014). Comparison of winter wheat growth with multi-temporal remote sensing imagery. *IOP Conference Series: Earth and Environmental Science, 17*(1), 12044. DOI: 10.1088/1755-1315/17/1/012044.

Zaitchik, B. F., Macalady, A. K., Bonneau, L. R., & Smith, R. B. (2006). Europe's 2003 heat wave: A satellite view of impacts and land–atmosphere feedbacks. *International Journal of Climatology, 26*(6), 743-769.

Appendix

Model Evaluation Land Cover Type Agriculture (Scheyern)

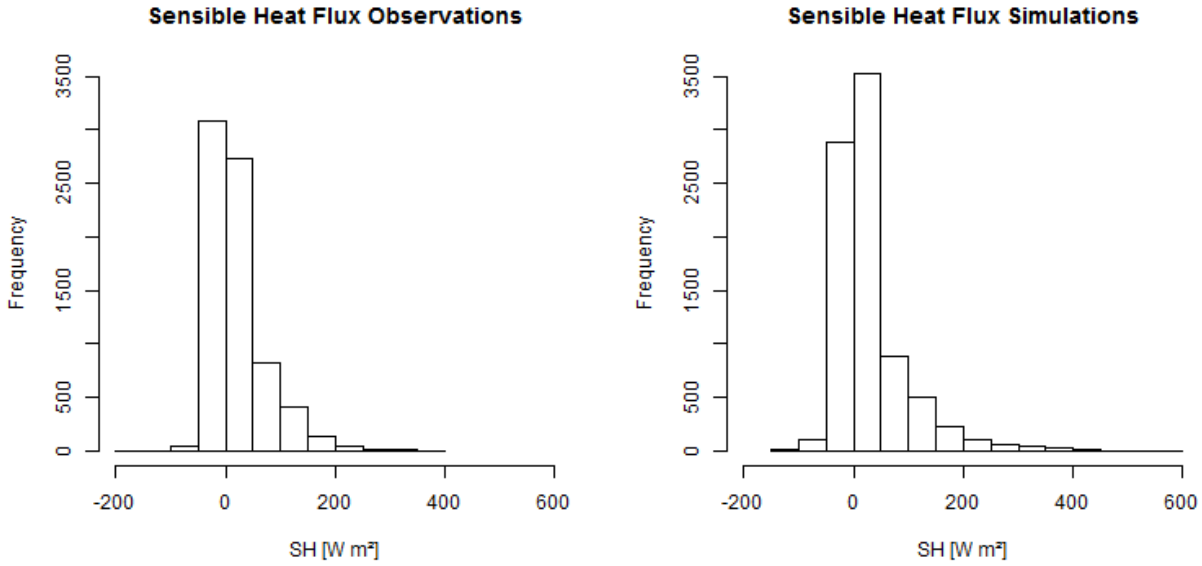

Figure A 1: Histograms of sensible heat flux observations and simulations at Scheyern

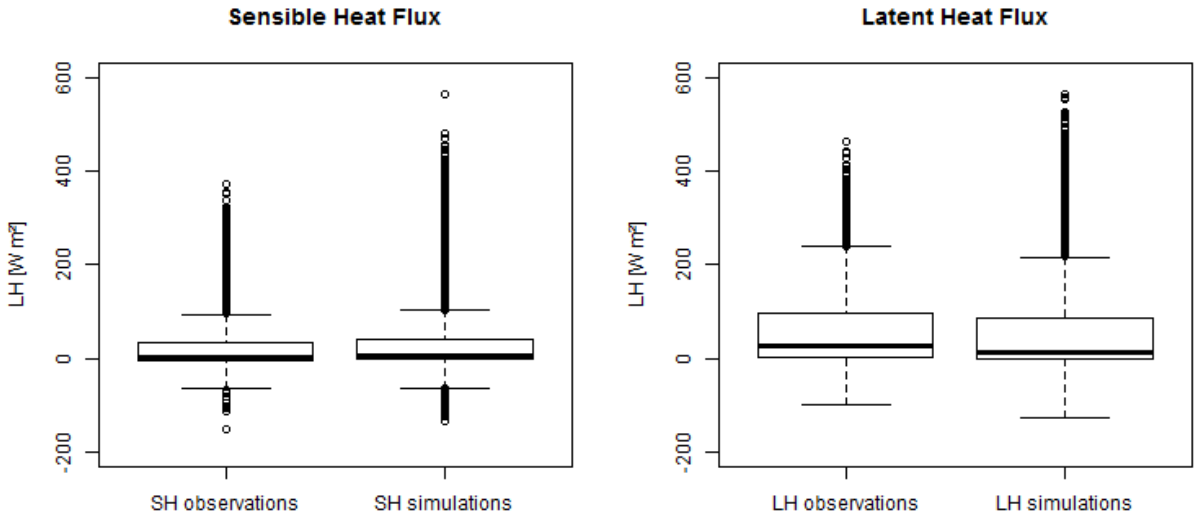

Figure A 2: Boxplots of sensible and latent heat flux observations and simulations at Scheyern.

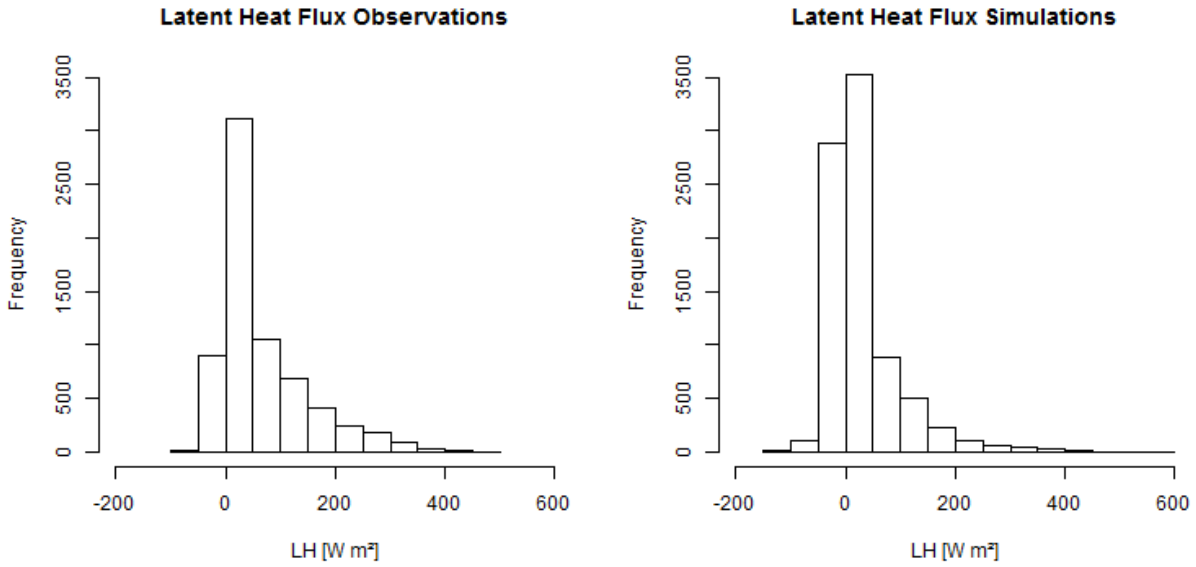

Figure A 3: Histograms of latent heat flux observations and simulations at Scheyern.

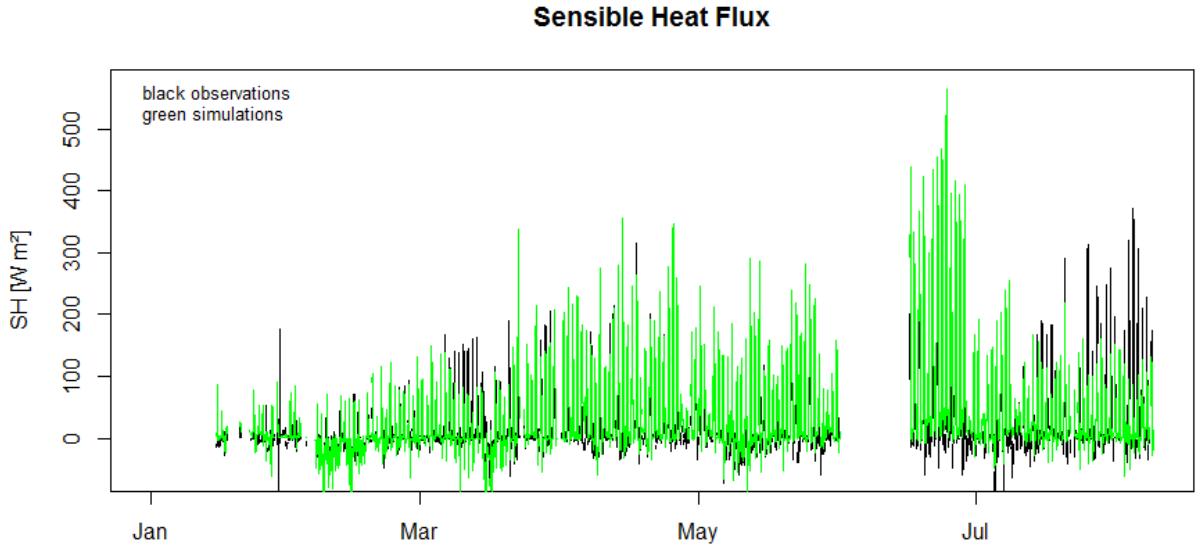

Figure A 4: Time series plot for the whole evaluation period for sensible heat flux at Scheyern.

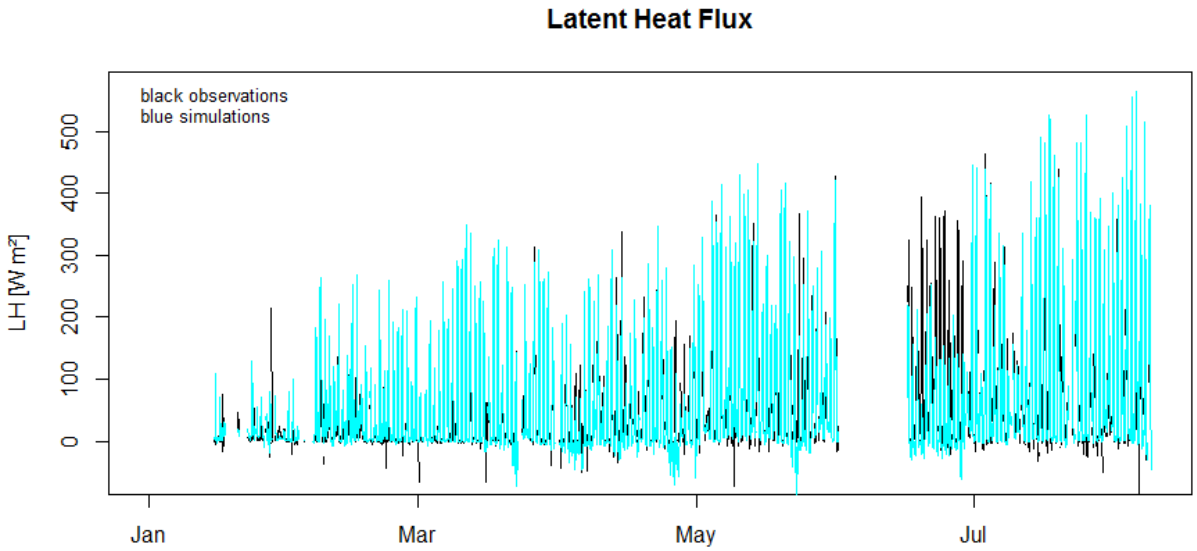

Figure A 5: Time series plot for the whole evaluation period for latent heat flux at Scheyern.

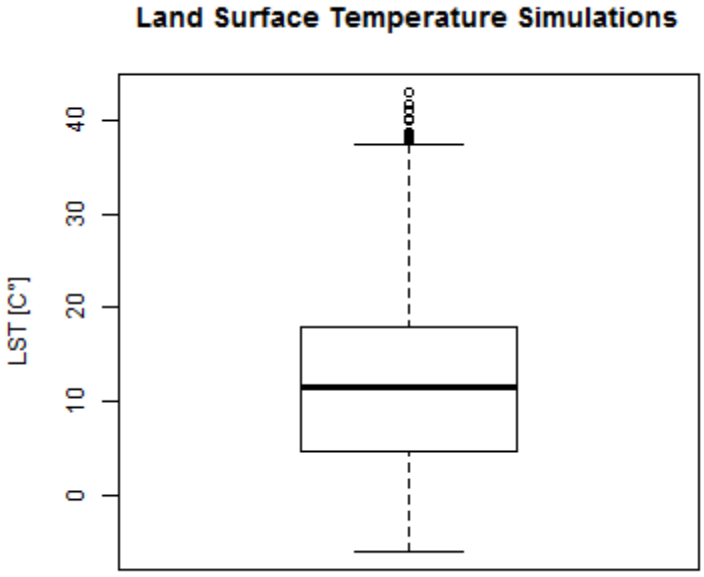

Figure A 6: Boxplot of land surface temperature simulations at scheyern.

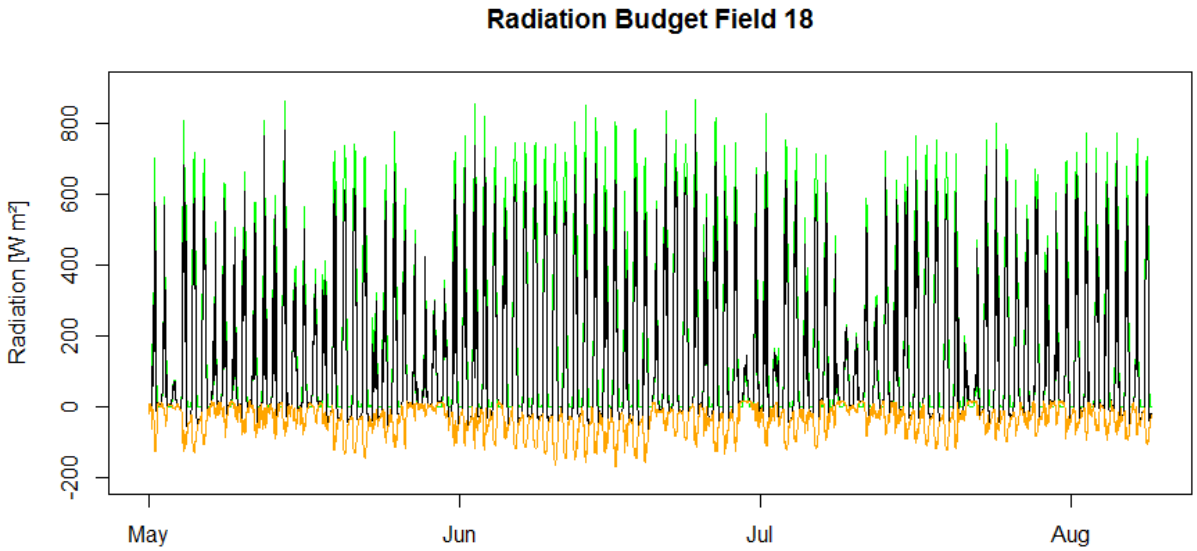

Figure A 7: Time series plot (May-Aug) for the radiation budget at Scheyern. Black = net radiation, Green = net shortwave radiation, orange = net long wave radiation.

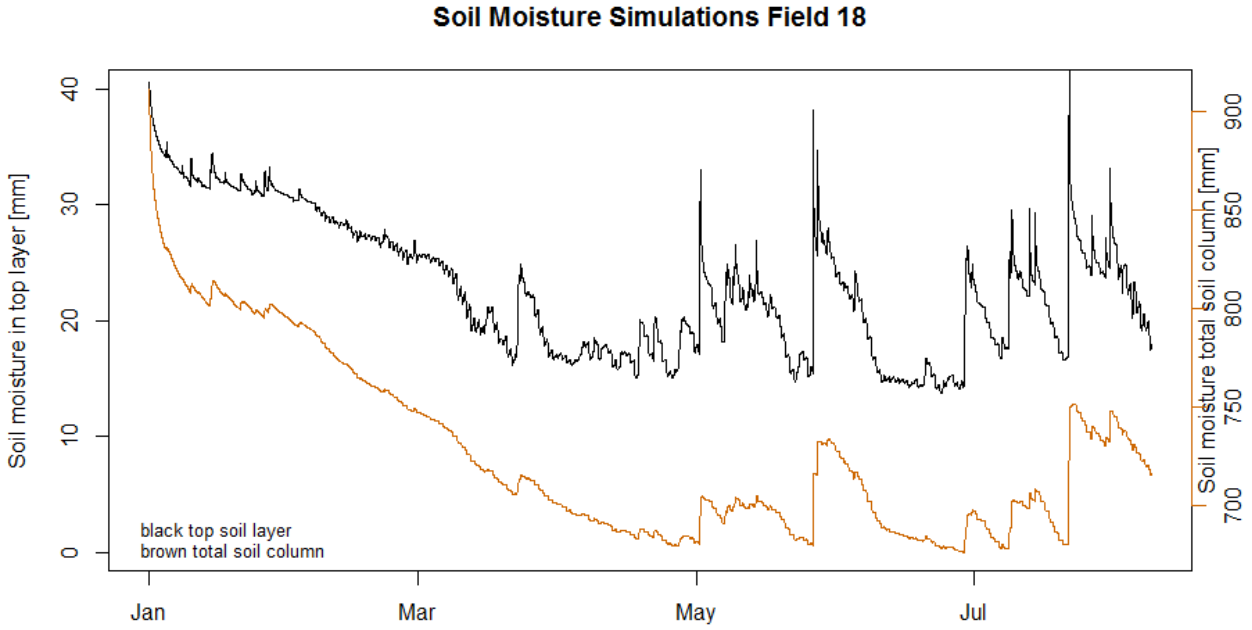

Figure A 8: Fig.9 Time series plot (year 2014) for the development of soil moisture content at Scheyern.

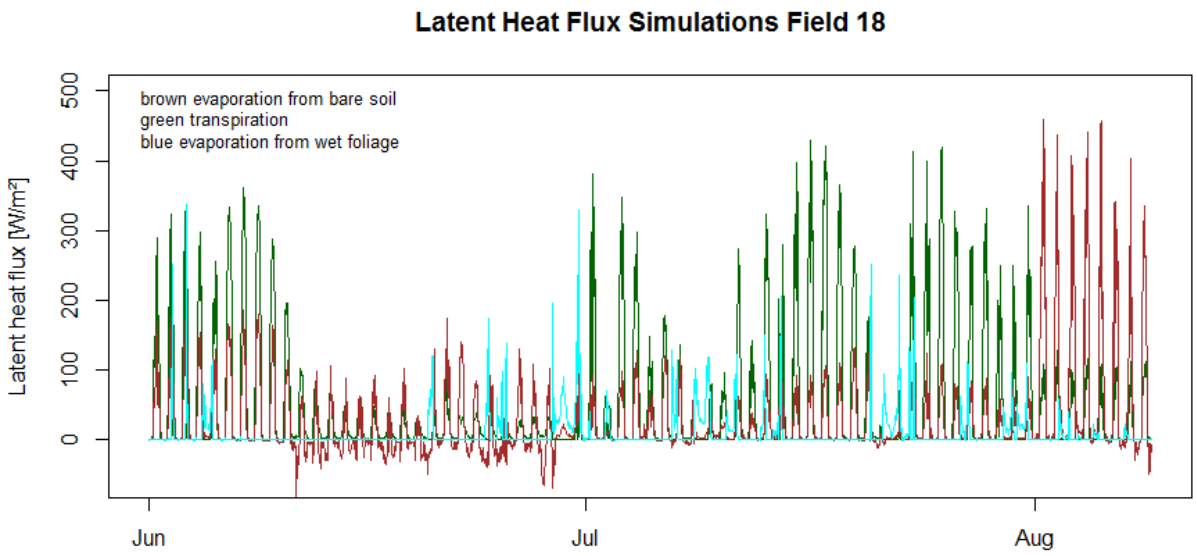

Figure A 9: Latent heat flux from transpiration and evaporation from bare soil (June – August) over field 18 (winter wheat).

Model Evaluation Land Cover Type Forest (Waldstein)

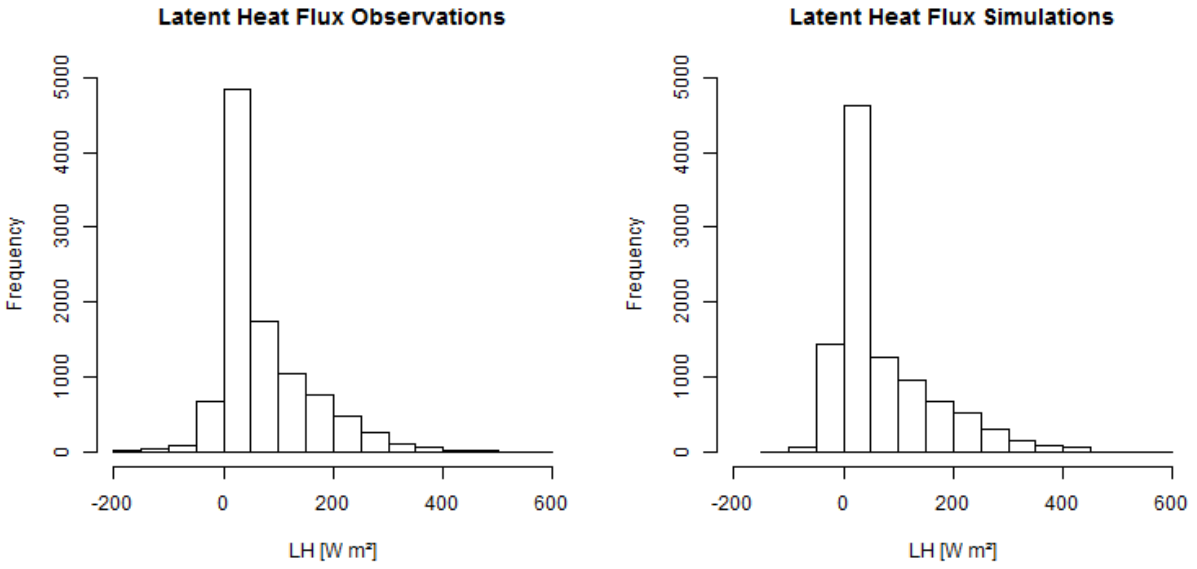

Figure A 10: Histograms of latent heat flux observations and simulations at Waldstein.

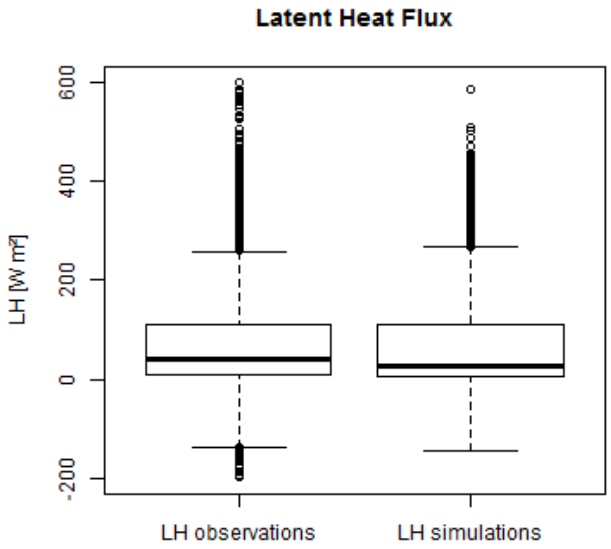

Figure A 11: Boxplots of latent heat flux observations and simulations at Waldstein.

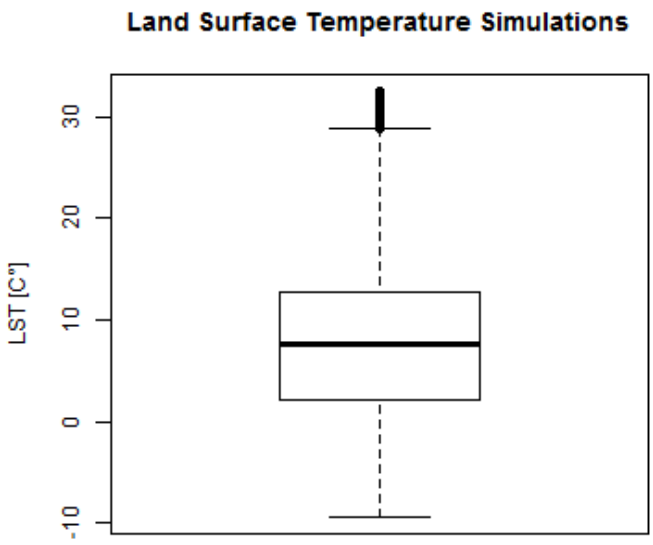

Figure A 12: Boxplots of land surface temperature simulations at Waldstein.

Model Application at Research Area

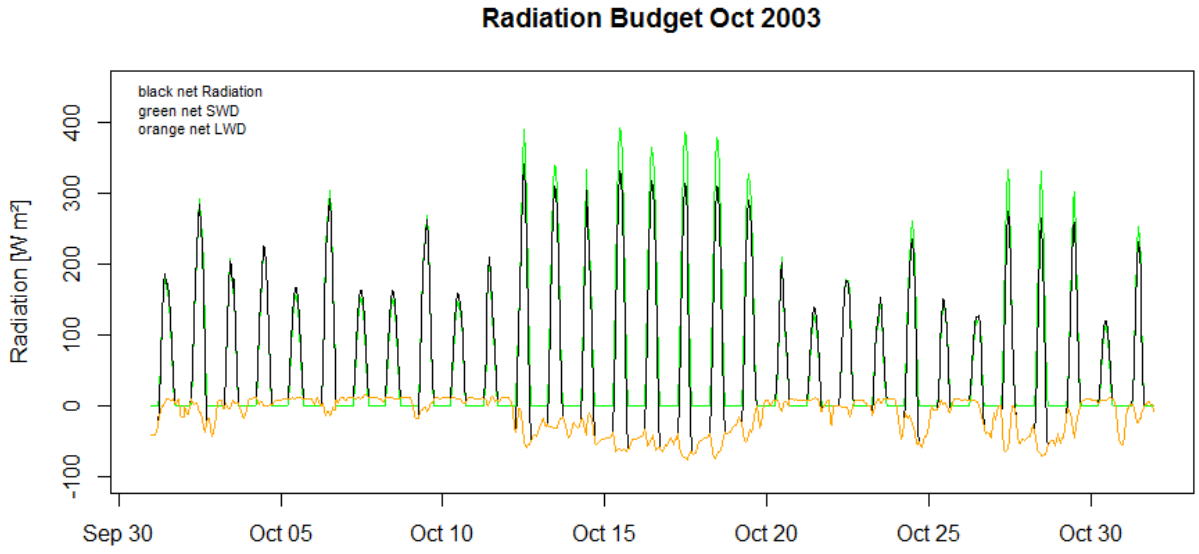

Figure A 13: Radiation Budget (October 2003) at Straubing.

Table A 1: Overview of the temporal occurrences of lowest and highest mean values, and minimum and maximum values for the main climate variables (model results and spatial analyses).

	SEWAB						**MODIS**		**SEWAB**					
	Homogenous Agriculture							**Heterogeneous LC**						
	2003			2004			**2003**		**2003**			2004		
	SH [Wm^{-2}]	LH [Wm^{-2}]	LST [°C]	SH [Wm^{-2}]	LH [Wm^{-2}]	LST [°C]	LST 2003 [°C]	LST 2003 [°C]	SH [Wm^{-2}]	LH [Wm^{-2}]	LST [°C]	SH [Wm^{-2}]	LH [Wm^{-2}]	LST [°C]
	Range of mean 29.73 – 322.45	Range of mean 25.70 – 251.30	Range of mean 6.67 – 41.46	Range of mean 29.15 – 324.51	Range of mean 31.33 – 268.35	Range of mean 10.82 – 34.40	Range of mean 8.93 – 39.19	Range of mean 8.49 – 37.24	Range of mean 13.21 – 341.17	Range of mean 45.75 – 245.90	Range of mean 6.16 – 37.61	Range of mean 12.48 – 330.70	Range of mean 52.20 – 276.72	Range of mean 10.35 – 31.79
March 30th – April 6th				Min - 58.55	Max 534.42	Min 2.28								Min 2.30
April 7th – 14th														
April 15th – 22nd		Min - 87.00												
April 23rd – 30th														
May 1st – 8th														
May 9th – 16th														
May 17th – 24th														
May 25th – June 1st					Min - 101.57								Min - 119.53	
June 2nd – 9th					Highest mean 268.35								Highest mean 276.27	

Table A 1 continued

	SEWAB						**MODIS**		**SEWAB**					
	Homogenous Agriculture							**Heterogeneous LC**						
	2003			2004			**2003**		**2003**			2004		
	SH [Wm^{-2}]	LH [Wm^{-2}]	LST [°C]	SH [Wm^{-2}]	LH [Wm^{-2}]	LST [°C]	LST 2003 [°C]	LST 2003 [°C]	SH [Wm^{-2}]	LH [Wm^{-2}]	LST [°C]	SH [Wm^{-2}]	LH [Wm^{-2}]	LST [°C]
June 10th – 17th		Max 472.17 & highest mean 251.30								Max 499.74 & highest mean 245.90				
June 18th – 25th														
June 26th – July 3rd												Max 457.76		
July 4th – 11th														
July 12th 19th														
July 20th – 27th										Min - 110.23				
July 28th – Aug 4th			Max 59.52								Max 50.70			
Aug 5th – 12th	Max 449.26 & Highest mean 322.45	Lowest mean 25.70		Max 442.32 Highest mean 324.51	Lowest mean 31.33	Max 38.18	Max 42.17	Max 40.10	Max 464.95 & highest mean 341.17	Lowest mean 45.90		Highest mean 330.70		Max 34.99
Aug 13th – 20th														
Aug 21st – 28th														
Aug 29th – Sept 5th												Min - 260		

Table A 1 continued

	SEWAB						**MODIS**		**SEWAB**					
	Homogenous Agriculture							**Heterogeneous LC**						
	2003			2004			**2003**		**2003**			2004		
	SH [Wm^{-2}]	LH [Wm^{-2}]	LST [°C]	SH [Wm^{-2}]	LH [Wm^{-2}]	LST [°C]	LST 2003 [°C]	LST 2003 [°C]	SH [Wm^{-2}]	LH [Wm^{-2}]	LST [°C]	SH [Wm^{-2}]	LH [Wm^{-2}]	LST [°C]
Sept 6th – 13th														
Sept 14th – 21st														
Sept 22nd – 29th												Lowest mean 12.48		
Sept 30th – Oct 7th									Min 190.78					
Oct 8th – 15th									Lowest mean 13.21					
Oct 16th – 23rd														
Oct 24th – 31st	Min -23.39 & lowest mean 29.73		Min - 1.79				Min 7.34	Min 6.37			Min -2.1		Lowest mean 52.20	
Nov 1st – 8th				Lowest mean 29.15										